2022 RMZ – M&G **Vol. 69** No. 1

RMZ

MATERIALS and GEOENVIRONMENT

MATERIALI in GEOOKOLJE

RMZ – M&G, **Vol. 69**, No. 1
pp. 1–66 (2022)

Ljubljana, March 2022

RMZ – Materials and Geoenvironment
RMZ – Materiali in geookolje
ISSN 1408-7073

Old title/Star naslov
Mining and Metallurgy Quarterly/Rudarsko-metalurški zbornik
ISSN 0035-9645, 1952–1997

Published by/Izdajatelj
Faculty of Natural Sciences and Engineering, University of Ljubljana/
Naravoslovnotehniška fakulteta, Univerza v Ljubljani

Associated Publisher/Soizdajatelj
Institute for Mining, Geotechnology and Environment, Ljubljana/
Inštitut za rudarstvo, geotehnologijo in okolje
Velenje Coal Mine/Premogovnik Velenje
Slovenian Chamber of Engineers/Inženirska zbornica Slovenije

Editorial Office/Uredništvo
Technical editors/Tehnična urednika Blaž Janc and Jože Žarn
Secretary/Tajnica Nives Vukič

Editorial Address/Naslov uredništva
RMZ – Materials and Geoenvironment
Aškerčeva cesta 12, p. p. 312
1001 Ljubljana, Slovenija
Tel.: +386 (0)1 470 46 10
Fax.: +386 (0)1 470 45 60
E-mail: bostjan.markoli@ntf.uni-lj.si
joze.zarn@ntf.uni-lj.si

Published/Izhajanje
4 issues per year/4 številke letno

Partly funded by Ministry of Education, Science and Sport of Republic of Slovenia./Pri financiranju revije sodeluje Ministrstvo za izobraževanje, znanost in šport Republike Slovenije.

Articles published in Journal "RMZ M&G" are indexed in international secondary periodicals and databases:/Članki, objavljeni v periodični publikaciji „RMZ M&G", so indeksirani v mednarodnih sekundarnih virih:
CA SEARCH® – Chemical Abstracts®, METADEX®, GeoRef.

Annual subscription for individuals in Slovenia: 20 EUR, for institutions: 30 EUR. Annual subscription for the rest of the world: 30 EUR, for institutions: 50 EUR/Letna naročnina za posameznike v Sloveniji: 20 EUR, za inštitucije: 30 EUR. Letna naročnina za tujino: 30 EUR, inštitucije: 50 EUR

Transaction account/Tekoči račun
Nova Ljubljanska banka, d. d., Ljubljana: UJP 01100-6030708186

VAT identification number/Davčna številka
24405388

Online Journal/Elektronska revija
https://content.sciendo.com/view/journals/rmzmag/rmzmag-overview.xml?result=4&rskey=iClOT4#

Table of Contents

Kazalo

Original scientific articles
Izvirni znanstveni članki

Original Scientific Article • DOI: 10.2478/rmzmag-2021-0019

Received: March 11, 2022
Accepted: March 28, 2022

Petroleum source rock characteristics of the Mesozoic units, Mekelle Basin, northern Ethiopia

Značilnosti mezozojskih plasti v Mekelle bazenu severne Etiopije kot izvornih plasti oglikovodikov

Damenu Adefris[1,2,*], M.E. Nton[3], O.A. Boboye[3], Balemwal Atnafu[4]

[1]Department of Geology, Debre Berhan University, P.O. Box 445, Debre Berhan, Ethiopia

[2]Petroleum Geosciences Program, Pan African University, Life and Earth Sciences Institute (including Health and Agriculture), University of Ibadan, Ibadan, Nigeria

[3]Department of Geology, University of Ibadan, Ibadan, Nigeria

[4]School of Earth Sciences, Addis Ababa University, P.O. Box 1176, Addis Ababa, Ethiopia

*Corresponding author: E-mail: damegeol@gmail.com

Abstract in English

The Mekelle Basin comprises carbonate and siliciclastic rocks which could have potential for petroleum as previous studies reported without enough evidence. This research is intended to assess source rock characteristics of selected samples from the Adigrat Sandstone, Antalo Limestone and Agula Shale. Four outcrop sections were investigated and fifteen limestone and shale samples were collected. TOC was deduced by *Leco SC-632* carbon analyzer, and Rock-Eval pyrolysis was determined using *Rock-Eval 6*. The TOC values range from 0.11 wt.% to 0.42 wt % for 80% of the samples which is less than the minimum requirements for source rocks. However, a few samples have TOC between 0.5 wt % and 1.0 wt %, indicating fair organic matter richness. The kerogen is mainly Type IV and inert. The S_1 (0–0.02 mgHC/g) and S_2 (0–0.07 mgHC/g) values are very low, with very high T_{max} (475–527 °C), indicating very poor potential with over-mature dry gas. Therefore, the analyzed samples have low organic content for hydrocarbon, implying that the studied units have no feasible source rock potential.

Keywords: Mesozoic units, Rock-Eval pyrolysis, Source rock, Thermal maturity, Total organic carbon

Abstract in Povzetek

Mekelle bazen vsebuje karbonatne in siliciklastične kamnine, ki bi, glede na predhodne raziskave, lahko vsebovale ogljikovodike. Namen raziskave je določitev lastnosti izbranih vzorcev Adigratskega peščenjaka, Antalskega apnenca in Agulskega skrilavega glinavca. Raziskali smo štiri izdanke ter nabrali petnajst vzorcev apnenca in skrilavega glinavca. Vsebnosti TOC so bile določene z Leco SC-632 analizatorjem ogljika. RockEval piroliza je bila določena z uporabo Rock-Eval 6. Vsebnosti TOC v vzorcih so v razponu od 0,11 masnih odstotkov do 0,42 masnih odstotkov, kar je manj kot so najnižje zahteve za izvorne kamnine. Redki vzorci imajo vrednosti TOC med 0,5 in 1,0 masnega odstotka, kar nakazuje zmerno visoko vsebnost organske snovi. Kerogen je večinoma tipa IV in inerten. Vrednosti S1 (0–0,02 mgHC/g) in S2 (0–0,07 mgHC/g) so zelo nizke, z zelo visoko T_{max} (475–527 °C), kar kaže na zelo nizek potencial s prezrelim suhim plinom. Preiskani vzorci imajo tako majhno količino organske snovi za ogljikovodike, kar kaže, da raziskane enote nimajo pomembnejšega potenciala izvornih plasti.

Ključne besede: mezozojske enote, Rock-Eval piroliza, izvorna kamnina, termična zrelost, skupna količina ogljika

Introduction

Petroleum is considered as one of the geologic resources of Ethiopia and potential oil and gas occurrences are expected from the Ogaden, Blue Nile, Mekelle, Gambela and Southern Rift Basins [1]. Paleozoic shale units served as sources of hydrocarbon that fed sandstone and carbonate reservoirs and led to the formation of a significant amount of the world's oil and

gas resource [2] [3]. Large reserves of oil and gas were discovered within the Permian sandstone and carbonate reservoirs sourced mainly by Silurian shales throughout the Middle East (e.g., Iran, Iraq and Arabia) [4]. The Permian Calub Sandstone and Bokh Shale are also good reservoirs and source rocks respectively in the Ogaden Basin, Ethiopia [5, 6]. The middle to upper Jurassic formations which comprised limestone, dolostone, marl, shale and sandstone are also known to have the potential for petroleum occurrences [5–12]. The Ogaden Basin was intensively investigated and has become the focus of oil companies to look for petroleum due to potential discoveries of gas fields at Shilabo, Calub and Hilala [5]. And, the Blue Nile Basin was the second target and studied in terms of petroleum system [9, 13], whereas the petroleum potential of Mekelle Basin has not been studied except the discovery of oil shale deposits within the Paleozoic glacial sediments [14]. However, the presence of possible potential source rocks within the Mesozoic units was reported by different workers even if detailed evaluation of quality, quantity and maturity of the organic matters have not been carried out. These units include the Agula Shale and Antalo Limestone with brown to black micritic limestone, beds of mudstone, brown shale and greenish-black limestone interbeds [15–16]. The Mekelle Basin requires a detailed evaluation of hydrocarbon prospectivity [1]. Therefore, this study is aimed at evaluating the petroleum source rock potential of these limestone and shale units including the Adigrat Sandstone.

Geological setting

The evolution of the Mekelle Basin is thought to have a close relationship with the East Africa Mesozoic rift basins, developed following the breakup of Gondwana [17]. Subduction along the Tethyan margin was considered to be the cause for the development of tensional stress in the Gondwana plate and its eventual breakup (Figure 1a) [18]. The breakup process was also triggered by the Permo – Triassic mantle plume, situated beneath the Karoo province, South Africa, that thermally weakened the lithosphere and contributed to the intracontinental rifting, widespread crustal extension and subsidence [18, 19]. These processes led to the development of the Permo – Triassic rift systems in the eastern part of Africa and created northwest-southeast trending aulacogen-like basins, reaching up to western and central Ethiopia [17, 20–22] (Figure 1b).

The sedimentation began in the late Paleozoic within these fault-controlled depositional environments [17, 19, 20, 23–28]. These rift-controlled sedimentary basins, in Ethiopia, include the Ogaden, Blue Nile and Mekelle Basins. The Mekelle Basin has also been considered as an intracontinental sag basin, formed due to cooling and thickening of a juvenile sub-continental lithospheric mantle and subsequent subsidence [29].

Some previous studies documented the petroleum potential of the Ogaden Basin [5, 6, 30–33]. [9, 13] investigated the hydrocarbon potential in the Blue Nile Basin. The Mekelle and Omo basins were investigated by [14, 34] respectively. The Mekelle Basin covers 8000 km^2 and comprises over 2000 meters thick Paleozoic to Mesozoic sedimentary successions [35] (Figure 2) which are considered to have geologically good properties to look for hydrocarbon [16].

The Paleozoic units comprise about 300 meters thick of glacial origin clastic rocks [36] which were, first, described and subdivided into glacial sandstone (Enticho Sandstone) and tillite facies (Edaga Arbi Tillite) [37]. The Edaga Arbi Tillite was later named Edaga Arbi Glacial which comprises tillite, siltstone and shale facies [35]. Enticho Sandstone was also subdivided into two members; Lower Enticho Sandstone and Upper Enticho Sandstone [38]. Detailed facies analysis revealed that the late Paleozoic sediments (Upper Enticho Sandstone and Edaga Arbi Glacial) were formed due to a wide range of glaciogenic processes and depositional environments including subaquatic environments with two major glacier advance-retreat cycles [39]. Oil shale deposit was discovered, sandwiched between the Enticho Sandstone and Edaga Arbi glacials and, in some places, underlying the Adigrat Sandstone which has an average mineable bed-thickness of 55 meters, covering an area

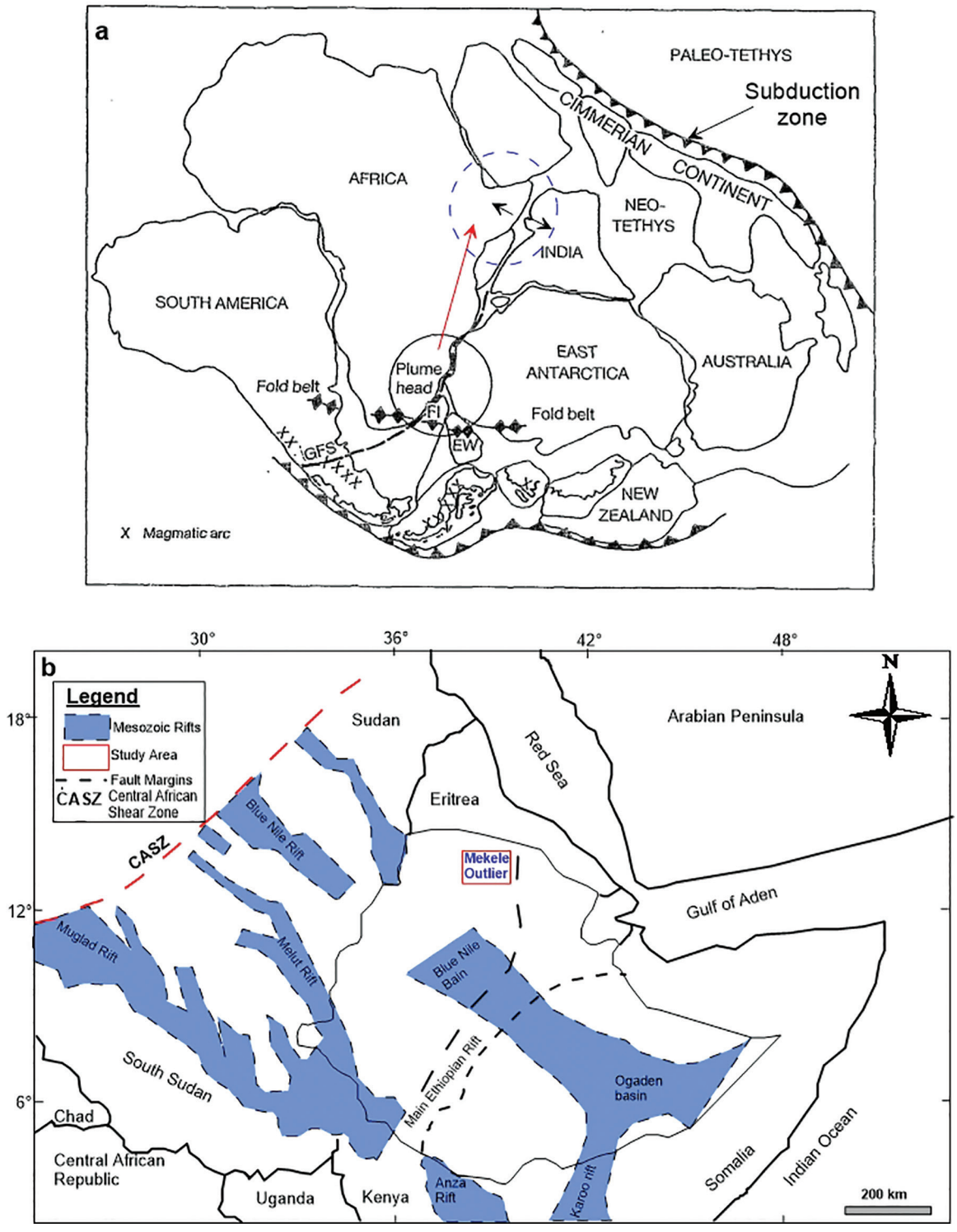

Figure 1: *(a) Map showing Gondwana breakup (after [18]); (b) Mesozoic rift basins of the Horn of Africa including Ethiopia (after [21]).*

of 30 km^2 with an estimated reserve of 4 billion tonnes [14]. The Triassic to middle Jurassic unit (Adigrat Sandstone) is about 300–650 meters thick and is considered to have a very good reservoir potential for petroleum [15, 16, 35]. The unit comprises fine-grained to coarse-grained sandstones and interbeds of siltstone and clay which were deposited in continental

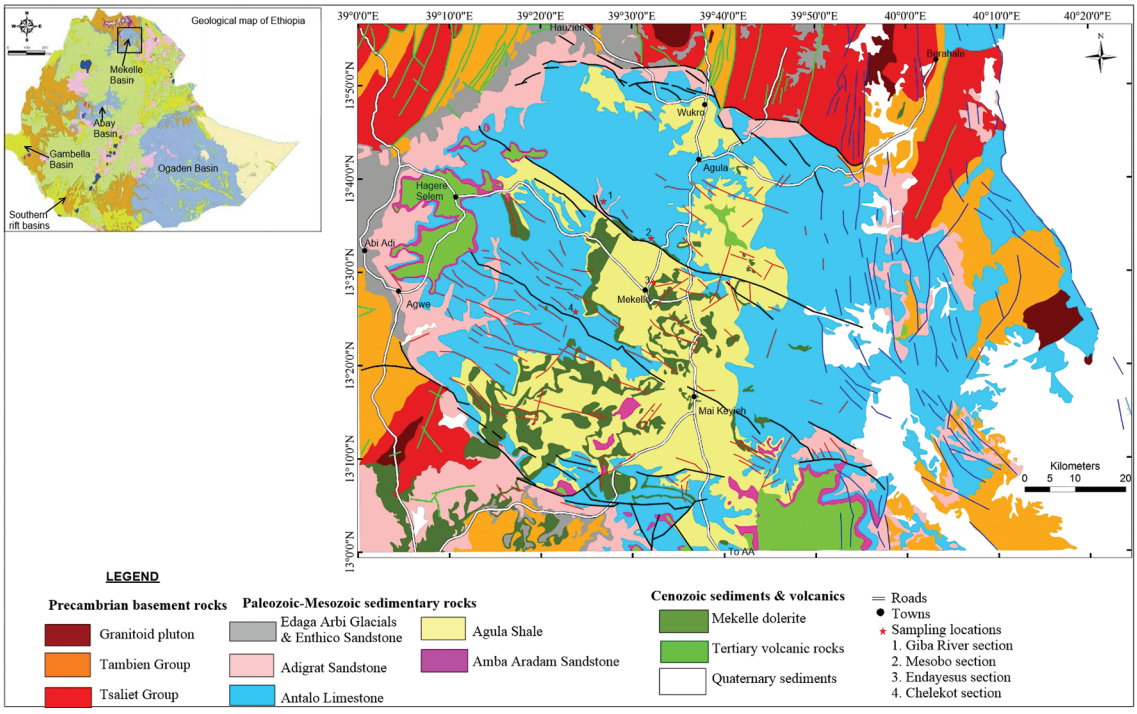

Figure 2: *Geological map of the Mekelle Basin with sampling locations (after [42]). The inset map is a simplified geological map of Ethiopia (after [43]).*

and shallow marine environments during the Triassic-middle Jurassic [35, 36].

The middle to upper Jurassic unit is carbonate (Antalo Limestone) with about 740 meters thick dominated mainly by yellow, white to black limestone with significant interbeds of marl, lenses of chert and cross-bedded sandstone [15–17, 35]. The brown shale and black limestone interbeds of the Antalo Limestone could serve as very good potential source rocks [16]. The unit has some reservoir potential [40]. The unit is also considered as a marine shelf carbonate facies, equivalent to the Mesozoic carbonate units of the Middle East Arabian Basins having potential for oil and gas occurrences [41]. In the Ogaden Basin, the marl and shale layers of Uarandab Formation are potential source rocks, with Type II kerogen, having petroleum potential that ranges from 2 kg/ton to 20 kg HC/ton of rock [5]. The black shales and mudstones of the Upper Hamanlei of the Blue Nile Basin, are also matured source rocks for oil generation, with TOC up to 7 wt.% and hydrogen index (HI) between 465 mgHC/g and 660 mgHC/g [9]. The Agula Shale is characterized by gray to black shale, marl and clay subunits with inter-laminae of black limestone, gypsum and dolomite, and has 60 to 250 meters thickness that was deposited in lagoons under semiarid conditions [15] [35]. The Amba Aradam Sandstone is upper Jurassic-lower Cretaceous in age [15, 17] which conformably overlies the Agula Shale. It is 60–200 meters thick and comprises medium to coarse-grained white to pink color sandstone facies (at the northern part of the basin) and white sandstone and conglomerate facies with some clayey beds (at the southern part of the basin) [35]. It has been confirmed, from the present study, that a highly conglomeratic sandstone composed of very coarse pebble size and well rounded quartz grains is exposed in the southern part of the basin whereas in the northwestern part of the basin, it is very fine-grained with yellow, pink to reddish colors. This unit was deposited in fluvial-lacustrine depositional environments and is assumed to be a very good reservoir rock in the basin [16, 35].

Materials and methods

A total of fifteen samples made up of five black limestones and ten shales were collected from

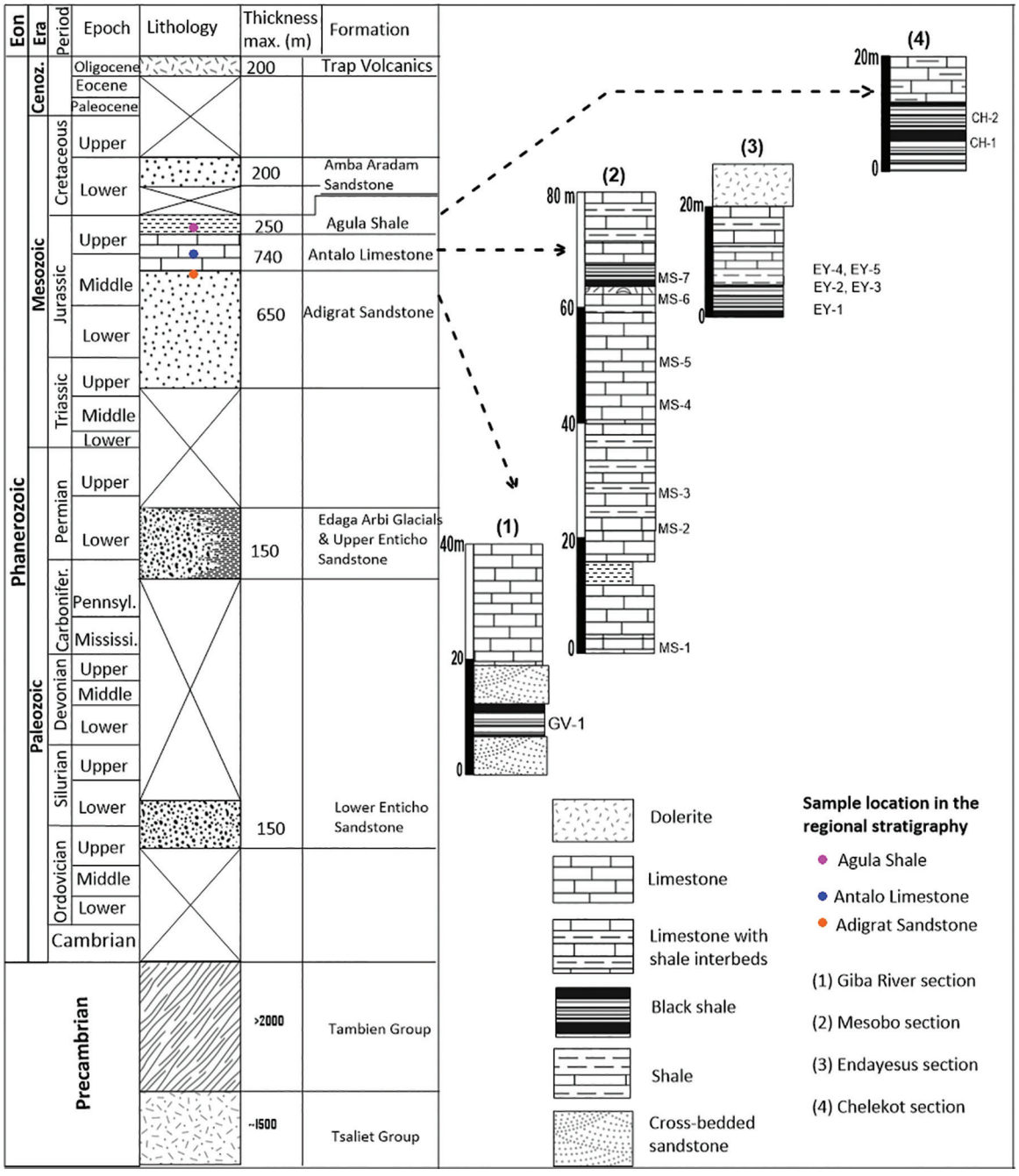

Figure 3: *Lithologic logs showing the locations of samples collected for source rock characterization.*

four outcrop locations for organic geochemical analyses. The samples were collected from the Adigrat Sandstone (one sample), Antalo Limestone (twelve samples) and Agula Shale (two samples). The petroleum potential of the samples was assessed from the Total Organic Carbon (TOC) and Rock-Eval pyrolysis. All laboratory procedures were carried out following the Norwegian Industry Guide to Organic Geochemical Analyses, fouth edition [44], at the Applied Petroleum Technology Ltd, (ALS Oil & Gas), UK. About 100 mg of sample was pulverized and diluted hydrochloric acid (HCl) was added to the pulverized rock samples to remove carbonate. The samples were then introduced into the *Leco* combustion oven, and the organic matter was directly converted to carbon dioxide through combustion. The

Table 1: *Outcrop samples collected for organic geochemical analyses*.

Sample no.	Sampling location	Sample type	Formation
CH-1	13°25′36″, 39°23′39″, 1912 m asl.	limestone	Agula Shale Antalo Limestone
CH-2		shale	
EY-1	13°29′26″, 39°29′07″, 2113 m asl.	shale	
EY-2		shale	
EY-3		shale	
EY-4		limestone	
EY-5		shale	
MS-1	13°33′23″, 39°30′36″, 2094 m asl.	limestone	
MS-2		shale	
MS-3		shale	
MS-4		limestone	
MS-5		limestone	
MS-6		shale	
MS-7		shale	
GV-1	13°37′55″, 39°24′51″, 1818 m asl.	shale	Adigrat Sandstone

amount of carbon in the samples was measured, as carbon dioxide, by an infrared (IR) detector. A *Leco SC-632* carbon analyzer was used to measure the TOC and the amount of carbon was obtained and expressed in weight percent (wt.%). Rock-Eval pyrolysis was carried out using the *Rock-Eval 6* instrument. Jet-Rock 1 was run and checked against the acceptable range given in [44]. Different hydrocarbon components (S_1, S_2 and S_3) were volatilized and determined, with the help of a Flame Ionization Detector (FID). The samples were placed in the oven and heated to a temperature of 300 °C for 3 minutes, and S_1 values were detected. The oven temperature was again increased to 650 °C, at a programmed rate of 25°C/minute to detect S_2 and S_3values. Then, the pyrolysis products; S_1, S_2 and S_3 peaks were normalized to the weight of the sample (mg HC/g sample). T_{max} values were also determined with the S_2 peaks.

Results and discussion

Field data

The investigated outcrop locations are Giba River, Mesobo, Enadayesus and Chelekot sections (Figure 3) where the studied layers from the Adigrat Sandstone, Antalo Limestone and Agula Shale represent black limestone and shale (Table 1). About 70 meters thick black limestone with the associated shale layer was logged from the Mesobo section which is found approximately 5 km north of the Mekelle town (Figure 4a). The shale layers are gray to black, with variable thicknesses ranging from 10 cm to 3 m (Figure 4b). At the vicinity of Mekelle town, thickly bedded black fine-grained limestone (30 cm to 1.3 m in thickness) associated with cyclic layers of black to gray shale, was identified along a stream-cut which represents about 16 meters thick part of the Antalo Limestone (Figure 4c). The shale beds are relatively consolidated, slightly greenish to gray, with well-developed, very thin laminations. Fissility is observed within the loose to semiconsolidated layers, whereas the consolidated layers are characterized by conchoidal fractures. At the bottom of this outcrop, there is a very thick loose to highly consolidated black shale, with thickness ranging from 40 cm to 4 m (Figure 4d). Around Giba River which is located about 25 km northwest of Mekelle town, gray-black shale layers with thickness ranging from 5 cm to 10 cm were also identified from the upper part of Adigrat Sandstone

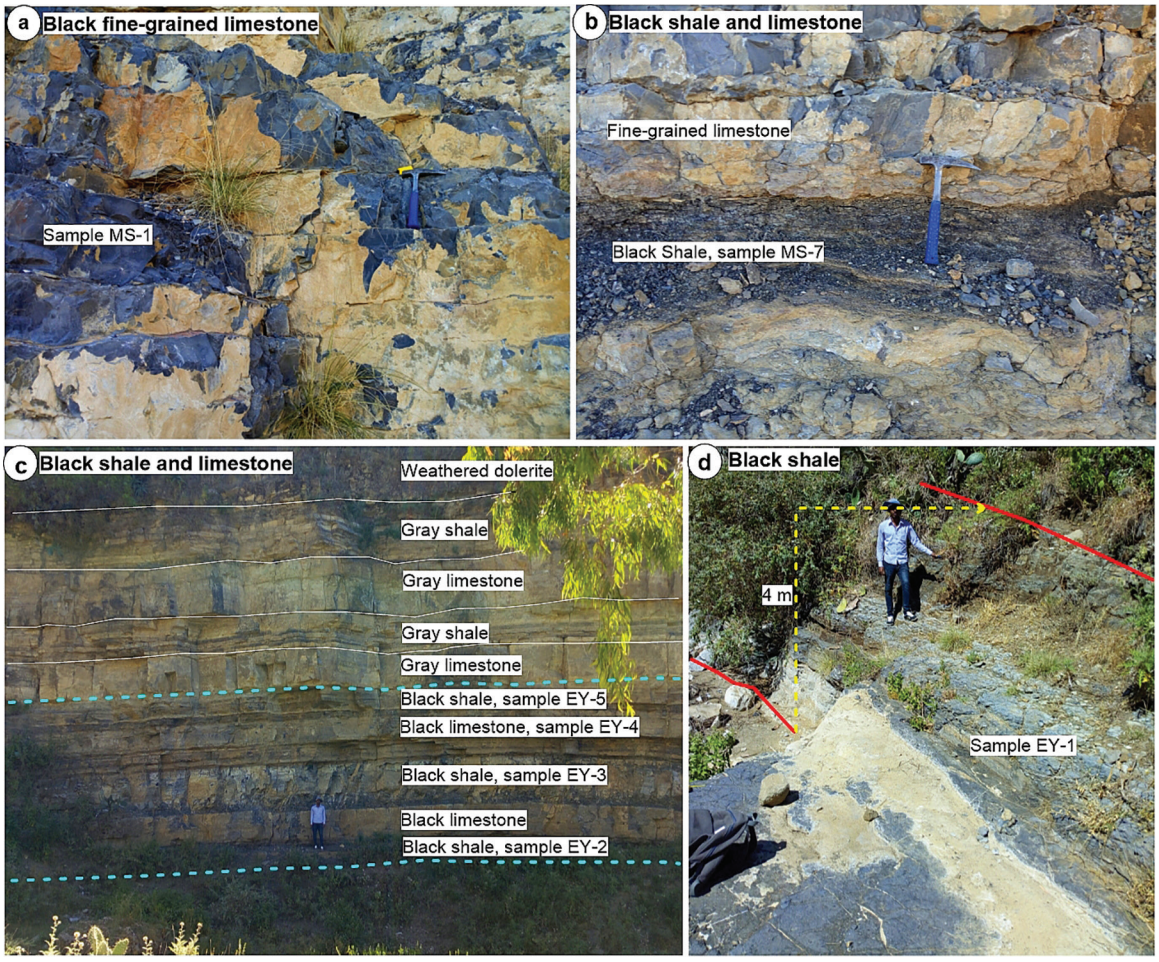

Figure 4: *Outcrop photographs showing black shale layers and limestone beds within the Antalo Limestone at the central part of the Mekelle Basin. (a) thickly bedded black fine-grained limestone (Mesobo section, sample MS-1); (b) black shale within black micritic limestone beds (sample MS-7); (c) 16 m thick stream-side cliff exposure comprising limestone and shale beds (samples EY-2 to EY-5) around Mekelle town (Endayesus section); (d) Black shale along stream at the bottom of Endayesus section (sample EY-1).*

(Figures 5a, b). Gray-black shale layers also represent a significant part of the Agula Shale (Figure 5c).

Organic geochemistry

The results of measured and calculated source rock parameters for fifteen (15) limestone and shale samples are shown in Table 2. Two shale samples of the Mesobo section (MS-2 and MS-7), have 0.50 wt.% and 0.92 wt.% TOC values respectively, whereas the remaining five samples (MS-1, MS-3, MS-4, MS-5, MS-6), have TOC between 0.10–0.41 wt.%. From the Endayesus section, only one shale sample (EY-2), has 0.77 wt.% TOC while the remaining four samples have TOC values ranging from 0.2 to 0.25 wt.%. A shale sample from the underlying Adigrat Sandstone, in the Giba River section, recorded 0.42 wt.% TOC. In the Chelekot section, two samples from the overlying Agula Shale have 0.18 wt. % and 0.40 wt. % of TOC respectively. Only three samples (EY-2, MS-2 and MS-7) have TOC values above the 0.5% threshold [45]. The S_3 values which represent CO_2 content within the kerogen are relatively high compared to the S_1 and S_2 values (Table 2).

Organic matter richness

The most critical parameters such as; TOC and Rock-Eval S_1 and S_2 values for most of the studied samples are below the standard for any form of hydrocarbon generation, which are unlikely to be considered as petroleum

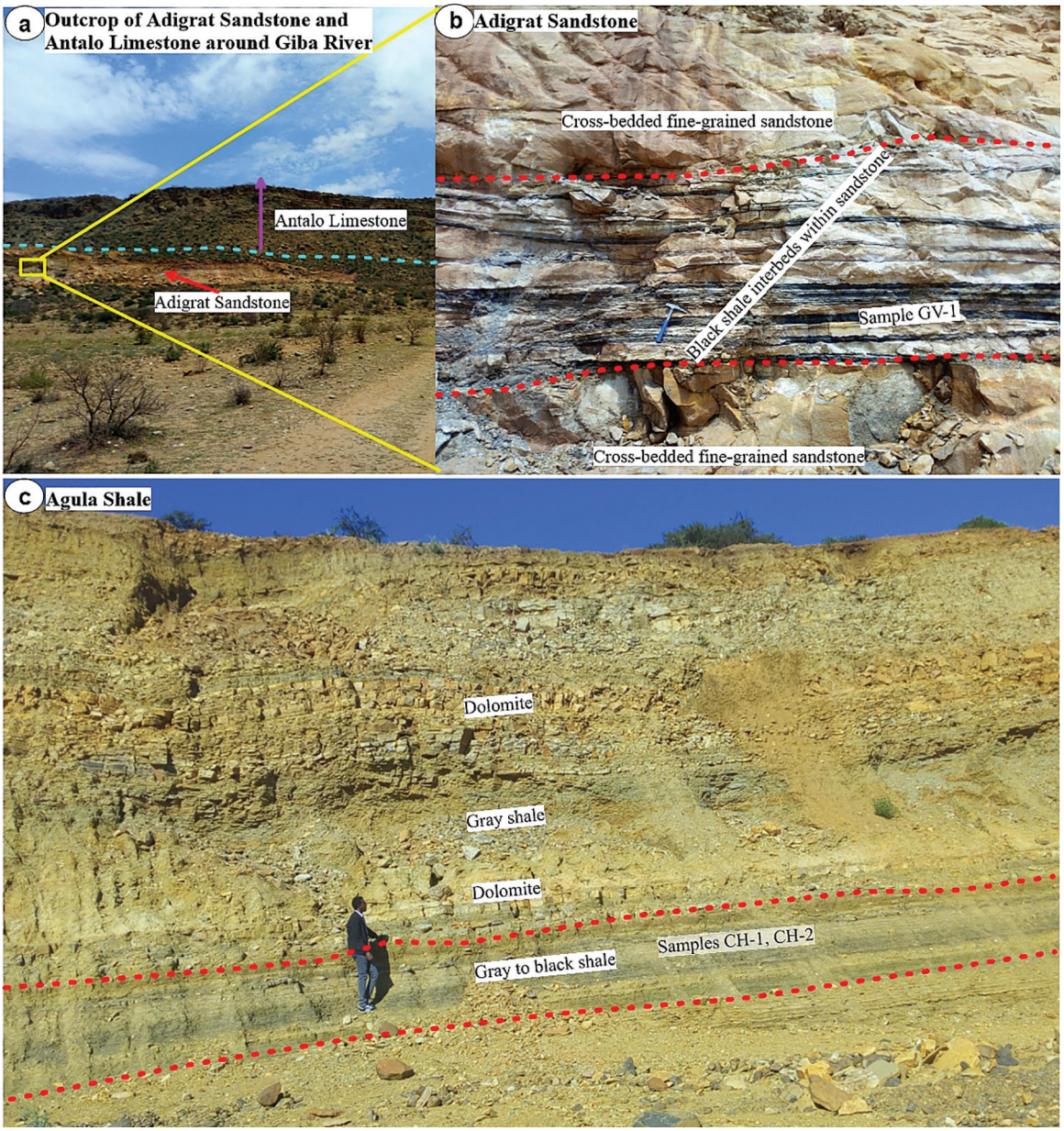

Figure 5: *Outcrop photographs showing black shale layers within the Adigrat Sandstone and Agula Shale, at the central part of the Mekelle Basin. (a) lower part of Antalo Limestone conformably overlies the upper part of Adigrat Sandstone at Giba River section; (b) about 5–10 cm thick oil shale beds (sample GV-1) from the upper part of Adigrat Sandstone; (c) Some part of the Agula Shale at Chelekot section (samples; CH-1, CH-2).*

source rocks. The total organic content (TOC) below 0.5 wt. % and S_2 values below 2.5 mg HC/g are generally considered as poor source rocks [46–49]. Twelve of the studied samples have TOC between 0.11–0.42 wt.% which is in the range of poor quality whereas three of the shale samples with 0.5–0.92 wt.% indicate fair organic matter richness. However, S_2 values are too low with very high pyrolysis T_{max}. The type of kerogen and its source organic matter has been determined from a cross plot of hydrogen index (HI) and oxygen index (OI) (Figure 6a) by which Type IV kerogen with a high amount of organic carbon dioxide was identified for all of the analyzed limestone and shale samples. Type IV kerogen is derived from highly oxidized or reworked material of any origin [48, 50, 51]. The TOC and pyrolysis yield (S_2) cross-plot also show very poor quality organic matter [47, 50] (Figure 6b).

Table 2: *Rock-Eval pyrolysis data of the analyzed samples.*

Sample no.	Sample type	TOC (wt.%)	S_1	S_2	S_3	T_{max}	HI	OI	PI	PP
CH-1	limestone	0.18	0.00	0.00	0.17	327	0	94	--	0.00
CH-2	shale	0.40	0.01	0.00	0.25	524	0	62	1.00	0.01
EY-1	shale	0.25	0.00	0.00	0.26	498	0	106	--	0.00
EY-2	shale	0.77	0.01	0.01	0.20	485	1.3	26	0.50	0.02
EY-3	shale	0.20	0.00	0.01	0.98	495	5	488	0.00	0.01
EY-4	limestone	0.21	0.02	0.07	0.64	475	34	309	0.22	0.09
EY-5	shale	0.23	0.00	0.00	0.26	496	0	111	--	0.00
MS-1	limestone	0.11	0.00	0.00	0.30	--	0	275	--	0.00
MS-2	shale	0.50	0.00	0.02	0.39	493	4	78	0.00	0.02
MS-3	shale	0.41	0.00	0.01	0.51	505	2.44	125	0.00	0.01
MS-4	limestone	0.10	0.00	0.00	0.28	484	0	294	--	0.00
MS-5	limestone	0.22	0.00	0.00	0.26	484	0	119	--	0.00
MS-6	shale	0.20	0.00	0.00	0.39	491	0	194	--	0.00
MS-7	shale	0.92	0.02	0.02	1.10	519	2	119	0.50	0.04
GV-1	shale	0.42	0.00	0.00	0.35	527	0	83	--	0.00

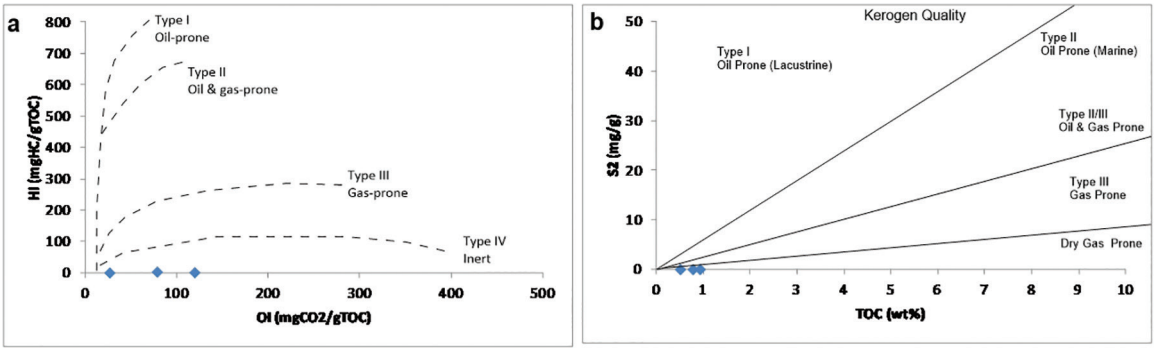

Figure 6: *(a) Oxygen index (OI) and hydrogen index (HI) cross plot for the recognition of kerogen types (after [57]); (b) Kerogen type based on TOC versus pyrolysis yield (S_2) cross-plot, showing very poor quality organic matter for hydrocarbon generation (after [47]).*

Organic matter maturity

The thermal maturity of the analyzed shale and limestone samples was determined from the Rock-Eval T_{max} which is the temperature at which the S_2 peak occurs during pyrolysis and can be correlated with the type of organic matter (kerogen) [46, 52–55]. The different levels of thermal maturity of the organic matters which are determined from T_{max} could qualitatively and quantitatively be expressed as immature (<435 ^{0}C), early mature (435–445 ^{0}C), peak mature (445–450 ^{0}C), late mature (450–470 ^{0}C) and post-mature (>470 ^{0}C) [48]. Therefore, thermal maturity together with the other source rock parameters such as the total organic carbon (TOC) is significant to determine the quality of a given source rock [56]. The measured T_{max} value for one sample is 327 ^{0}C which shows an immature stage and nine samples have T_{max} that ranges 475–498 ^{0}C and four samples are in between 505–527 ^{0}C indicating post mature stage. The level of thermal maturity could also graphically be determined from T_{max} and hydrogen index cross plot (Figure 7a). Hence, the maturity level of the organic matter in all of the analyzed samples indicates a post-mature stage.

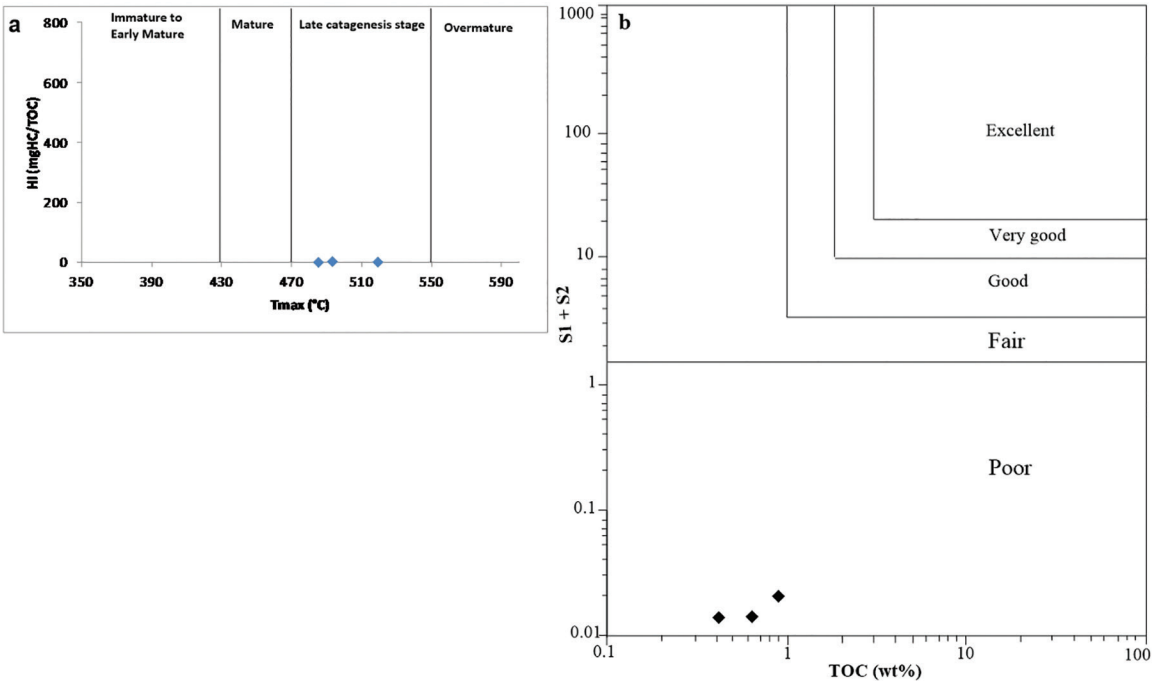

Figure 7: *(a) Rock-Eval T_{max} versus hydrogen index (HI) plot showing the thermal maturity level of the organic matter (after [57]); (b) TOC versus ($S_1 + S_2$) cross-plot, indicating poor hydrocarbon generating potential (after [47]).*

Hydrocarbon generating potential

The hydrocarbon generating potential of source rocks is indicated with the sum of Rock-eval S_1 and S_2 values, which could be expressed qualitatively and quantitatively as; poor (0–3 mgHC/g), fair (3–6 mgHC/g), good (6–12 mgHC/g), very good (12–24 mgHC/g) and excellent (>24 mgHC/g) [46–48]. The S_1 values for most of the samples are 0.00 mgHC/g, with some samples having 0.01–0.02 mgHC/g values. S_2 values for nine (9) of the studied samples are 0.00 mgHC/g, whereas the remaining six (6) samples range from 0.01 to 0.07 mgHC/g. Therefore, both the S_1 and S_2 values indicate that the studied samples have a very low potential for any form of hydrocarbon generation. Cross plot of $S_1 + S_2$ vs TOC shows that the samples have poor oil generating potential (Figure 7b).

Conclusions

Field evidence showed that the studied units comprised black shale and black limestone beds which seem having adequate organic matter. However, the organic geochemical analyses revealed low organic content of the analyzed samples, indicating that the black color of the samples is not a diagnostic feature of organic richness which could most probably be due to iron oxide impurities. The TOC values of a few samples indicate fair organic matter richness whereas about 80% of the samples have poor organic matter quality. The cross-plots of oxygen and hydrogen indices as well as S_2 versus TOC indicate Type IV and dray gas-prone kerogen. The T_{max} versus hydrogen index cross-plot shows that the organic matter is in a late catagenesis stage and thermally over-mature. Therefore, the source rock parameters indicate poor petroleum generating potential. However, since some outcrop samples of the Antalo Limestone have shown fair organic richness, further study is required, especially from core samples, to assure the source rock potential of this unit.

Acknowledgments

This research was funded by the African Union (AU). The authors would like to thank AU for the grant.

References

[1] World Bank (2016): Ethiopia Oil and Gas Sector Development: Support for Review and Update of Policy and Regulatory Framework. *Final Report*. The World Bank, 72 p.

[2] Ehrenberg, S.N., Nadeau, P.H. (2005): Sandstone vs. Carbonate petroleum reservoirs: A global perspective on porosity-depth and porosity-permeability relationships. *American Association of Petroleum Geologists Bulletin*, 89(4), pp. 435–445.

[3] Ahr, W.M. (2008): *Geology of Carbonate Reservoirs: The Identification, Description, and Characterization of Hydrocarbon Reservoirs in Carbonate Rocks*. John Wiley and Sons: New Jersey, 277 p.

[4] Edgell, H.S. (1977): The Permian system as an oil and gas reservoir in Iran, Iraq and Arabia. *Proc. Second Iranian Geological Symposium*, pp. 161–201.

[5] Hunegnaw, A. Sage, L., Gonnard, R. (1998): Hydrocarbon Potential of the Intracratonic Ogaden Basin, SE Ethiopia. *Journal of Petroleum Geology*, 21, pp. 401–425.

[6] Tsegaye, S.G. Nton, M.E. Boboye, O.A., Ahmed, W. (2018): Geochemical Characteristics and Hydrocarbon Generation Modelling of Early Triassic to Late Cretaceous Formations within Ogaden Basin, Ethiopia. *Journal of Petroleum Science and Technology*, 8(4), pp. 58–75.

[7] Carrigan, W.J. Cole, G.A. Colling, E.L., Jones, P.J. (1995): Geochemistry of the Upper Jurassic Tuwaiq Mountain and Hanifa Formation Petroleum Source Rocks of Eastern Saudi Arabia. In: *Petroleum Source Rocks*, Katz, B.J. (eds.). Springer-Verlag: Berlin, pp. 67–87.

[8] Csato, I., Habib, A., Kiss, K., Koncz, I. (2001): Play concepts of oil exploration in Yemen: MOL's experience in 1996-2000. *Oil and Gas Journal*, 99(23), pp. 68–74.

[9] Wolela, A. (2007): Source Rock Potential of the Blue Nile (Abay) Basin, Ethiopia. *Journal of Petroleum Geology*, 30(4), pp. 389–402.

[10] Hakimi, M.H. Abdullah, W.H., Shalaby, M.R. (2010): Organic geochemistry and thermal maturity of the Madbi Formation, East Shabowah Oil fields, Masila Basin, Yemen. *Bulletin of the Geological Society of Malaysia*, 56, pp. 41–48.

[11] Hakimi, M.H., Abdullah, W.H. (2014): Thermal maturity history and petroleum generation modeling for the Upper Jurassic Madbi source rocks in the Marib-Shabowah Basin, western Yemen. *Marine and Petroleum Geology*, 59, pp. 202–216.

[12] Hakimi, M.H., Abdullah, W.H., Shalaby, M.R. (2012): Madbi-Biyadh/Qishn (!) petroleum system in the onshore Masila Basin of the Eastern Yemen. *Marine and Petroleum Geology*, 35, pp. 116–127.

[13] Mammo, T. (2010): Delineation of sub-basalt sedimentary basins in hydrocarbon exploration in North Ethiopia. *Marine and Petroleum Geology*, 27, pp. 895–908.

[14] Yihdego, Y., Salem, H.S., Kafui, B.G., Veljkovic, Z. (2018): Economic geology value of oil shale deposits: Ethiopia (Tigray) and Jordan. *Energy Sources, Part A: Recovery, Utilization and Environmental Effects*, 40(17), pp. 2079–2096.

[15] Bosellini, A., Russo, A., Fantozzi, P.L., Assefa, G., Solomon, T. (1997): The Mesozoic Succession of the Mekele Outlier (Tigre Province, Ethiopia). *Memorie di Scienze Geologiche*, 49, pp. 95–116.

[16] EMoM. (2011): Petroleum Exploration in Ethiopia: Information and Opportunities. *Unpublished Report*, Ethiopian Ministry of Mines, Addis Ababa, pp. 1–20.

[17] Kazmin, V. (1975): *Explanation of the geological map of Ethiopia*. Geological Survey of Ethiopia. *Bulletin,* 1, pp. 1–14.

[18] Storey, B.C. (1993): Tectonic Controls on Gondwana break-up Models: Evidence from the Proto-Pacific Margin of Antarctica and the Southern Andes. *Second ISAG*, pp. 551–554.

[19] Worku, T., Astin, T.R. (1992): The Karoo to Recent Rifting in the Western Branch of the East-African Rift System: A Bibliographical Synthesis. *Musée Royal de l'Afrique Centrale*, 83, pp. 63–82.

[20] Binks, R.M., Fairhead, J.D. (1992): A plate tectonic setting for Mesozoic rifts of West and Central Africa. In: *Geodynamics of Rifting, Volume II. Case History Studies on Rifts: North and South America and Africa*, Ziegler, P.A. (eds.). *Tectonophysics*, 213, pp. 141–151.

[21] Gani, N.D.S., Abdelsalam, M.G., Gera, S., Gani, M.R. (2009): Stratigraphic and structural evolution of the Blue Nile Basin, Northwestern Ethiopian Plateau. *Geological Journal*, 44, pp. 30–56.

[22] Russo, A., Assefa, G., Atnafu, B. (1994): Sedimentary evolution of the Abay River (Blue Nile) Basin, Ethiopia. *Neues Jahrbuch Für Geologie und Paläontologie*, 5, pp. 291–308.

[23] Bosellini, A. (1988): The continental margins of Somalia. *Geology and Geophysics of continental margins*. *American Association of Petroleum Geologists Memoir,* 53, pp. 185–205.

[24] Coffin, M.F., Rabinowitz, P.D. (1988): Evolution of the Conjugate East African-Madagascan margins and the

Western Somali Basin. *Geological Society of America, Special Paper,* 226, pp. 1–78.

[25] Bosworth, W. (1992): Mesozoic and early Tertiary rift tectonics in East Africa. In: *Seismology and Related Sciences in Africa*, Ebinger, C.J., Gupta, H.K., Nyambok, I.O. (eds.). *Tectonophysics*, 209, pp. 115–137.

[26] Worku, T., Astin, T.R. (1992): The Karoo sediments (Late Palaeozoic to Early Jurassic) of the Ogaden Basin, Ethiopia. *Sedimentary Geology*, 76, pp. 7–21.

[27] Bosworth, W., Morley, C.K. (1994): Structural and stratigraphic evolution of the Anza rift, Kenya. *Tectonophysics*, 236, pp. 93–115.

[28] Hankel, O. (1994): Early Permian to Middle Jurassic rifting and sedimentation in East Africa and Madagascar. *Geologische Rundschau*, 83, pp. 703–710.

[29] Alemu, T., Abdelsalam, M.G., Dawit, E.L., Atnafu, B., Mickus, K.L. (2018): The Paleozoic-Mesozoic Mekele Sedimentary Basin in Ethiopia: An example of an exhumed IntraCONtinental Sag (ICONS) basin. *Journal of African Earth Sciences*, 143, pp. 40–58.

[30] Assefa, G. (1988): Potential hydrocarbon-generating rock units within the Phanerozoic sequence of the Ogaden Basin, Ethiopia: A preliminary assessment using the Lopatin model. *Journal of Petroleum Geology*, 11(4), pp. 461–472.

[31] Worku, T. (1988): *Sedimentology, diagenesis and hydrocarbon potential of the Karoo sediments (Late Paleozoic to early Jurassic) Ogaden Basin, Ethiopia*. M. Phil. Thesis. University of Readnig: UK, 222 p.

[32] Geleta, S. (1998): *Biostratigraphy, depositional environment, basin evolution and hydrocarbon potential of the late Triassic to late Jurassic succession, Ogaden Basin, Ethiopia*. PhD Thesis. Institute und Museum fur Geologie und palontologie: Tubingen, 78 p.

[33] Oljira, T., Nton, M.E., Sonibare, O.O. (2020): Organic Geochemical Evaluation of Shale Units of Bokh Formation, Ogaden Basin, Ethiopia. *Open Journal of Geology,*10, pp. 565–578.

[34] Mammo, T. (2012): Analysis of gravity field to reconstruct the structure of Omo basin in SW Ethiopia and implications for hydrocarbon potential. *Marine and Petroleum Geology*, 29, pp. 104–114.

[35] Beyth, M. (1972): Paleozoic-Mesozoic Sedimentary Basin of Mekele Outlier, Northern Ethiopia. *American Association of Petroleum Geologists Bulletin*, 56(12), pp. 2426–2439.

[36] Bussert, R., Dawit, E.L. (2009): Unexpected diversity: New results on the stratigraphy and sedimentology of Palaeozoic and Mesozoic siliciclastic sediments in Northern Ethiopia. *Zentralblatt Für Geologie und Paläontologie,* Teil I, pp. 181–198.

[37] Dow, D., Beyth, M., Hailu, T. (1971): Palaeozoic glacial rocks recently discovered in northern Ethiopia. *Geological Magazine*, 108, pp. 53–60.

[38] Bussert, R., Schrank, E. (2007): Palynological evidence for a latest Carboniferous-Early Permian glaciation in Northern Ethiopia. *Journal of African Earth Sciences*, 49, pp. 201–210.

[39] Bussert, R. (2014): Depositional environments during the Late Palaeozoic ice age (LPIA) in northern Ethiopia, NE Africa. *Journal of African Earth Sciences*, 99, pp. 386–407.

[40] Adefris, D., Nton, M.E., Boboye, O.A., Atnafu, B. (2021): Aspects of Diagenetic and Sequence Stratigraphic Framework on Reservoir Potential of Antalo Limestone, Mekelle Basin, northern Ethiopia. *Nigerian Association of Petroleum Explorationists Bulletin,* 30, pp. 26–37.

[41] Peterson, J.A. (1985): Geology and petroleum resources of central and east-central Africa. *Open-File Report 85-589. United States Geological Survey*, 48 p.

[42] Arkin, Y., Beyth, M., Dow, D.B., Levitte, D., Haile, T., Hailu, T. (1971): *Geological Map of Mekele Sheet Area ND 37-11, Tigre Province*. Geological Survey of Ethiopia, Addis Ababa, 1p.

[43] MoWR (2009): Water information and knowledge management project: strengthening water quality data generation and management. Draft Final Report, August 2009; 240 p.

[44] Weiss, H.M., Wilhelms, A., Mills, N., Scotchmer, J., Hall, P.B., Lind, K., Brekke, T. (2000): NIGOGA–The Norwegian Industry Guide to Organic Geochemical Analyses [online]. Edition 4.0, Norsk Hydro, Statoil, Geolab Nor, SINTEF Petroleum Research and the Norwegian Petroleum Directorate, 102 p.

[45] Tissot, B.P., Welte, D.H. (1984): *Petroleum Formation and Occurrence*. Springer-Verlag: Berlin, 699 p.

[46] Krokstad, W., Schou, L., Leith, L.T., Vigran, J.O., Due, A., Andersen, W., Berg, T., Haugen, G., Vinge, T. (1986): *Source Rock Evaluation of Well 15/12-4. Hydrocarbon Characterisation of Oil, Cuttings and Cores*. Issue 16, 300 p.

[47] Peters, K.E. (1986): Guidelines for evaluating petroleum source rock using programmed pyrolysis. *American Association of Petroleum Geologists Bulletin*, 70(3), pp. 318–329.

[48] Peters, K.E., Cassa, M.R. (1994): Applied Source Rock Geochemistry. In: *The petroleum system-from source to trap*, Magoon, L.B., Dow, W.G. (eds.). *American*

Association of Petroleum Geologists Memoir, 60, pp. 93–120.

[49] Al-Selwi, A., Joshi, M. (2015): Oil and Gas Research Source Rock Evaluation using Total Organic Carbon (TOC) and the Loss-On-Ignition (LOI) Techniques. *Oil and Gas Research*, 1(1), pp. 1–5.

[50] Waples, D.W. (1985): *Geochemistry in Petroleum Exploration*. D. Reidel Publishing Company: Boston, 232 p.

[51] McCarthy, K., Niemann, M., Palmowski, D., Peters, K. (2011): Basic Petroleum Geochemistry for Source Rock Evaluation. *Oilfield Review*, 23, pp. 32–43.

[52] Espitalie, J., Laporte, J.L., Madec, M., Marquis, F., Leplat, P., Paulet, J., Boutefeu, A. (1977): Rapid method of characterizing source rocks and their petroleum potential and degree of maturity. *Revue de 1'Institut Francais du Petrole*, 32, pp. 23–42.

[53] Barker, C.E., Johnson, R.C., Poole, F. (1990): Rock-Eval pyrolysis data for petroleum-potential evaluation based on veil cuttings and core samples from Eastern Nevada collected during 1990. *Open-File Report 90-698*, pp. 1–15.

[54] Stanley, R.G., Valin, Z.C., Pawlewicz, M.J. (1992): Rock-Eval pyrolysis and vitrinite reflectance results from outcrop samples of the Rincon Shale (lower Miocene) collected at the Tajiguas Landfill, Santa Barbara County, California. *Open-File Report 92-571*. *United States Geological Survey*, 27 p.

[55] Lafargue, E., Espitalié, J., Marquis, F., Pillot, D., Français, I., Préau, A.D.B. (1998): Rock-Eval 6 Applications in Hydrocarbon Exploration, Production and in Soil Contamination Studies. *Revue de l'Institut Français Du Pétrole*, 53(4), pp. 421–437.

[56] Cooke, I.L. (2014): User Guide Total Organic Carbon (TOC) data. *Open Report*, OR/14/056. *British Geological Survey,* Natural Environment Research Council (NERC). 14 p.

[57] Van Krevelen, D.W. (1984): Organic geochemistry-old and new. *Organic Geochemistry*, 6, pp. 1–10.

Original Scientific Article • DOI: 10.2478/rmzmag-2021-0015

Received: March 05, 2022
Accepted: March 24, 2022

Identification of favourable geological formations for the determination of groundwater

Prepoznavanje geoloških formacij, ugodnih za akumulacijo podzemne vode

Moussa Diallo[1,2], Ahmed Amara Konaté[1,2,*], Mory Kourouma[1,2], Fassidy Oularé[1,2], Muhammad Zaheer[3]

[1]Laboratoire de Recherche Appliquée en Géoscience et Environnement, Institut Supérieur des Mines et Géologie de Boké, BP 84, Boké, Baralandé, Republic of Guinea

[2]Centre Emergent Africain Mines et Société, Institut Supérieur des Mines et Géologie de Boké, BP 84, Baralandé, Republic of Guinea

[3]Department of Earth & Environmental Sciences, Hazara University Mansehra 21300, Khyber Pakhtunkhwa, Republic of Pakistan

*Corresponding author: E-mail: konate77@yahoo.fr

Abstract in English

Clean drinking water supply is a major concern to the population of the urban municipality of Boké, Republic of Guinea. This study is aimed to investigate the favourable geological structure for the accumulation of groundwater in Boké. Apparent resistivity data was collected by using the Schlumberger-type vertical electrical sounding technique. The apparent resistivity values were obtained on a bi-logarithmic scale in which the distances AB/2 were plotted on the abscissa and the resistivities are on the ordinate. It found the number of terrains and their characteristics (resistivity and thickness) in the area and the behaviour of the current in the soil through a curve. The results show that the structures favourable to the accumulation of groundwater were fractured dolerites, cracked shales and cracked or crushed sandstones. The sandstones were the most important in terms of the amount of water. They are located at a depth of more than 100 metres. It was also found that dolerites and shales are located at shallower depths (less than 100 m).

Keywords: Groundwater, geo-electric method, lithological section, fracture zones, Prefecture of Boké

Abstract in Povzetek

Zagotavljanje zalog čiste pitne vode je eden ključnih izzivov za prebivalce mestne občine Boké v Republiki Gvineji. Namen članka je raziskava geoloških struktur, ki so primerne za akumulacijo podzemne vode v mestni občini Boké. S Schlumbergerjevo metodo navpičnega električnega sondiranja je bila določena navidezna upornost. Vrednosti navidezne upornosti so bile prikazane na logaritemskem diagramu z razdaljami AB/2 na abscisi in upornostjo na ordinati. Opredeljenih je bilo več območij in njihove značilnosti (upornost in debelina). Določena je bila krivulja obnašanja toka v tleh. Rezultati kažejo, da so strukture, ki so ugodne za akumulacijo podzemne vode, pretrti doleriti, pretrti skrilavi glinavci in pretrti ali zdrobljeni peščenjaki. S stališča količine podzemne vode so slednji najbolj pomembni. Ležijo na globini preko 100 m. Doleriti in skrilavi glinavci ležijo na plitvejših globinah (manj kot 100 m).

Ključne besede: podzemna **voda, geoelektrična metoda, litološki profil, razpoklinska območja, Prefektura Boké**

Introduction

The urban municipality of Boké which is the subject of this study, like the rural municipalities of Boké, benefits from significant mining investments due to the presence of several bauxite deposits in its surroundings. In recent years, a dozen mining companies have settled there. This also justified its designation as a special economic zone of Guinea through the decree of April 25, 2017. The presence of companies has led to a population growth in recent years. The population of the prefecture increased from 760,119 inhabitants in 1996 to 1,092,291 inhabitants in 2014 before reaching 1,157,540 inhabitants in 2016 [1]. This exponential population growth has had consequences on the socio-economic activities of local populations. Access to basic social services (electricity, water and health) is a real problem these days. Referring to [1], compared to previous years and to other regions of the country, the population of Boké has experienced a decline in its accessibility to drinking water. Its water accessibility rate fell from 71.3% in 2007 to 48.3% in 2012. However, the country average was 67.8% in 2012. Regarding domestic consumption in the Boké region, the rate is 8.3% against 10.6% in the country. The rate of village hydraulic boreholes in the region is 25.5% against 35.3% for the country [1].

Groundwater is found below the surface of the earth within the saturated layers of sand, gravel and pore spaces in sedimentary as well as crystalline rocks. Surface water (rivers, lakes) and superficial aquifers (perched aquifers), which constitute the current main sources of supply, are rapidly drying up due to climate change (drought), human activities (deforestation, salt extraction, charcoal production, aggregate extraction, etc.), and mining. In addition to rapidly drying up, these waters are affected by pollution in the vicinity of large cities and mining facilities [2]. Hence the need to seek out and exploit new sources of drinking water for the population, such as water from deep fractures. Being deep, sufficient in quantity, and less polluted, these waters are suitable for supplying agglomerations and industrial installations.

Several studies of different methods have been carried out in the area for the research of groundwater in order to ensure the supply of drinking water to the population. [3] conducted a study of the groundwater research project on the Boffa geological sheet and examined the characteristics of the different aquifers by using geophysical methods composed of seismic refraction, electrical sounding, profiling by the two-spaced device and resistivity logging. In the same vein, [2] carried out studies to determine the best geophysical method and stated that the most suitable were electrical methods (electrical drag and sounding), the seismic method (seismic refraction), and the magnetic method (magnetic profile). In addition, the National Water Point Development Service (SNAPE) carries out village hydraulic boreholes each year in the Boké region to fill the void of drinking water. These boreholes are carried out based on classical methods supported by the interpretation of aerial photos and geomorphological observations (talweg line, valley, slopes, etc.). As a result, it records a rate of failure or low flow boreholes of around 25% [4].

The electrical resistivity survey such as the Schlumberger configuration enables the changes of apparent resistivity with depth to identify the water-saturated bodies, which are characterized by lower resistivity zones [5]. The resistivity value is changed corresponding to water content in the geological materials. The fracture's features are usually filled with groundwater and have a lower resistivity value of the rock layer than water-bearing strata [6]. According to [7], the four-electrode quadrupole (AMNB) of Schlumberger is considered satisfactory by technicians in previous studies and remains the most widely used.

From the analysis of the aforementioned studies, it appears that they rarely use methods to decrease the failure rate and obtain high-throughput boreholes; others propose very complex and expensive methods that do not take into account certain important parameters (depth of aquifers, types of aquifers with high flow rates, the forms of the anomalies sought, lead time, etc.).

When proposing a method or a complex of methods for investigating groundwater, several factors must be taken into account, including

ease of use, reliability, speed and cost. With this logic, [8] used the geophysical method to determine the productivity of boreholes in the Toumodi region (Côte d'Ivoire). At the end of this study, it was found that the coupling of geomorphological and geophysical methods reduces the negative drilling rate and optimizes the exploitation of positive drilling. A study carried out by [9] in Burkina Faso on the optimization of the geophysical implantation of boreholes in the base area and focused on the drilling and electrical drag improved the overall success rate by more than 10%. According to [8] the geophysical investigation through the survey and electric train carried out in Côte d'Ivoire (Center-North) made it possible to identify the structures and characterize the aquifers (thicknesses of the alteration and the depth of the cracked horizon) of this region. In another study by [10] carried out in Tanda (eastern part of the Ivory Coast), the use of geophysical prospecting by electrical resistivity for the search for groundwater made it possible to determine with good precision the exact position of conductive anomalies and several fractures of a different direction.

[11] found that the geoelectric survey of Schlumberger types gives good results in the characterization of subsurface structures. Similarly, [12–15] have each in the context of their studies demonstrated the reliability of geoelectric soundings in determining the nature of geological layers and aquifers. Geophysical methods were proved to be the most active technique in the exploration of groundwater resources. With a support borehole parameter and their interpretation from the resistivity imaging method, consistent information regarding the groundwater can be produced. From the above development, it appears that geophysical methods are appropriate for the siting of boreholes to decrease the failure rate and achieve high throughput boreholes. This work, therefore, aims to precisely locate areas or structures favourable to the accumulation of groundwater in the urban municipality of Boké.

The first part of this work will focus on the overall presentation of the study area; the materials and methodology used will be described in the second part; the results obtained will be presented and interpreted in the third part, and a conclusion accompanied by perspectives will bring this work to a close.

Materials and methods

Study area

Our study area is located between 14°00' and 15°00' West longitude; 10°00' and 11°00' North latitude. Figure 1 shows the location map of the study area.

In terms of relief, soil, vegetation, climate and economy, the study area is characterized by plains, plateaus, hills and lowlands with an elevation ranging from -5 m to 217 m. The relief map is shown in Figure 2.

The soil is lateritic skeletal, hydromorphic and alluvial; the soil texture is: clay 0–45%, sand 20% approximately, silt 30% approximately; the soil is permeable and porous in places [16].

Most of the area is covered with wooded savannah. Trees characteristic of the tropical forest are located in a narrow band along the river valleys, both on the slopes and on the tops of the hills. The plateaus are characterized by herbaceous and tree vegetation [17].

The Boké area has a tropical climate with two seasons, each of which lasts six months (the dry season from May to October, and the rainy season from November to April). With 0 millimeters of precipitation, December is the driest month. With an average of 613 mm, the month of August records the heaviest rainfall. The inter-annual average of precipitation is 2,227 mm [17].

March is the hottest month of the year with an annual temperature of 33.5 ° C in 2019 and the coldest month is January with an average temperature of 22.2 ° C in 2019 [16].

The main economic activities in the study area are mining, agriculture, fishing, livestock, transport and trade.

From the hydrographic point of view, the urban municipality of Boké is watered by two main rivers. They are the Cogon River, terminated by the Rio Compony with a length of 390 km, and the Tinguilinta River, which forms from the city of Boké the Rio Nuñez. In addition to these two main rivers, many rivers water our study region such as the Kassongony, Sangui,

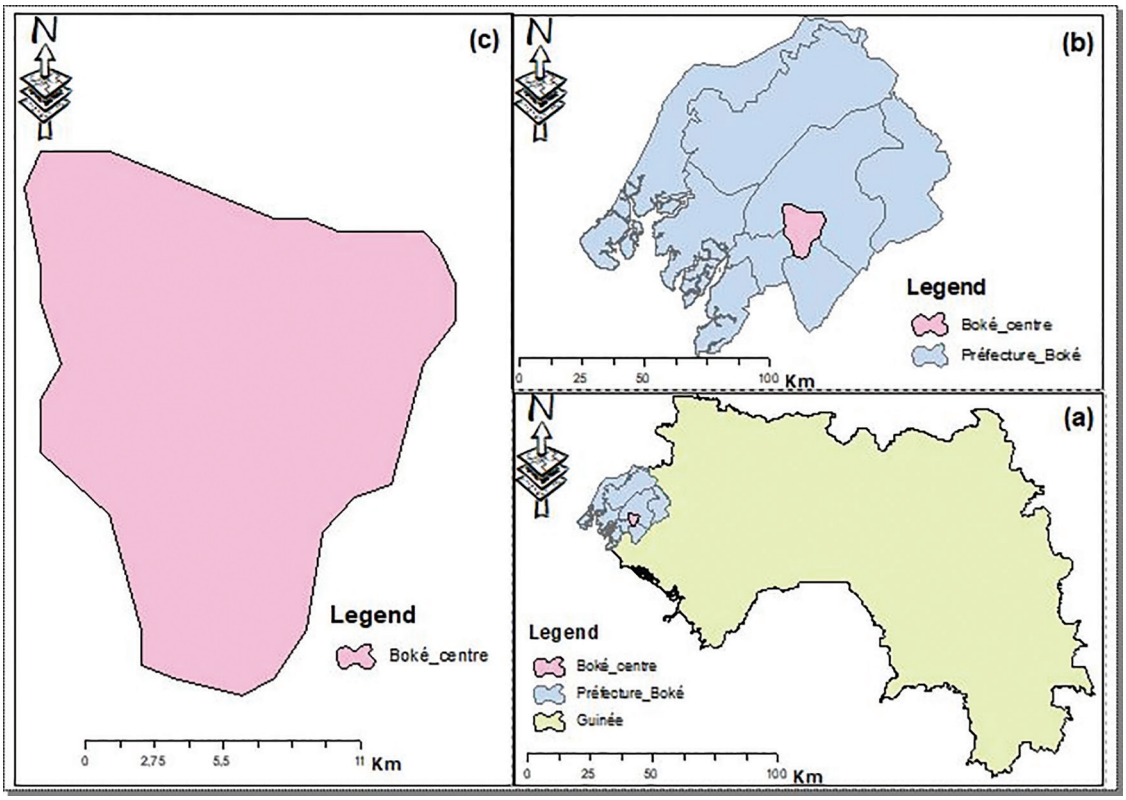

Figure 1: *Location map of urban municipality of Boké (Boké centre).*

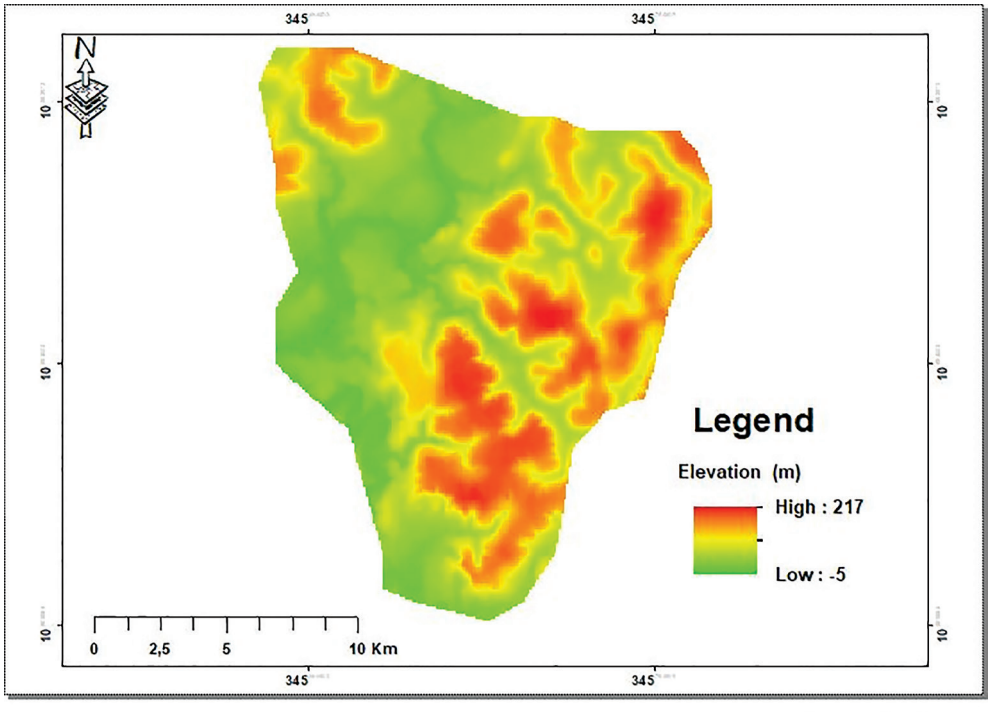

Figure 2: *Elevation map of urban municipality of Boké (Boké centre).*

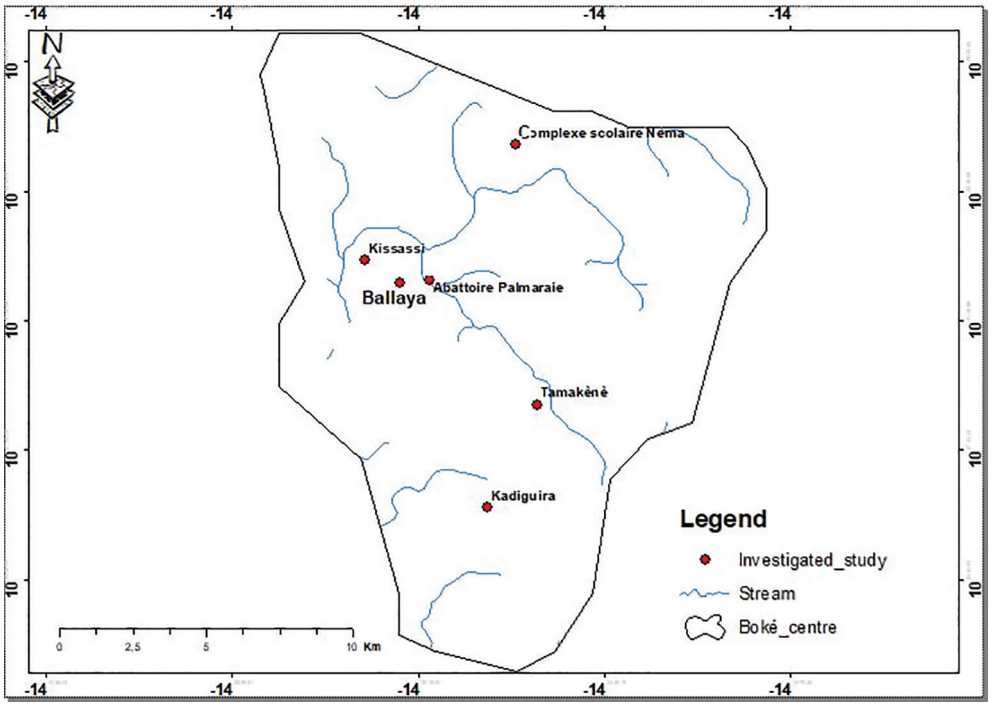

Figure 3: *Hydrographic map of urban municipality of Boké (Boké centre).*

Dolonkhi, etc. The hydrographic map is shown in Figure 3.

Several major basins are shared in the study area. In particular, the Batafon basin (7,478 hectares), the Tinguilinta basin (4,812 ha) and the Nunez basin (2,761 ha) [17]. Based on the nature of the slopes, the altitude of the sources, the nature of the terrain and the seasons, the regime of the waterways is irregular.

Geologically, our study area belongs to the sedimentary cover. It was relatively calm with great magmatic activity in the Mesozoic [18].

The terrigenous terrains of the Ordovician (argillites, aleurolites and sandstones), Silurian (quartz sandstones, schists, argillites, etc.), and Devonian (sandstones, coarse-grained aleurolites, etc.) are developed in the urban municipality of Boké. These terrains are all covered by unconsolidated deposits of marine or lacustro-fluvial origin from the Paleogene (represented in our region by clays, argillites and quartz sands) and from the Quaternary (the Quaternary formations are represented by different facies: Marine, continental, lacustro-fluvial) [3].

An intense eruptive activity dating from the Mesozoic and due to the tectonic movements of the North African platform occurred in our study area. These Mesozoic intrusions are represented by dolerites, gabbro-dolerites, Congo-diabases and gabbro-quartzes [18].

The Boké zone belongs to the West African craton and its lands occupy part of the Bowé syneclise. In Boké, the base does not outcrop [18]. The Boké area is affected by two tectonic faultts. Namely: the deep faults which served for the rise of the basic magma, and the secondary faults developed on the cover. These two faults constitute the current hydrographic network.

According to [19], the study region is located within the limits of three major morphological zones: Fouta-Djalon plateau, coastal plain and shelves.

From the hydrogeological point of view, our study area belongs to the northwestern part of Guinea which abounds in significant water reserves fed by atmospheric precipitation and by rivers [3]. The geological conditions of the region make it possible to distinguish two groundwater sampling environments: bedrock and the superficial formations that cover them. Mesozoic doleritic rocks and healthy shales constitute the bedrock. In

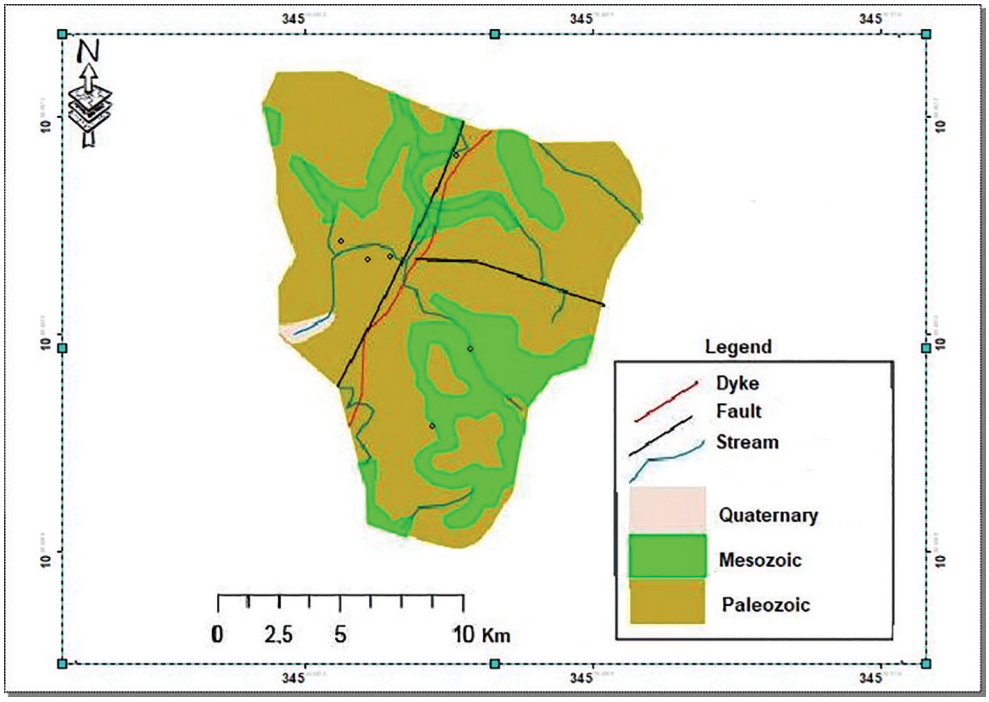

Figure 4: *Geological map of urban municipality of Boké (Boké centre).*

these formations, water is linked to cracking or crushing zones [2].

In the study area, the waters of tectonic fractures are generally attached to doleritic magmatic rocks and argillites which are fractured and crushed by tectonic movements. These areas are not well known, but they can be one of the main sources of good quality water supply. The study area contains several nappes in the weathering crust. This is evidenced by the high number of artisanal wells in all settlements and the presence of groundwater sources in the area [2]. The geological map of the urban commune of Boké is shown in Figure 4.

Materials

For the collection of geophysical data, a compact RSP6 resistivity meter of the SCINTREX Canada type and its accessories were used to determine the resistivity of the sites; a Garmin-type GPS was used as a tool for the geo-referencing of the measurement points; and WINSEV software (version 6.4) was used for data processing.

Methods

To achieve our objective, a geophysical survey was conducted on six sites (see Figure 5) which were: Kissassi; Abattoire Palmeraie; Tamakènè; Nema school complex; Kadiguira; and Ballaya.

According to [20], in practice, the choice of geophysical methods depends on:

- The nature of the sought target which must cause an anomaly sufficient to be measured;
- The quality of precision sought which must correspond to the resolving power of the method and the device used;
- The objective of prospecting work and in particular the scale at which it is undertaken, which determines the framework for implementing field measurements.

In the context of groundwater research, the parameters sought concern the reservoir: its position, its geometry and the quality of the water it contains [20].

For the present work, since it is a question of the survey for groundwater, our choice takes into account not only the capacity of a method to locate the zones of fractures or crushing considered as zones of accumulation of groundwater, but also the cost, the implementation time and the ease of use in the field. This justifies the

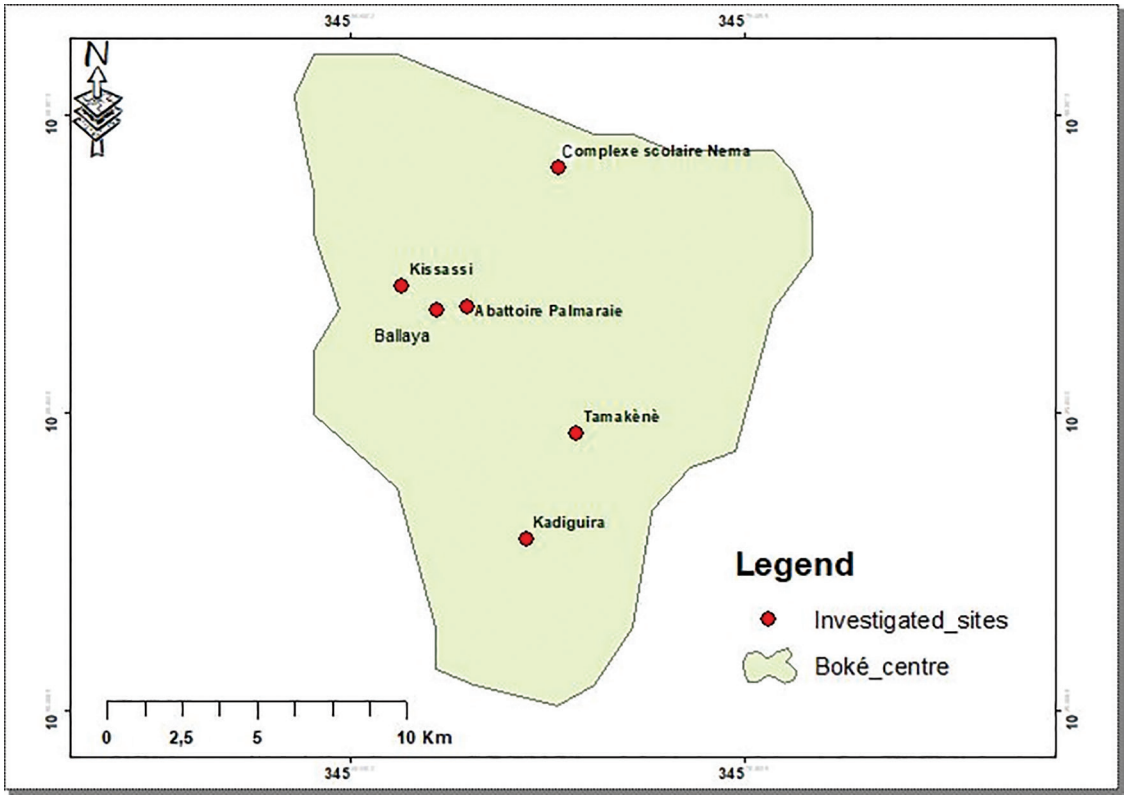

Figure 5: *Location map of study sites.*

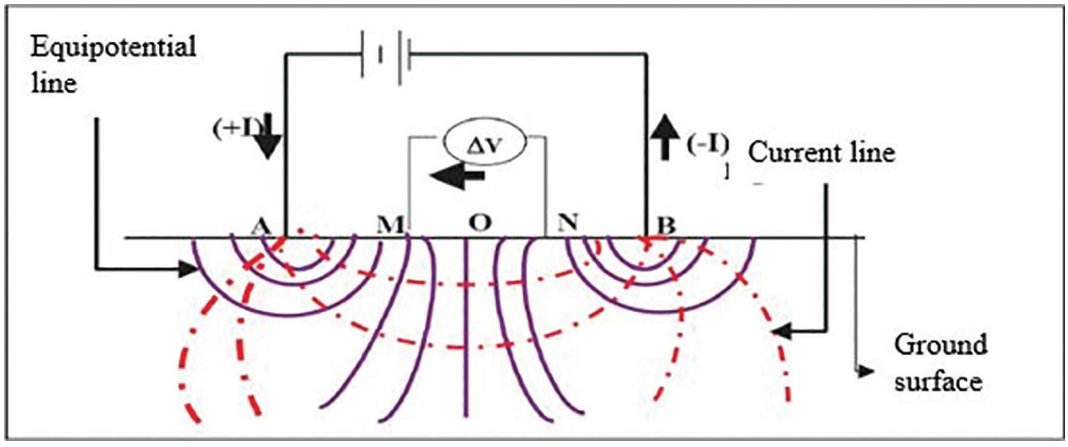

Figure 6: *Schlumberger device.*

choice of the geo-electrical method (electrical sounding) of the Schlumberger type.

- Work device: Several devices are envisaged to determine the distribution of resistivities in the subsoil. The choice of device depends on the depth of investigation. Any measuring device has in fact four electrodes, two electrodes A and B, for sending currents (transmission circuit) and two others M and N, for measuring the potential ΔV (measuring or receiving circuit). The Schlumberger configuration is shown in Figure 6.
- Measurement technique: The measurement technique consists of separating the injection circuit from the measurement circuit. Four electrodes are used for this in practice, AMNB (the measuring quadrupole). From

two electrodes, called injection electrodes A and B, an electric current of intensity I is sent into the ground and the potential difference (ΔV) is measured between two other electrodes, called measurement electrodes MN [21].

- Processing: The results of the resistivity measurements are entered into the software, and after processing, the apparent resistivity values are obtained on a bi-logarithmic scale whose distances AB/2 are reported on the abscissa and the resistivities are on the ordinate. The petro-geophysical model defining the number of terrains and their characteristics (resistivity and thickness) in the area and the physical-geological model which highlights the behavior of the current in the ground through a curve are finally obtained. Knowing the geology of the area, the nature of the terrain is defined by analogy with the resistivity values of the rocks in the region.

Results and discussion

The results and their interpretation, the coordinates of the points and the parameters of the measuring device on the sites are as follows:

A- Kissassi site

1) Curve of electrical positioning sounding 1 (SEP1): the geometric characteristics of the device at this point are: AB/2 = 40 m; MN/2 =10 m; k = 275. The geographic coordinates are:

   X = 57,448; Y = 1,208,604; and Z = 36 m.

   At this point, the petro-physical model reveals an area of three layers. Taking into account the geology and the physical properties of the rocks of the area, the lithology is presented from top to bottom as follows (Figure 7):
   - A layer of cuirass having a resistivity of 5,851 Ωm and a thickness of 1.6 m;
   - An alteration crust with a resistivity of 2,517 Ωm and a thickness of 2 m, and;
   - A formation of low resistivity (820 Ωm) compared to the first and second which is fractured clays. It is beyond 3.6m deep and this layer constitutes the superficial aquifer.

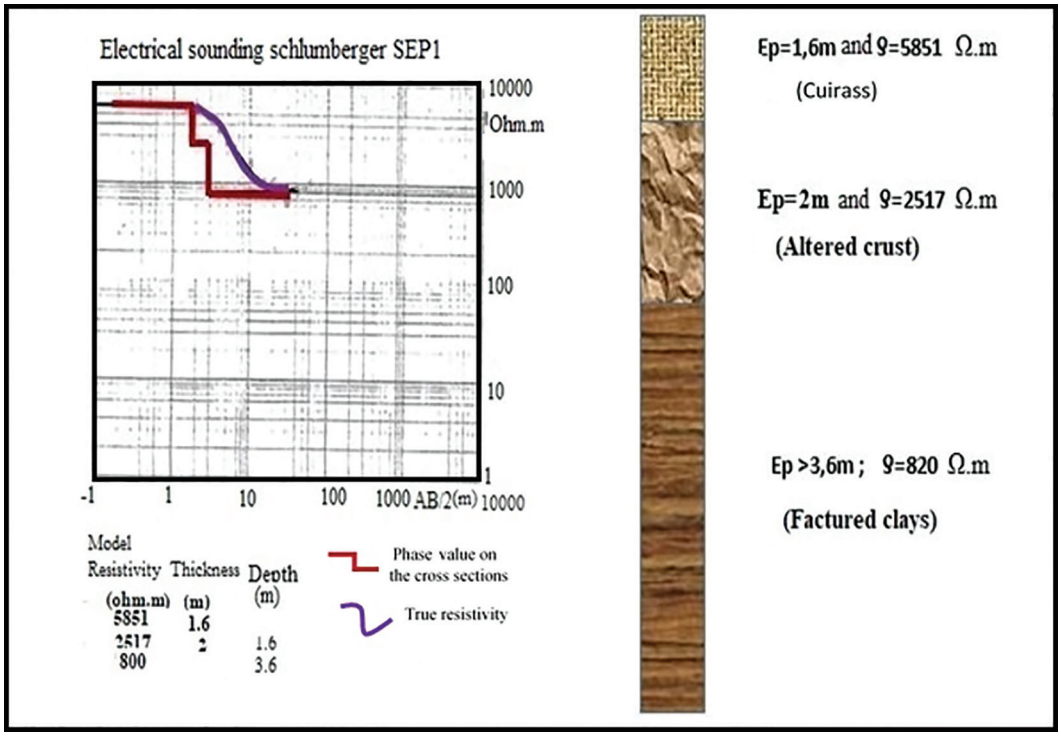

Figure 7: *Lithological section of SEP1. Ep = Thickness.*

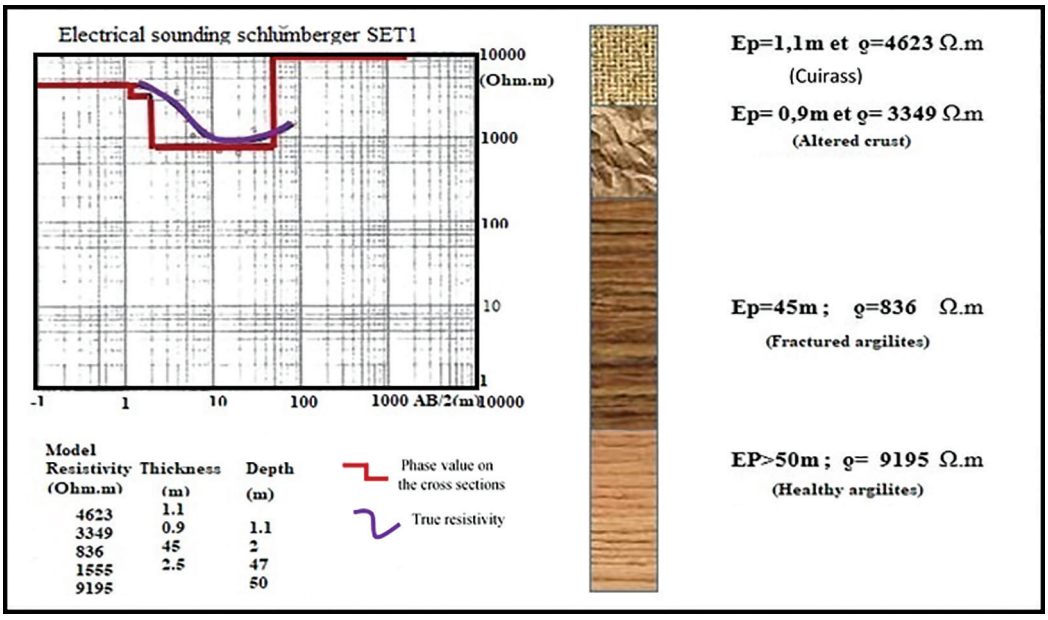

Figure 8: *Lithological section of SET1. Ep = Thickness.*

2) Electrical Test Sounding 1 (SET1): the geometric characteristics of the device at this level are: AB/2 = 30 m; MN/2 = no measurement = 10 m; and k = 275.
   Compared to the first survey, the electrical test survey specifically intersected four layers including (Figure 8):
   – A layer of cuirass having a resistivity of 4,623 Ωm and a thickness of 1.1m;
   – A layer of crust altered having a resistivity of 3,349 Ωm;
   – A thick layer of fractured argillites with an average resistivity of 836 Ωm and a thickness of 45 m;
   – A last layer having a high electrical resistivity (9,195 Ωm); it is the bedrock (healthy argillites).

B- Abattoire Palmeraie site

The geometric characteristics of the device on this site are: AB/2 = 40 m; MN/2 = 10 m. The geographic coordinates are: X = 576,652; Y = 1,207,919; Z = 7 m.

1) Curve of electrical positioning sounding 2 (SEP2).
   The petro-physical model of the survey (SEP2) presented the lithology from top to bottom as follows (Figure 9):
   – A thin surface layer having a thickness of 0.64 m and a resistivity of 543 Ωm (sandy clays soil);
   – A layer of altered crust with a thickness of 1.3 m and a resistivity of 1602 Ωm;
   – Thin layer of clay with a resistivity of 758 Ωm and a thickness of 1 m;
   – A layer of fractured shale 45m thick and a resistivity of 378 Ωm; The water table is at this level;
   – A healthy layer of shales.
   The bedrock roof was cut to a depth of 35 m.
2) Test electrical sounding 2 (SET2):
   The lithological section of this survey is as follows (Figure 10):
   – A layer of cuirass which has a thickness of 1.7 m and a resistivity of 4,410 Ωm;
   – A weakly altered layer (altered crust);
   – A layer of weakly fractured dolerites is located beyond 5.7 m depth. This zone admits an electrical resistivity of 453 Ωm.
   The top of the bedrock (fractured dolerites) of this hole was intersected at a depth of 35 m.

C- Tamakènè site

The characteristic parameters of the device are: AB/2 = 40 m; MN/2 = 10 m; k = 275. The geographic coordinates are as follows: X = 580,265; Y = 1,203,704; Z = 57 m.

1) Electrical positioning sounding curve (SEP3):

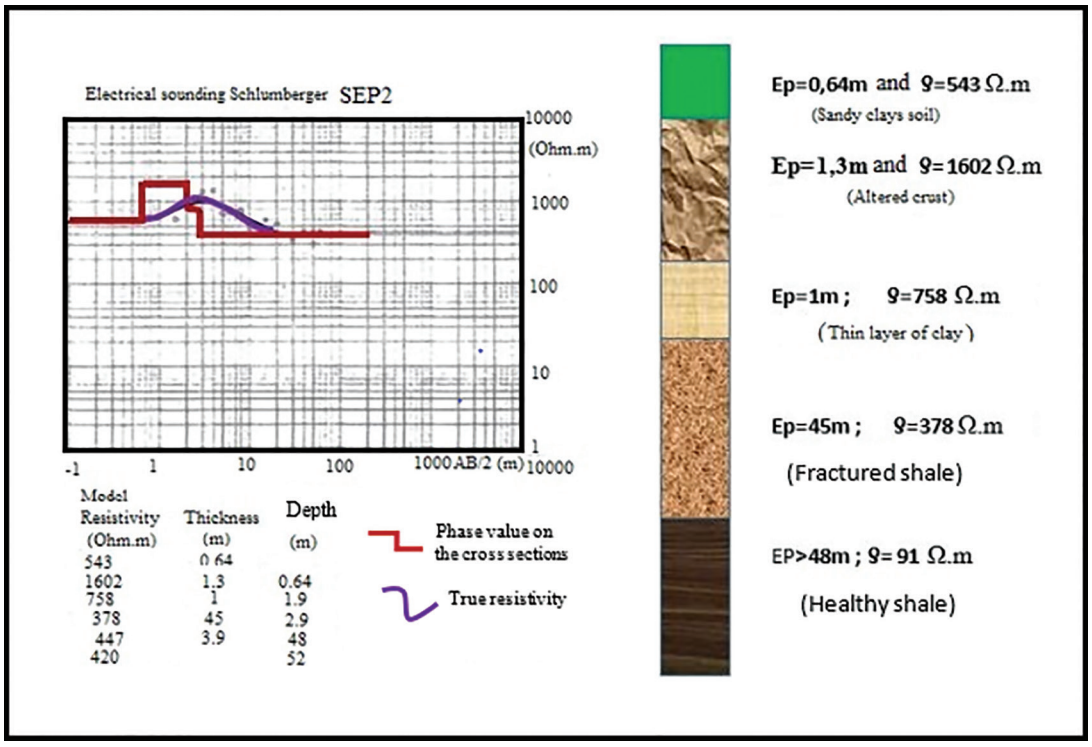

Figure 9: *Lithological section of SEP2. Ep = Thickness.*

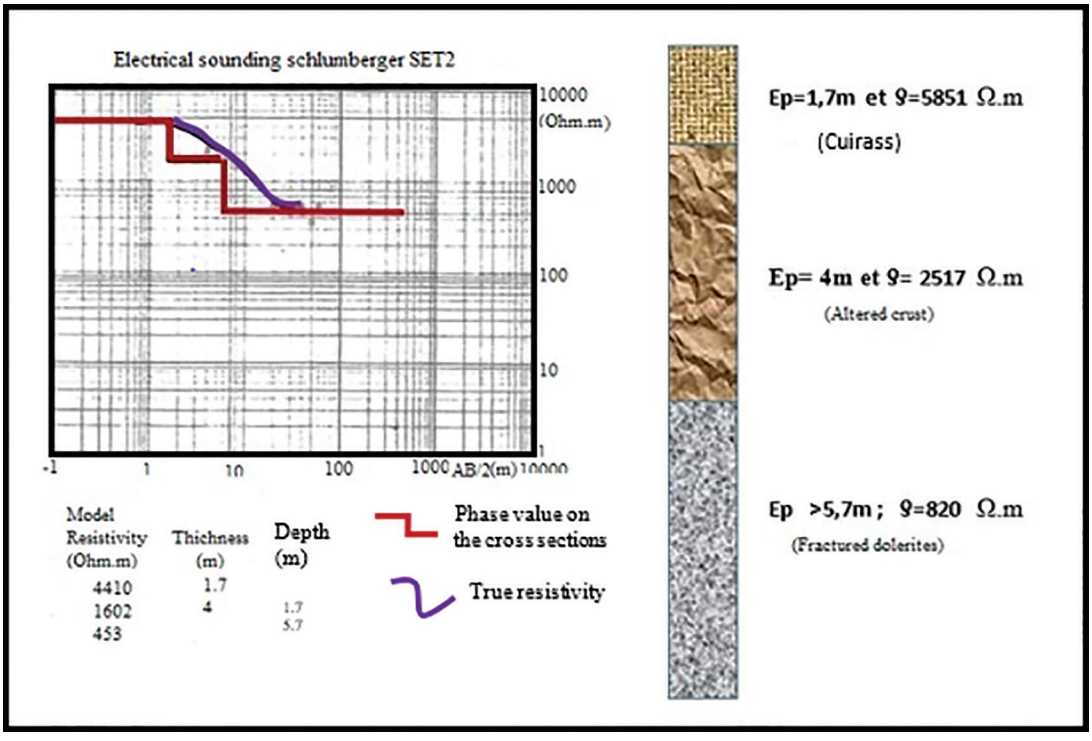

Figure 10: *Lithological section of SET2. Ep = Thickness.*

The lithological section revealed by the latter is as follows:

From top to bottom (Figure 11):

- A superficial formation having a thickness of 1.4m and a resistivity of 1,741 Ωm;
- A layer of slightly altered crust with a resistivity of 2,379 Ωm and 3.65 m thick;
- A thin layer of clay with a thickness of 1.5 m and a resistivity of 1,008 Ωm;
- A thick layer (199 m) of highly fractured shale characterized by an electrical resistivity of 261 Ωm. The aquifer is located at this level. Below this layer is bedrock (healthy shale).

2) Electrical Test Sounding 3 (SET3).

The geographical coordinates of this site are mentioned in Figure 12.

At this level (SET3), the lithology is presented from top to bottom as follows (Figure 12):

- A layer of cuirass which extends over a thickness of about 2.12 m and an average resistivity of 5,000 Ωm;
- A layer of altered crust with an average resistivity of about 1,300 Ωm and a thickness of about 6 m;
- A thick layer of sandstone beyond 21 m characterized by an electrical resistivity of 41,201 Ωm.

D- Nema school complex site

The geometric characteristics of the device on this site are: AB/2 = 40 m; MN/2 = 10 m; and K = 275.

1) Curve of electrical positioning sounding 4 (SEP4):

The lithology at this point is, from top to bottom, as follows: (Figure 13):

- A layer of cuirass which has a resistivity of 5,345 Ωm and a thickness of 1.5 m;
- A layer of altered crust with a resistivity of 1,115 Ωm is beyond 1.5 m.

2) Electrical sounding test 4 (SET4):

The electrical test sounding performed shows the following lithology (Figure 14):

- A layer of altered crust with a thickness of 5.8 m and a resistivity of 1,278 Ωm;
- A layer of wet clay located about 13 m deep with a resistivity of 829 Ωm;
- Beyond 10 m depth, there is a layer of fractured and wet clay. It has a resistivity of 121 Ωm.

E- Kadiguira site

The geometric characteristics of the device are like the previous sites (Nema school complex, Tamakènè).

1) Curve of the electrical positioning sounding (SEP5).

The lithological section of SEP5 gave us the following, from top to bottom:

- A layer of altered crust which extends over a thickness of 7.5 m and a resistivity of 908 Ωm;
- A thick layer of wet clay constituting the aquifer with a thickness of 52 m and a resistivity of 290 Ωm;
- A last layer which constitutes the bedrock (healthy clay). It is located beyond 60 m deep and has a resistivity of 3397 Ωm

2) Electrical sounding test 5 (SET5).

The lithologic section of SET5 is presented from top to bottom as follows (Figure 15):

- Altered crust with a thickness of 6.05 m and a resistivity of 814 Ωm;
- A layer of fractured clay located at a depth of 6.05m, characterized by a resistivity of 367 Ωm and a thickness of 18 m (this is the aquifer);
- Beyond 24 m, we have the upper part of the bedrock (healthy clay).

F- Ballaya site

1) Curve of electrical positioning sounding 6 (SEP6).

The lithological section of SEP6 is presented from top to bottom as follows (Figure 16):

- An altered and wet (altered crust) layer 2.3 m thick with a resistivity of 262 Ωm;
- A layer of fractured argillites, characterized by levels, with a thickness of 29.1 m and an average resistivity of 167 Ωm;
- A layer of healthy argillites located more than 31 m deep with a resistivity of 2,418 Ωm.

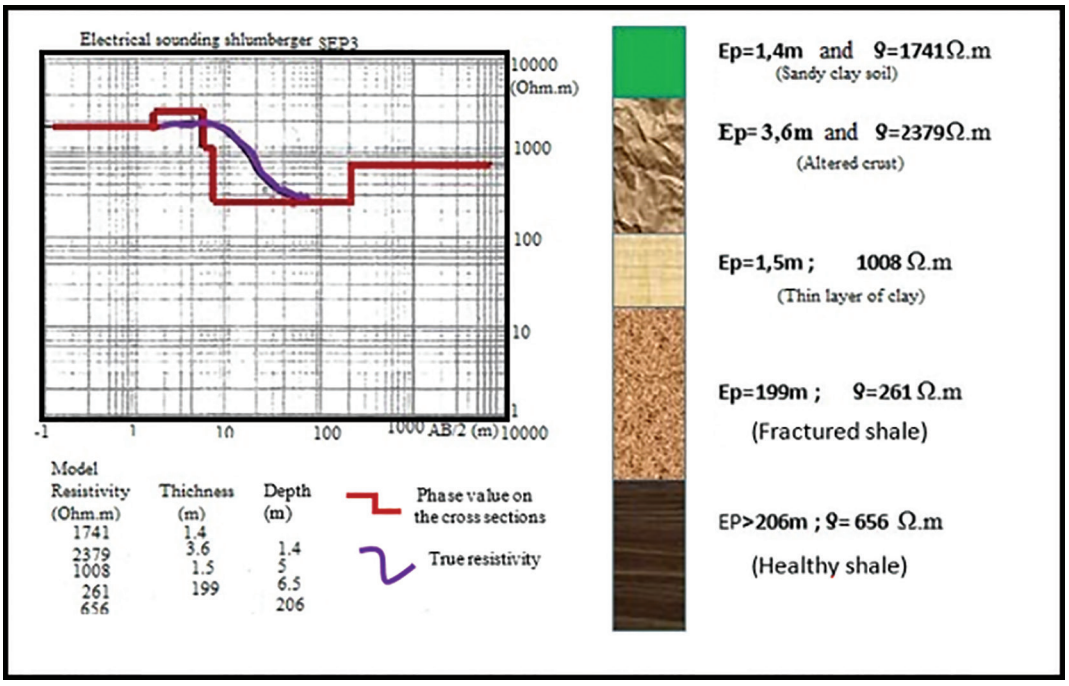

Figure 11: *Lithological section of SEP3. Ep = Thickness.*

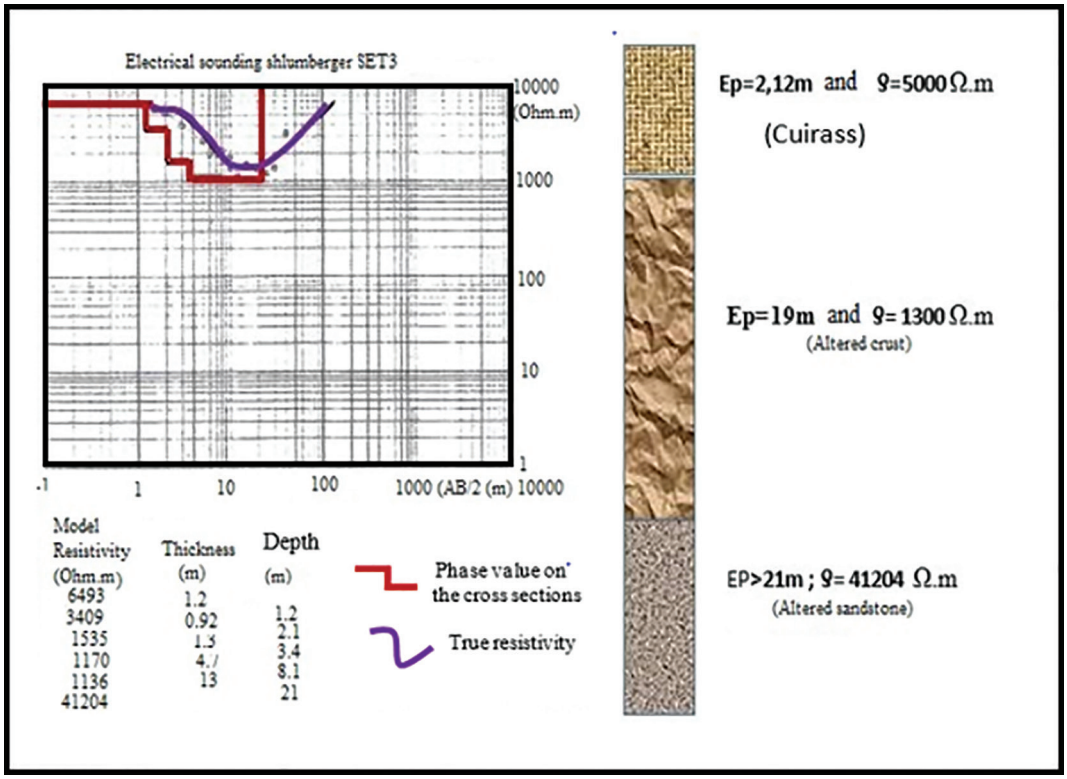

Figure 12: *Lithological section of SET3. Ep = Thickness.*

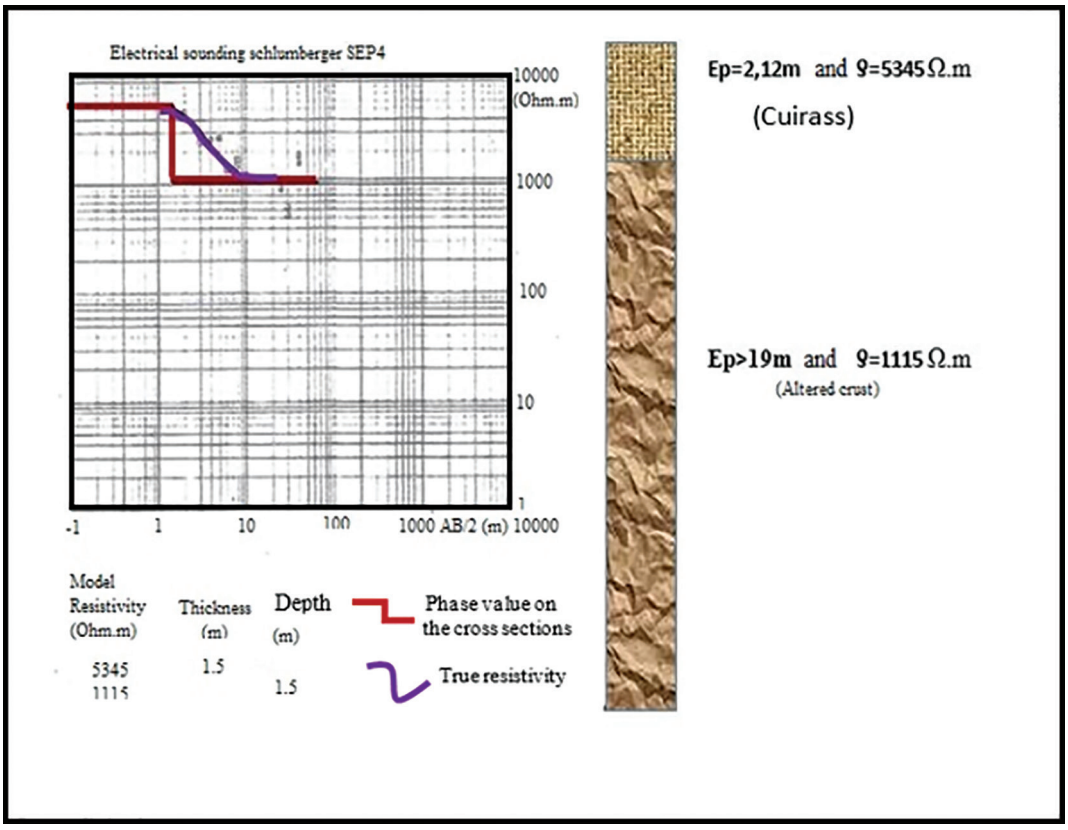

Figure 13: *Lithological section of SEP4. Ep = Thickness.*

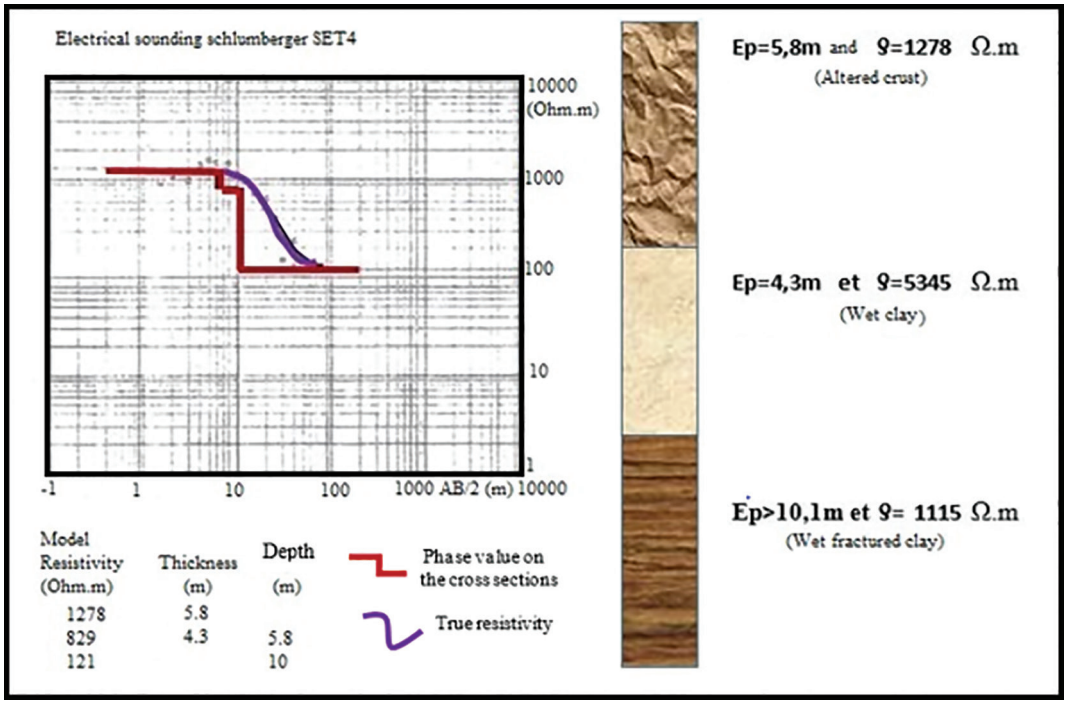

Figure 14: *Lithological section of SET4. Ep = Thickness.*

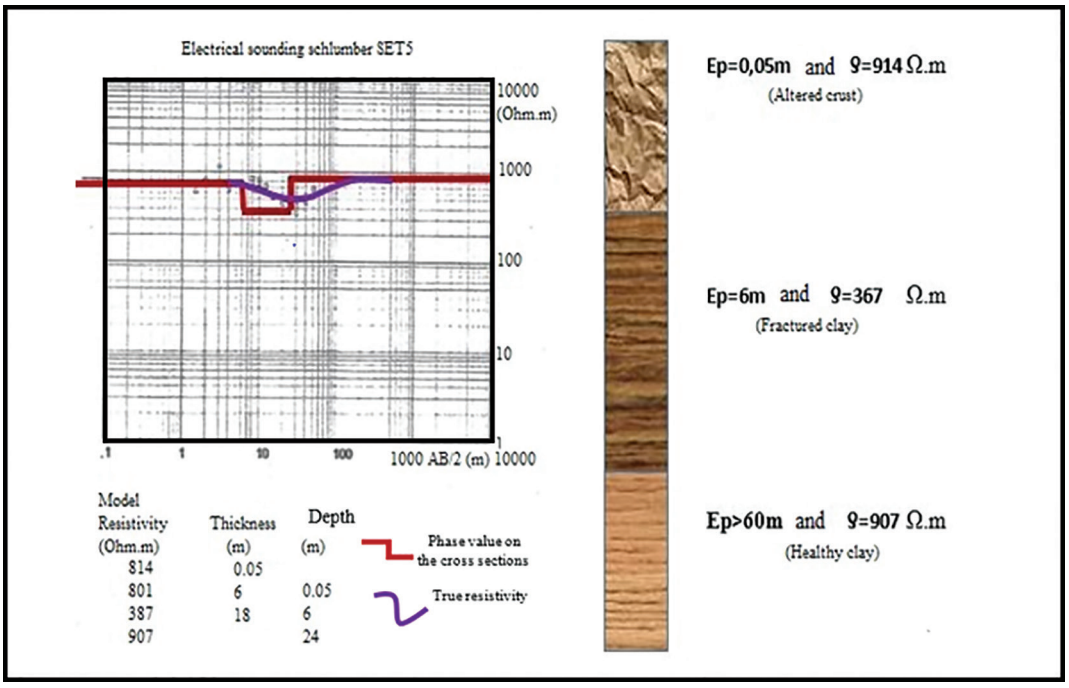

Figure 15: *Lithological section of SET5. Ep = Thickness.*

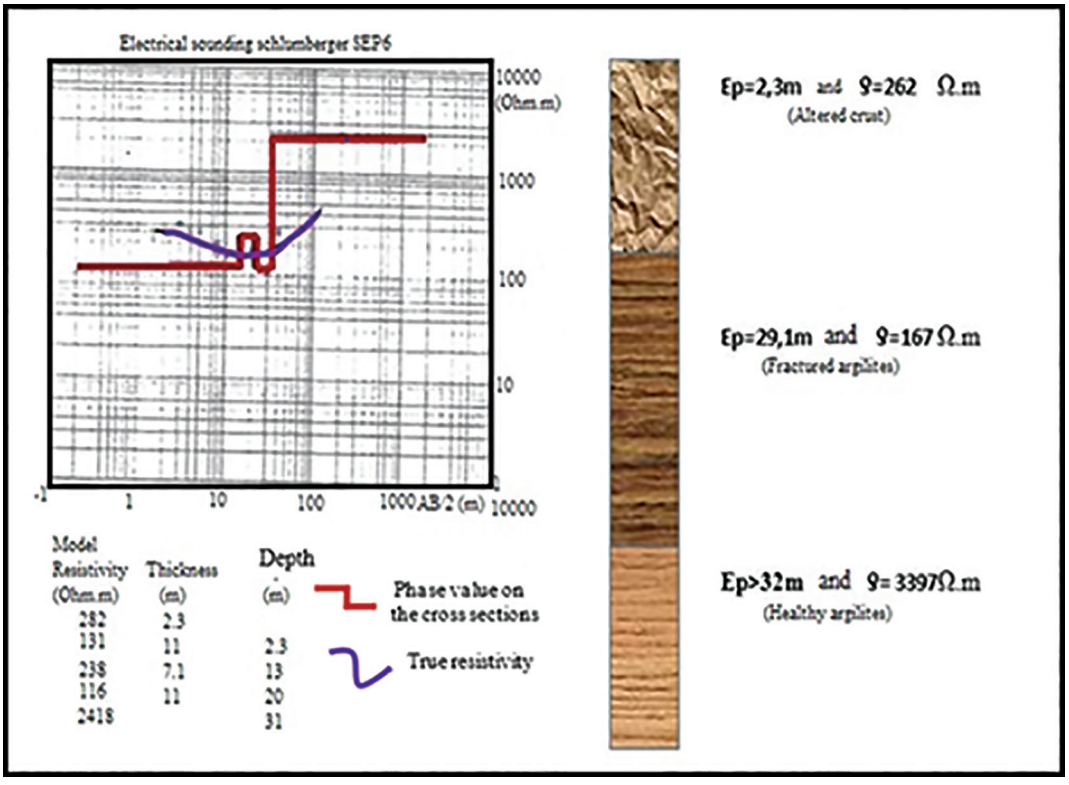

Figure 16: *Lithological section of SEP6. Ep = Thickness.*

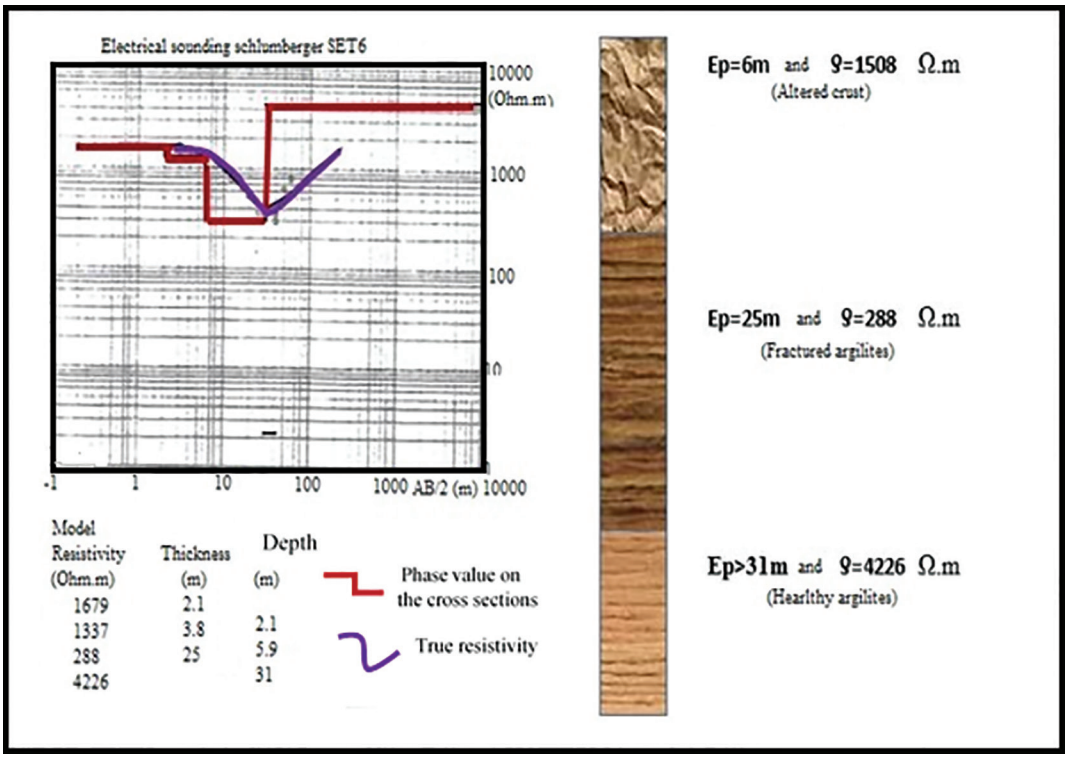

Figure 17: *Lithological section of SET6. Ep = Thickness.*

2) Electrical sounding test (SET6):
The lithologic section of SET6 is presented from top to bottom as follows (Figure 17):
   – A layer of altered crust with two levels, the upper part resistant and the lower part less resistant; it has an average resistivity of 1,508 Ωm and a thickness of about 6 m;
   – A thick layer of fractured argillites with a resistivity of 288 Ωm and a thickness of 25 m;
   – Beyond 31 m, we have healthy substratum (argillites). It has a resistivity of 4,226 Ωm.

Discussion

The analysis and interpretation of the results of the electrical soundings carried out at the six sites studied in the area enabled us to highlight three superimposed zones or layers in such a way that the comparison of the resistivities is presented as follows: $\varrho 1 > \varrho 2 < \varrho 3$.

The first layer of the study area extending over approximately 40 m corresponds to the covering of the sedimentary cover; the second constitutes an arena of low resistivity and being on a depth of surroundings 5 m; the third layer is the very resistant and fissured in places bedrock. Several authors, in the context of hydrogeological studies with different objectives, have determined the lithology of the sites using electrical soundings. This is the case of [22], [9–10] who, in their studies, succeeded in highlighting the geological structures, increasing the production of the drillings and decreasing the negative drilling rate. This supported our choice of the method and the results obtained.

Conclusions

At the end of this study, we find that our area has a lithology of several terrains arranged from top to bottom:

– A layer of weathering crust covered in places by a thin layer of the cuirass or topsoil. The average thickness of this layer is 40 m;
– A thin layer of wet clay with an average thickness of 4.5 m which is intercalated between

the weathered crust and the top of the fissured bedrock;
- A layer of cracked shales, dolerites or sandstones (roof of the substratum) follows the layer of clays. It is at this level that the most important fractures for the accumulation of groundwater are located. This zone is located at more than 40 m depending on the location;
- A healthy formation which constitutes the substratum. It consists of healthy shales, doleritic intrusions and sandstones.

Structures favourable to the accumulation of groundwater are fractured shales, fissured dolerites and fissured or crushed sandstones. The latter (sandstone) has a significant thickness and is generally located at a great depth (100 to 150 m).

Despite the efforts, it must be recognized that like any other study, this one has limitations. They are: ignorance of the direction of groundwater flow and lack of knowledge of the physicochemical properties of the waters in the area. These shortcomings are justified by the lack of material and financial resources necessary during the works.

References

[1] INS Guinée (2018): *Rapport annuel. Conakry*. Institut National de la Statistique de Guinée, 28 p.

[2] Kourouma, M. (2016): *Choix d'un complexe rationnel de méthodes géophysiques pour la recherche des eaux souterraines au Nord-Ouest de la Guinée.* Thèse. CERESCOR, Centre de Recherche Scientifique de Guinée: Guinée, 176 p.

[3] Diallo, I. (1979): *Projet de recherche des eaux souterraine sur la Boffa en vue de l'adduction de la population en eau potable*. Mémoire de fin d'étude supérieure. Boké, Institut Supérieur des Mines et Géologie de Boké (ISMGB), Guinée, 102 p.

[4] SNAPE (2018): *Rapport annuel.* Conakry, 18 p.

[5] Kim, M.K.J.K.N., Jeong, G. (2011): Surface geophysical investigations of landslide at the Wiri area in southeastern Korea. *Environmental Earth Sciences*, 63(5), pp. 999–1009, DOI: 10.1007/s12665-010-0776-z.

[6] Kadri, M., Nawawi, M.N.M. (2010): Groundwater exploration using 2D Resistivity Imaging in Pagoh, Johor, Malaysia*.* In: *AIP Conference Proceedings*, pp. 151–155.

[7] Morad, M.D. (2012): *Utilisation des dispositifs de géophysique électrique non classiques pour l'étude des couches géologiques profondes: cas des chotts el Gharbi et chergui (Algérie).* Thesis. Université d'Oran: Algérie, 198 p.

[8] Michel, K.A., Coulibaly, D., Koffi, Y.B., Biemi, J. (2013): Application de méthodes géophysiques à l'étude de la productivité des forages d'eau en milieu cristallin: cas de la région de Toumodi (Centre de la Côte d'Ivoire). *International Journal of Innovation and Applied Studies,* 2(3), pp. 324–334.

[9] Dieng, B., De Heusch, K.A., Bakyono, B. A. (2004): *Optimisation de l'implantation géophysique des forages en zone de socle au Nord du Burkina Faso*. Groupe des Ecoles EIER-ETSHER, Ouagadougou 03, Burkina Faso.

[10] Kouakou, E.G.K. (2012): Utilisation de la prospection géophysique par résistivité électrique pour la recherche d'eau souterraine dans le département de Tanda (Est de la Côte d'Ivoire). *European Journal of Scientific Research,* 83(2).

[11] Falco, P. (2013): *Sondages géoélectriques "Null-Arrays" pour la caractérisation des structures de subsurface*. Thesis. Université Neuchatel.

[12] Njueya A.K., Kengni, L., Fonteh, M.F., Dongmo, A.K., Ntankouo., R.N., Nkouathio, D.G., Tazo, C. (2016): Apport des Sondages Électriques Verticaux à la Localisation et la Caractérisation des Aquifères en zone Volcanique au Cameroun: Cas d'Ebone et ses Environs. *European Journal of Scientific Research*, pp. 54–65.

[13] Kouakou, E.G.K., Dosso, L., Kouame, L.N., Sombo, A.P., Sombo, B.C. (2015): Contribution des méthodes de résistivité électrique a la recherche d'eau en milieu cristallin: cas de Yakassé-Attobrou et d'Abié, région de la Mé, Côte d'Ivoire. *La Revue Ivoirienne des Sciences et Technologie,* 26, pp. 194–211.

[14] Koussoubé, Y., Nakolendoussé, S., Bazié, P., Sawadogo, A.N. (2003): Typologie des courbes de sondages électriques verticaux pour la reconnaissance des formations superficielles et leur incidence en hydrogéologie de socle cristallin du Burkina Fasso. *Pangea infos, Société Géologique de France,* 1999, 31/32, pp. 33–36.

[15] Bernardi, A., Detay, M., De Gramont, H.M. (1988): Recherche d'eau dans le socle africain. Corrélation entre les paramètres géoélectriques

et les caractéristiques hydrodynamiques des forages en zone de socle. *Hydrogeology Journal,* 4, pp. 245–253.

[16] INS Guinée (2020): *Annuaire des statistiques de l'environnement,* 256 p.

[17] Dansoko, K. (2019): *La mise en œuvre d'un protocole suivi-évaluation environnementale et sociale du permis Alliance Minière Responsable (AMR).* Rapport de fin d'études supérieures, Institut Supérieur des Mines et Géologie de Boké (ISMGB), Guinée, 68 p.

[18] Mamedov, V.I., Bouféév, Y.V., Nikitine, Y.A. (2010): *Géologie de la République de Guinée.* Geoprospects Ltd: Université d'état de Moscou, 166 p.

[19] Nabé, L. (2017): *Géologie et étude des faciès bauxite de la feuille Boffa*. Rapport de fin de d'étude supérieur, Institut Supérieur des Mines et Géologie de Boké (ISMGB), Guinée, 97 p.

[20] Soro, D.D. (2017): *Caractérisation et modélisation hydrogéologique d'un aquifère en milieu de socle fracturé: cas du site expérimental de Sanon (région du plateau central au Burkina Faso)*. PhD Thesis. Université Pierre et Marie Curie-Paris VI, Institut international, 303 p.

[21] Cissé, O., Kourouma, A. (2006): *Utilisation des méthodes géophysiques pour la recherche des eaux souterraines à Lambanyi dans la commune de Ratoma*. Rapport de fin d'études supérieures. Institut Supérieur des Mines et Géologie de Boké (ISMGB), Guinée, 51 p.

[22] Lavoie, A.C. (1998): *Application de la méthode des sondages électriques à la caractérisation des aquifères et des dépôts meubles, Basses-Terres du St-Laurent, région Nord de Montréal*. Mémoire de maitrise, 210 p.

Original Scientific Article • DOI 10.2478/rmzmag-2021-0011

Received: July 02, 2021
Accepted: January 18, 2022

Hydrocarbon Potential and Biomarker Studies of EE-1 Well, Offshore Eastern Dahomey Basin, SW Nigeria

Matthew E. Nton[1], Emeka E. Emordi[1,*], Irewole Ayodele[2]

[1]Department of Geology, University of Ibadan, Ibadan
[2]South Atlantic Petroleum Limited, Lagos, Nigeria

*Corresponding author: E-mail: elmer.emordi@gmail.com

Abstract

The hydrocarbon potential, organic source input, and paleodepositional environment of subsurface sediments from EE-1 well, offshore Eastern Dahomey Basin, were assessed using Rock-Eval pyrolysis and biomarker geochemistry. The total organic carbon (TOC) and soluble organic matter (SOM) in the sediments ranged from 0.96wt% to 8.92wt% and 676.12 ppm to 2883.85 ppm, respectively, indicating adequate to excellent organic richness. The pseudo-Van Krevelen plot classified the sediments as types II and III kerogen, which have the potential to generate both oil and gas. The T_{max} and production index (PI) ranged from 422°C to 431°C (average, 426°C) and 0.03 to 0.24, respectively, suggesting low thermal maturity. The presence of C_{27}–C_{29} steranes, oleanane, and hopane/sterane ratio (1.53/16.11), indicated organic matter from mixed sources with more terrigenous input. Cross plots of Pr/nC_{17} against Ph/nC_{18}, C_{35}/C_{31} – C_{35} homohopane index (0.05 – 0.17) and other related biomarker ratios such as C_{21}/C_{23} trycyclic terpane ratio (0.33 – 0.82) signified that the sediments were deposited in mixed marine/terrigenous environment under oxic – suboxic conditions. This study has demonstrated that sediments had adequate organic matter with the potential to generate both oil and gas at appropriate thermal maturity.

Keywords: hydrocarbon potential, biomarker, Dahomey Basin

Introduction

The Dahomey Basin comprises a combination of inland, coastal, and offshore waters and stretches from Southeastern Ghana, through Togo and the Republic of Benin, to southwestern Nigeria [1] (Figure 1). The Eastern Dahomey Basin (Nigerian sector) has been of much geological interest as a result of the reported occurrences of bitumen, limestone, glass sands, and phosphates [2]. The initial motivation for oil exploration in the Eastern Dahomey Basin arose from the discovery of seepages and tar sand deposits as early as 1909. In the earlier days of exploration for oil in the basin, the wells drilled were classified as 'dry' and thus abandoned. Recent exploration and prospect re-evaluation efforts in the Nigerian segment of the basin have been encouraged following oil discovery and production in the neighbouring Benin Republic sector, west of the basin and the social unrest in the prolific Niger Delta, east of the basin [3].

Numerous studies have been carried out on the Eastern Dahomey Basin by a host of earlier workers such as those listed in references [3–14], amongst others. These studies have increased our knowledge of stratigraphic resolution, established petroleum systems, and the hydrocarbon potential of the basin. However, in comparison with the contiguous Niger Delta, much is yet to be clearly understood in the Eastern Dahomey Basin. In the Dahomey Basin, for instance, there is no consensus of opinion on the stratigraphic nomenclatures in the offshore and onshore sectors and different names are assigned to the same units at different places by different authors [5, 13, 15]. This study therefore examines the sediments of EE-1 Well, for hydrocarbon potential,

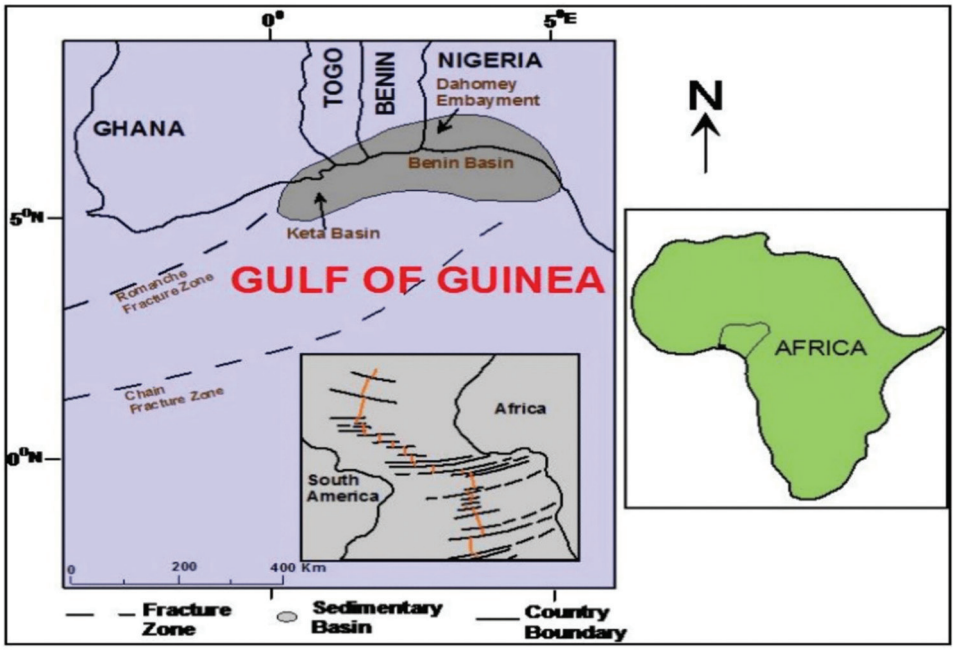

Figure 1: *Regional map of four countries showing the location of the Benin (Dahomey) Basin in the Gulf of Guinea [11].*

palaeodepositional environment using Rock-Eval and biomarker geochemistry in line with current understanding. The resulting information will be of great interest to explorationists and researchers.

Location of study area and geologic setting

The study area is located between latitudes 6°10'N and 6°20'N and longitudes 2°0'E and 2°30'E, offshore Eastern Dahomey Basin (Figure 2).

The Dahomey Basin is a coast-parallel basin, stretching from the western limit of the Niger Delta in Nigeria westwards, through Benin Republic and Togo, terminating in the Volta Delta in Ghana, with a total latitudinal stretch of about 500 km [16]. It is a marginal pull apart or marginal sag basin [17] which originated during the Early Cretaceous separation of African and South American plates [18]. The basin contains Late Cretaceous to recent sediments up to 3,000 m where they thicken markedly into the offshore and then thin beneath the deep water area. Onshore, the sediment-fill also thins both westward and eastward from the central area in Benin Republic. The maximum thickness of the sediments is around the Nigeria - Republic of Benin border. In the Nigerian sector, the sediments thin into the Basement Complex of the Okitipupa High, west of the Niger Delta. Earlier stratigraphic study of the basin by Jones and Hockey [19] recognized both Cretaceous and Tertiary sediments. Other subsequent workers recognized three chronostratigraphic units: Pre-lower Cretaceous folded sequence, Cretaceous sequence and Tertiary sequence [6, 9]. The Cretaceous stratigraphy as compiled from outcrop and borehole records comprising the Abeokuta Group is further subdivided into three informal formational units, namely, Ise, Afowo, and Araromi Formations [5]. Ise Formation is the oldest Cretaceous unit and comprises predrift succession of conglomerates, sands, and mudrocks overlying the Basement Complex. The succession continues upwards with medium to coarse, loose sands interbedded with kaolinitic clays. Omatsola and Adegoke [5] assigned a Lower Cretaceous (Neocomian) age to this formation. The deposits are products of alluvial fan setting at the basin edge, following initial rifting [16]. The Afowo Formation comprises mostly medium to coarse sandstone, with thin to thick interbeds of shales, siltstones, and claystones. It has been described as tar-bearing and petroliferous. The formation has been assigned a Turonian age [8, 15]. The Araromi Formation is the youngest Cretaceous unit that conformably overlies Afowo Formation in the Eastern Dahomey Basin. The formation consists of fine to medium

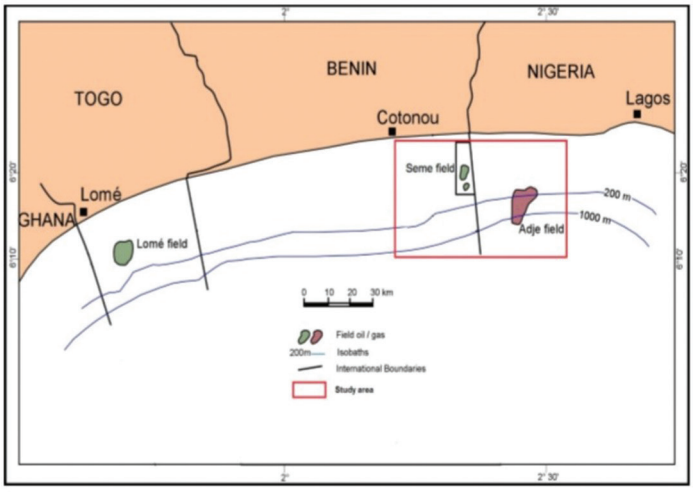

Figure 2: *Dahomey embayment showing the study area (after d'Almeida et al. [14])*.

sands at the base, overlain by a seaward thickening shale and siltstone with thin limestones and marls, as well as thin lignitic bands. The Araromi Formation has been assigned a Maastrichtian to Paleocene age [5]. Overlying the Cretaceous Abeokuta Group is the Ewekoro Formation. The Ewekoro Formation is predominantly limestone, but it is, however, not encountered offshore in coastal boreholes, where the shaley Imo Formation unconformably overlies the Afowo Formation [15]. Four microfaciesl, namely, bio-microsparite, shelly biomicrite, algal biosparite, and red phosphatic biomicrite, have been identified within this predominantly limestone body [4, 20]. The formation has been assigned Upper Paleocene by most authors [2, 21, 22]. The Akinbo Formation [23] overlies the Ewekoro Formation. The unit consists of fine-grained, dark micromicaceous shale, locally silty with glauconitic marl and conglomeratic at the base. The formation has been dated Upper Paleocene to Lower Eocene in age [12, 23]. The Oshosun Formation overlies the Akinbo Formation and consists of greenish grey or beige clay and shale, with interbeds of sandstones. The shale is thickly laminated and glauconitic [12]. According to Okosun [9], the basal beds consist of any of the following facies: sandstones, mudstones, claystones, clay-shale, or shale. This formation is phosphate-bearing [2, 19]. A Lower Eocene-Middle Eocene age is assigned to this formation. The Ilaro (Ijebu) Formation conformably overlies the Oshoshun Formation in the Eastern Dahomey Basin. This unit comprises massive, poorly consolidated, cross-bedded sandstones. Subrounded to rounded pure quartz grains dominate the base of the formation and it has been assigned an Eocene – Oligocene age. The Benin Formation, also called the Coastal Plain Sands [5] is the youngest sequence in the Eastern Dahomey Basin and comprises poorly sorted sands with lenses of clays. The sands are cross-bedded in part and show nearshore to continental distinctiveness. The formation age covers the Miocene to Recent periods.

There are lots of controversies concerning the stratigraphy of the Nigerian sector of the basin. This is due primarily to different stratigraphic names that have been proposed for the same formation in different localities in the basin [9, 24]. This situation can be fairly blamed on the lack of good borehole coverage and adequate outcrops for detailed stratigraphic studies [25].

Materials and methods

Samples

Subsurface samples of EE-1 Well from offshore Eastern Dahomey Basin were obtained for this study. Of a total depth of 315 m to 2257.5 m, the interval 1200–2260 m was used in this study. The detailed lithological description of the samples is shown in Figure 3. The lithologic sequence within the interval shows that the base to depth 2100 m is a thick sequence of silty

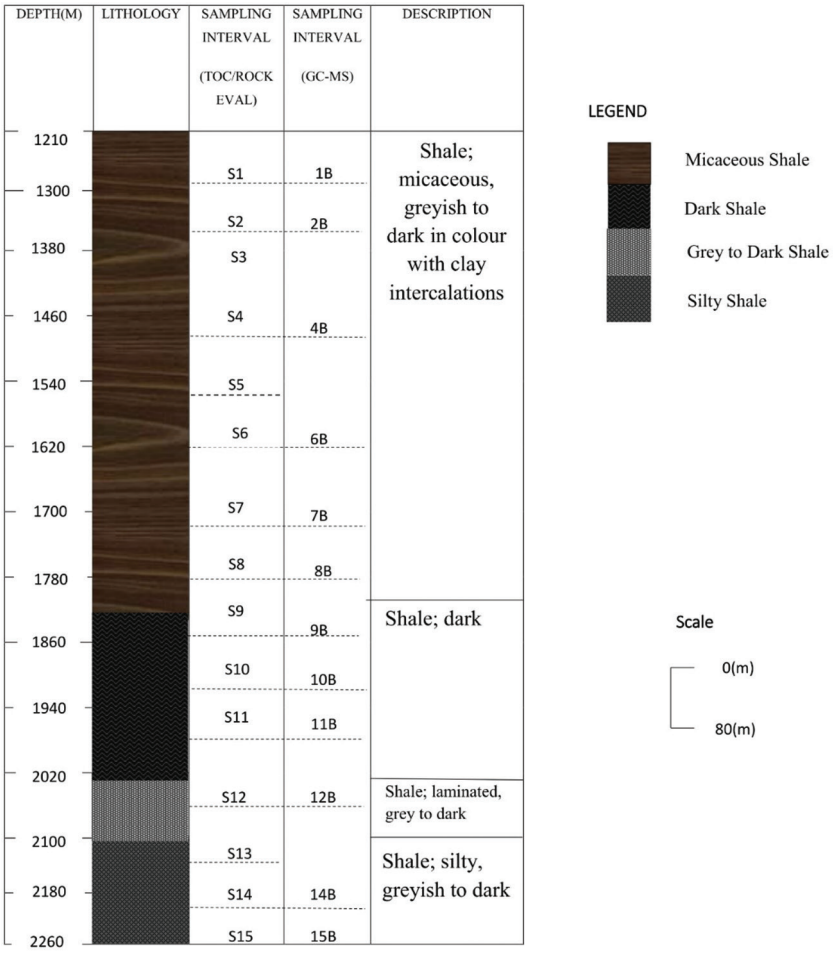

Figure 3: *Lithological log of the studied section of EE-1 Well.*

shale which is greyish to dark in colour. This is overlain by a greyish to dark shale sequence, a thick sequence of indurated, dark shale indicative of rich organic matter, which was encountered from 2020 m to 1810 m. From 1810 m to the top of the well (1210 m) is micaceous shale with clay intercalations, ranging in colour from grey to dark.

Analytical methods

Total Organic Carbon Determination

Approximately 10 g of each pulverized shale sample (15) was weighed out and decarbonated by treatment with concentrated hydrochloric acid (HCl) for two hours. After decarbonation, the samples were rinsed with distilled water and flushed through a filtration apparatus, fitted with a glass microfiber filter to remove the acid. The filtrate was then removed, placed into a LECO crucible and dried in a low temperature oven (110°C) for four (4) hours. The samples were then analyzed in a LECO 600 carbon analyzer for the total organic carbon (TOC) content.

Rock-Eval pyrolysis

Based on the TOC adequacy, 100 mg of selected samples (15) were gradationally heated to 550°C at a 25°C/min heating rate using a HAWK Pyrolyzer from which the pyrograms were produced as calculated parameters. Both the TOC and Rock-Eval pyrolysis were undertaken at Geomark Research Ltd. Laboratory, Humble, Texas, USA.

Soluble organic matter extraction and fractionation

About 30–50 g of each pulverized shale sample was extracted using a mixture of methylene chloride/methanol in a Soxhlet extractor Tecator Soxtec System HT 2 1045 Extraction Unit. After the extraction, the solvent was

distilled and the soluble organic matter (SOM) was evaporated in a rotary evaporator, and the extracts were weighed. The extracts were later fractionated on silica gel column chromatography into saturate, aromatic, polar (NSO) fractions by successive additions of n-hexane, n-hexane/dichloromethane (4:1, v/v), and dichloromethane/methanol (1:1, v/v), respectively.

Gas chromatography—mass spectrometry

The saturate and aromatic fractions recovered from the liquid chromatography were analysed for their biomarkers by gas chromatography/mass spectrometry (GC/MS) using the selected ion monitoring mode (SIM). The fingerprints (fragmentograms) acquired from this analysis were identified by relative retention times from the GC/MS traces using 5b-Cholane and o-terphenyl standards for saturate and aromatic fractions, respectively, and quantifying of biomarkers was done by measuring peak heights. The chromatographic data were acquired using MS Chemstation software, version G1701BA, for Microsoft NT. The bitumen extraction, fractionation and GC/MS analyses were carried out at Exxon Mobil Geochemical Laboratory, Qua Iboe Terminal (QIT), Eket. The detailed analytical procedures can be obtained from Emordi [26].

Results and discussion

Organic matter quantity

The quantity of organic matter present in a rock can be expressed as a percentage of total organic carbon (TOC), which is a measure of the organic richness of a sample expressed as the percentage weight of the dry rock sample [27]. The TOC values for the samples range between 0.96 and 8.92wt% (Table 1). These values are above the 0.5 wt% minimum for clastic source rocks to generate hydrocarbons [27]. The SOM content ranged from 676 ppm to 2883 ppm (average: 1893 ppm), which indicates good to very good organic richness while the genetic potential (GP) values range from 1.18 mg HC/g to

Table 1: *Results of TOC and Rock-Eval Pyrolysis of the studied samples.*

Sample ID	Depth (m)	SOM (ppm)	TOC	S1	S2	S3	Tmax	Calc. %Ro	GP (S1 + S2)	HI	OI	SOM/TOC	S1/TOC	PI
S1	1240	676.12	1.14	0.13	1.11	2.23	423	0.45	1.24	97	196	59.31	11	0.10
S2	1340	2004.31	1.01	0.16	1.02	2.36	422	0.44	1.18	101	234	198.45	16	0.14
S3	1410	ND	1.19	0.16	1.31	2.78	425	0.49	1.47	110	234	ND	13	0.11
S4	1480	1417.71	1.41	0.19	1.93	2.55	428	0.54	2.12	137	181	100.55	13	0.09
S5	1560	ND	0.96	0.15	1.15	2.51	429	0.56	1.3	120	262	ND	16	0.12
S6	1620	2456.23	0.97	0.15	1.26	1.96	429	0.56	1.41	131	203	43.03	16	0.11
S7	1700	2883.85	1.02	0.21	1.66	2.79	427	0.53	1.87	163	274	13.04	21	0.11
S8	1760	1835.19	1.47	0.25	2.60	2.39	430	0.58	2.85	177	163	15.28	17	0.09
S9	1830	1599.37	1.94	0.34	5.84	2.51	426	0.51	6.18	301	129	11.96	18	0.06
S10	1906	1205.55	2.63	0.93	8.24	2.53	427	0.53	9.17	313	96	6.13	35	0.10
S11	1965	2698.84	1.91	1.00	4.11	2.51	431	0.60	5.11	215	131	23.64	52	0.20
S12	2040	1826.01	2.03	0.95	2.99	3.29	425	0.49	3.94	147	162	6.28	47	0.24
S13	2118	ND	1.18	0.39	2.94	2.30	429	0.56	3.33	249	195	ND	33	0.12
S14	2180	2143.91	1.15	0.63	3.25	2.79	422	0.44	3.88	283	243	186.43	55	0.16
S15	2257.5	1978.45	8.92	1.35	43.18	3.15	426	0.51	44.53	484	35	22.18	15	0.03

TOC = weight percent organic carbon in rock, GP = petroleum genetic potential
T_{max} = °C, HI = hydrogen index
S_1+S_2 = mg HC/g of rock, OI = oxygen index
S_3 = mg CO_2/g of rock, PI = production index = S1 / (S1+S2)
S_1/TOC = normalized oil content, Calc. % Ro = Calculated vitrinite reflectance
SOM = Soluble Organic Matter, ND = Not done

44.53 mg HC/g (average: 5.972 mg HC/g), indicating moderate to good source rock potential [27].

Organic matter type

The quality of organic matter content of a source rock determines the type of hydrocarbon generated [27]. Cross plots of hydrogen index versus oxygen index (OI) (Figure 4) show that the samples consist of types II and III kerogen, which indicates that the organic matter can generate both oil and gas at appropriate thermal maturity [28]. The cross plot of the remaining hydrocarbon potential (S2) against TOC (Figure 5) further supports type II/III (oil/gas prone) kerogen.

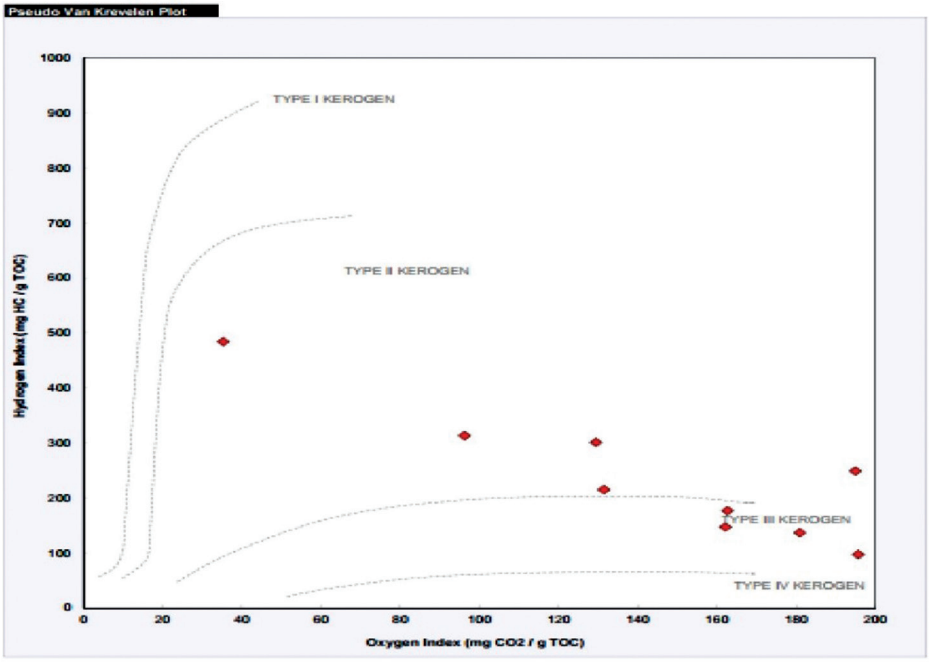

Figure 4: *A cross plot of hydrogen index (HI) versus oxygen index (OI) showing that the organic matter of the studied well is of types II and type III kerogen (Modified after Van Krevelen [29]).*

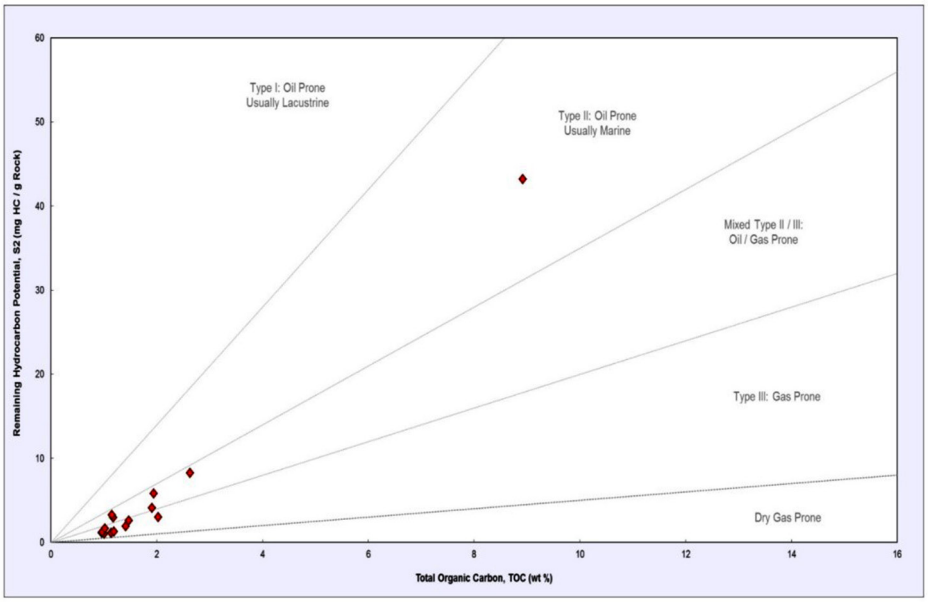

Figure 5: *A cross plot of remaining hydrocarbon potential (S2) against total organic content (TOC) showing the organic matter type and origin (after Jackson et al. [30]).*

Maturity of organic matter

The generation of petroleum from organic matter during its burial history is a part of the overall processes of thermal maturation of organic matter [27]. Thermal maturity describes the extent of heat-driven reactions, which convert sedimentary organic matter into petroleum [31]. In this study, the values of T_{max} ranged from 422°C to 431°C (average 426.6°C), indicating immature status for the studied well [31]. Similar values have been reported by Nton et al. [12] in sediments of the Aje-1 well, Eastern Dahomey Basin where T_{max} values that ranged from 359°C to 465°C indicated the immature to marginal maturity status of the well. Cross plots of HI against T_{max} (Figure 6) further revealed that >95% of the samples are immature. The calculated vitrinite reflectance R_o for this study ranged from 0.44 to 0.60 and lie in the immature status defined by Peters and Cassa [32].

The production index (PI) is defined as the ratio S1/ (S1 +S2) and is an indicator of the degree of thermal maturity. It is also an indication of the amount of hydrocarbon which has been produced geologically relative to the total amount of hydrocarbon that the sample can produce PI values of 0.03 – 0.24, indicated immature status for the sediments [31]. The ratio of extractable bitumen to total organic carbon (bitumen/TOC), sometimes called the transformation ratio (TR), is often used as a quantitative index to deduce the thermal maturity of sediments [31]. This ratio has been discovered to range from near zero in shallow sediments to about 250 mg/g TOC at the peak of oil generation. These values have also been observed to decrease at greater depths as a result of the conversion of bitumen to gas [31]. In the study well, the transformation ratio ranged from 22.18 to 282.73 mg/g TOC (average: 132.27) (Table 1), indicating immature to marginally mature status for the sediments. However, anomalous high figures observed in some of the samples may indicate contamination by migrated oil.

Normal alkanes and acyclic isoprenoids

The n-alkane data and biomarker maturity parameters were used to evaluate the level of thermal maturity of the sediments. Typical representative chromatograms showing distribution of n-alkanes and isoprenoids are shown in Figure 7. Using the chromatograms, parameters indicating source input, maturity, and depositional environment were generated as shown in Table 2.

The pristane/phytane (Pr/Ph) ratio, is one of the most commonly used geochemical parameters as an indicator of depositional environment, though with low specificity due to the interferences of thermal maturity and preliminary assessment of organic matter source

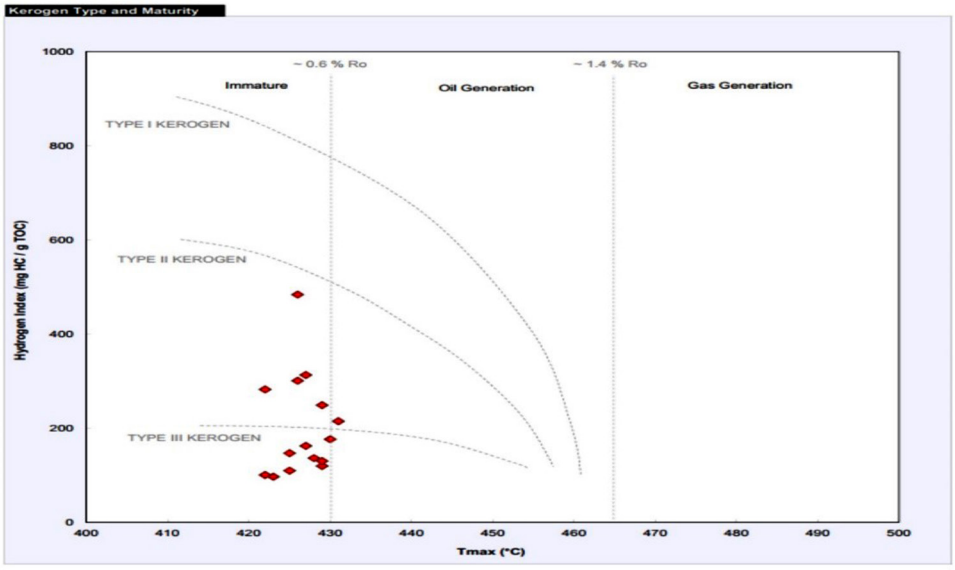

Figure 6: *Plot of hydrogen index (HI) against T_{max} showing that the kerogen is in the immature window [33].*

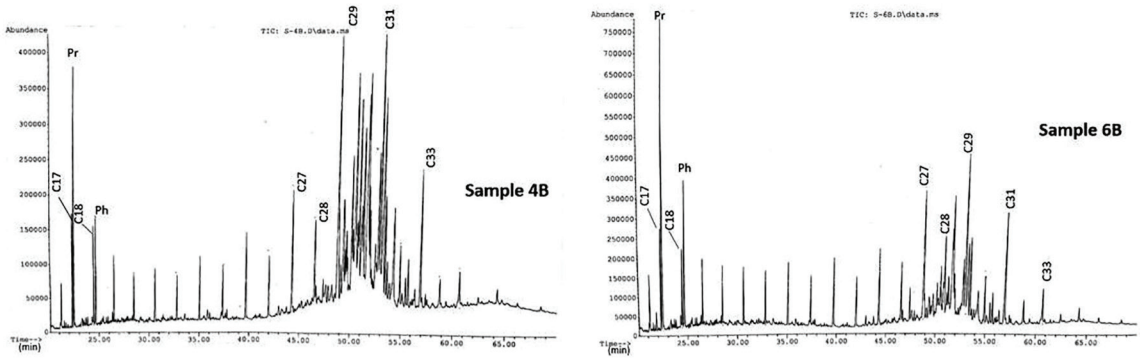

Figure 7: *Total ion chromatograms showing the distribution of the saturated hydrocarbon fraction of representative Samples 4B and 6B from the study well.*

Table 2: *Data showing values of isoprenoids, isoprenoids/n-alkane ratios and other parameters for EE-1 well.*

Sample ID	Pr/Ph	Pr/n-C_{17}	Ph/n-C_{18}	CPI	OEP-1	OEP-2
1B	1.47	0.98	0.62	1.93	0.51	0.83
2B	1.74	1.20	0.90	1.66	0.45	0.76
4B	2.38	2.41	1.08	1.70	0.51	0.8
6B	2.05	2.99	1.83	1.51	0.46	0.62
7B	3.20	2.42	1.40	1.67	0.53	0.7
8B	2.33	1.58	0.76	1.23	0.39	0.51
9B	1.49	2.31	1.55	1.27	0.47	0.49
10B	1.78	1.24	0.63	1.01	0.35	0.41
11B	2.20	0.99	0.51	1.12	0.39	0.44
12B	1.65	0.92	0.54	1.04	0.37	0.4
14B	1.94	0.60	0.46	0.37	0.4	0.08
15B	1.80	0.80	0.42	1.12	0.41	0.42

Abbreviations: Pr/Ph, pristane/phytane; Pr/nC_{17}, pristane/normal-C_{17} alkane; Ph/nC_{18}, phytane/normal-C_{18} alkane; CPI, carbon preference index, 2 (C_{23} + C_{25} + C_{27} + C_{29}) / (C_{22} + 2 C_{24} + C_{26} + C_{28}) + C_{30}); OEP-1, (C_{21} + C_{23} + C_{25}) / (4C_{22} + 4C_{24}); OEP-2, (C_{25} + C_{27} + C_{29}) / (4C_{26} + 4C_{28}); OEP, odd-to-even predominance.

inputs [34]. Ten Haven [35] stressed that high Pr/Ph (>3.0) indicates terrigenous input under oxic conditions, and low Pr/Ph (<0.8) indicates anoxic/hypersaline or carbonate environments. Values of Pr/Ph ranging from 1.47 to 3.20 (Table 2) indicate a mixed marine/terrigenous environment under suboxic to oxic conditions for the sediments. Cross plots of isoprenoids/n-alkanes (Figure 8) revealed that the samples are mainly in transitional environments with strong oxic influence and biodegraded.

The carbon preference index (CPI) and odd-even predominance (OEP) provide a crude estimate of source input, thermal maturity of petroleum, and dispersed organic matter [31, 36]. According to Hunt [37], CPI considerably greater than 1.0 shows contribution from terrestrial continental plants and immaturity. Over 90% of the samples have CPI >1% and strongly indicate terrestrial contribution and marine influence. The OEP values are less than 1.0 for all samples (Table 2), which further indicate low thermal maturity status of the well [38].

Biomarker geochemistry

The composition and distribution of certain diagnostic chemical fossils (biomarkers) can indicate the maximum stress experienced by

the rocks or petroleum in which the compounds are found [40]. Typical representative chromatograms showing distribution of steranes (m/z 217) and terpanes (m/z 191) from this study are shown in Figures 9 and 10. Using the chromatograms, an assessment of the thermal maturity levels was generated based on maturity parameters (Table 3).

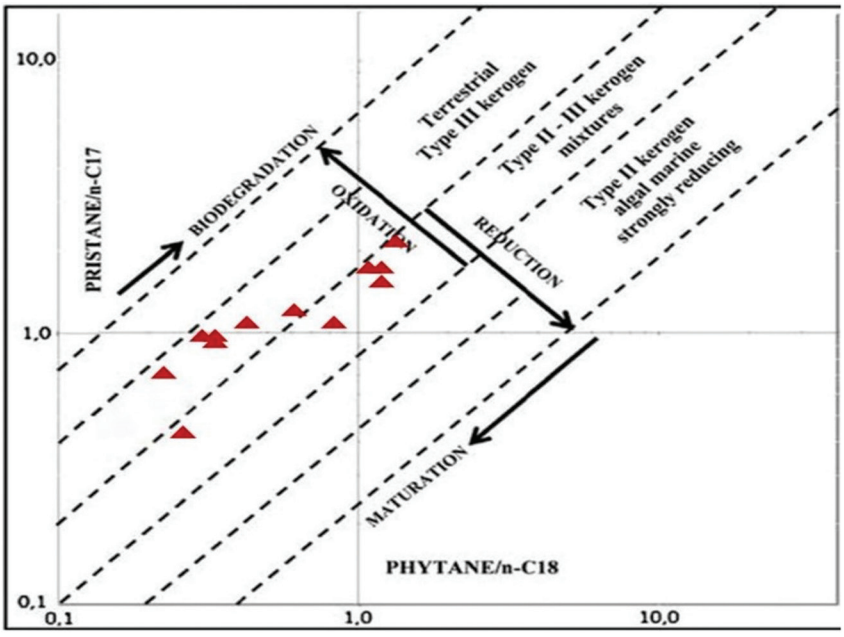

Figure 8: *Cross plot of Pr/n-C_{17} versus Ph/n-C_{18} showing the sources of organic matter and the depositional environment (Modified after Cortes et al. [39]).*

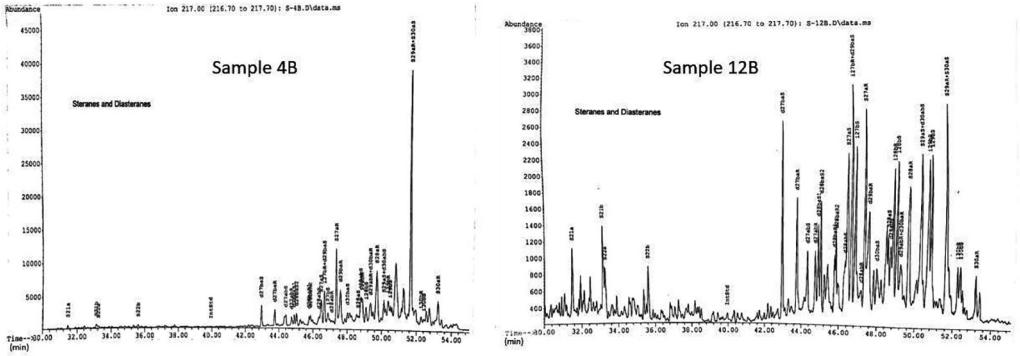

Figure 9: *m/z 217 mass chromatograms showing the distribution of steranes and diasteranes in the selected samples 4B and 12B.*

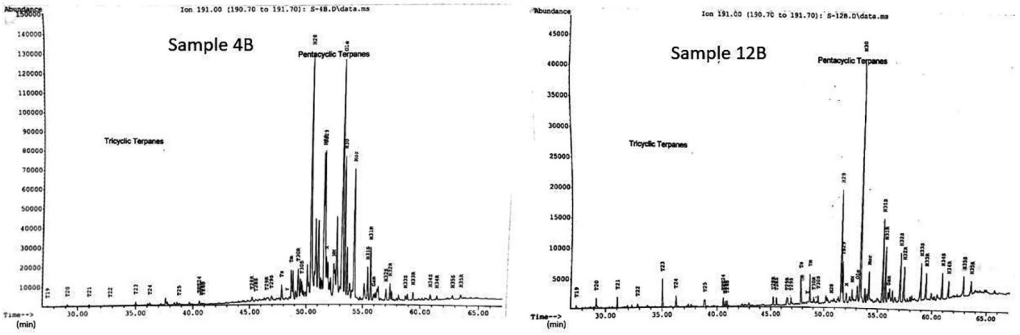

Figure 10: *m/z 191 mass chromatograms showing the distribution of terpanes and hopanes in the EE-1 Well samples 4B and 12B.12B.*

Table 3: *Biomarker maturity parameters computed for the studied well samples.*

Sample ID	Ts /Tm	Mor / Hop	αββ/ αββ+ααα C_{29} Sterane	22S/22S+22R	MPI-1	DMN	TMN-1	MDBT
1B	0.22	0.26	0.28	0.37	1.72	3.56	0.89	2.98
2B	0.25	0.26	0.25	0.34	1.46	2.96	0.73	3.35
4B	0.35	0.48	0.06	0.40	1.75	4.19	0.91	2.83
6B	0.32	0.29	0.21	0.38	1.37	4.04	1.13	3.11
7B	0.27	0.22	0.24	0.42	1.41	3.53	0.97	6.21
8B	0.34	0.18	0.23	0.46	1.35	2.25	1.06	1.81
9B	0.32	0.16	0.18	0.48	1.48	3.74	1.05	1.98
10B	0.35	0.14	0.30	0.57	1.12	3.01	1.17	0.82
11B	0.48	0.13	0.34	0.60	1.16	3.33	0.79	1.07
12B	0.50	0.11	0.44	0.58	1.01	3.25	0.67	1.51
14B	0.44	0.14	0.35	0.58	1.28	4.96	1.11	2.19
15B	0.45	0.10	0.42	0.59	1.32	4.36	0.79	1.47

Abbreviations: Ts/(Ts+Tm), trisnorneohopanes/trisnorhopanes ratio; Mor/Hop, 17β, 21α (H)Mortane/17 α, 21β (H) hopane ratio; 22S/22S+22R, 22S/22S+22R extended hopanes ratio; MPI-1 - methyl – phenanthrene index, 1,5 (2MP + 3MP) / (P + 1MP + 9MP); DMN – dimethyl naphthalene ratio, 2, 6 DMN + 2,7 DMN)/1,5 DMN; TMN-1 – trimethyl naphthalene ratio, (1,3,7 TMN)/ (1,3,7 TMN + 1,2,5 TMN); MDBT – methyl-dibenzothiopene ratio, 4MDBT/1MDBT.

The Ts/Tm ratio is used as a maturity indicator, because C_{27} 18α-trisnorneohopane, or Ts, exhibits greater thermal stability than its regular hopane counterpart, C_{27} 17α-trisnorhopane, or Tm, although the ratio is also source dependent [34]. The Ts/Tm values for the study well ranged from 0.22 to 0.5 (Table 3), indicating the immaturity status of the samples. The moretane/hopane ratio ranged from 0.10 to 0.48 and point to an immature to marginally mature status of the study well. The 20S/(20S + 20R) C_{29} steranes αββ/ααβ + ααα and 22S/(22S + 22R) extended hopanes, which are used as maturity indicators, were computed for the study well. An equilibrium value of 0.55 for 22S/(22S + 22R) extended hopanes ratio corresponds to the onset of hydrocarbon generation, while > 0.5 20S/(20S + 20R) C_{29} steranes αββ/ααβ + ααα signifies thermal maturity [31]. The values of the 20S/(20S + 20R) C_{29} steranes αββ/ααβ + ααα and 22S/(22S + 22R) extended hopanes ratios ranged from 0.06 to 0.44 and 0.34 to 0.6 (Table 3), respectively, supporting the low maturity status of the study well. Calculated aromatic biomarker parameters such as MPI-1 (methyl phenanthrene index), DNR-1 (dimethyl naphthalene ratio), TMNR (trimethyl naphthalene ratio), and MDR (methyl dibenzothiophene ratio) ranged from 1.01 to 1.72, 2.96 to 4.96, 0.67 to 1.17, and 0.82 to 6.21, respectively (Table 3). These values indicate that the samples are immature to marginally mature [41].

Depositional environment

Biomarkers provide information about the depositional environment of organic matter, the conditions during deposition as well as the lithology in which the organic matter is present [31]. Source and depositional environment parameters computed from the saturate biomarkers of the studied well are shown in Table 4.

The samples were characterized by the presence of C_{27} to C_{29} steranes and disateranes, which indicate derivation from mixed sources (marine and terrestrial) with capacity to generate both oil and gas. A ternary plot (Figure 11) showing sterane distributions and relationship with source indicates dominance of C_{29} over C_{27} and C_{28} and suggests a mixture of marine and terrigenous biomass to the study well, with stronger terrigenous input. The presence of oleananes, a biomarker for higher plants (angiosperms), strongly supports a terrestrial precursor for the studied well [42]. The distribution of 17α, 21β (H)—homohopanes 22R + 22S $C_{35}/(C_{31}–C_{35})$, also known as the homohopane index, can be used as an indicator of the redox potential

Table 4: *Source and depositional environment parameters computed from the saturate biomarkers of the EE-1 well.*

Sample ID	%C_{27} Sterane	%C_{28} Sterane	%C_{29} Sterane	$C_{21}T$/ $C_{23}T$	$C_{23}T$/ $C_{24}T$	Hop/ Ster	dia/ reg	Ole/ Hop	Gam/ Hop	C_{24} Tet / (C_{26} (S+R) + C_{24} Tet)	C_{25}/ C_{26} (S+R)	C_{35}/ C_{31}-C_{35} Hom
1B	33.50%	19.68%	46.82%	0.58	1.49	4.13	0.18	0.1	0.08	0.52	0.69	0.06
2B	34.79%	22.11%	43.10%	0.8	1.59	2.99	0.15	0.11	0.1	0.49	0.54	0.14
4B	27.36%	19.31%	53.33%	0.49	1.33	1.98	0.28	0.62	0.04	0.6	0.48	0.05
6B	33.10%	20.73%	46.18%	0.82	1.66	1.62	0.21	0.42	0.05	0.62	0.89	0.05
7B	33.35%	20.97%	45.68%	0.78	1.39	3.65	0.27	0.29	0.04	0.67	0.48	0.05
8B	36.81%	21.02%	42.17%	0.62	1.73	4.1	0.23	0.33	0.04	0.64	0.41	0.05
9B	36.85%	25.19%	37.96%	0.55	1.98	1.53	0.13	0.21	0.04	0.6	0.44	0.07
10B	40.18%	25.85%	33.97%	0.33	3.45	6.04	0.33	0.07	0.04	0.52	0.69	0.09
11B	38.09%	24.36%	37.55%	0.39	3.1	11.45	0.42	0.04	0.03	0.72	0.67	0.06
12B	38.86%	27.19%	33.95%	0.36	2.57	16.11	0.48	0.06	0.04	0.45	0.67	0.09
14B	36.49%	23.80%	39.71%	0.46	1.91	6.27	0.35	0.14	0.06	0.5	0.56	0.11
15B	37.53%	41.63%	45.42%	0.37	1.92	6.91	0.38	0.08	0.09	0.45	0.63	0.17

Abbreviations: Ole/Hop, oleanane index; Hop/Ster, hopane/sterane ratio; dia/reg, diasterane index; Gam/Hop, gammacerane index; C_{35}/C_{31}-C_{35} Hom, homohopane index; C_{25}/C_{26}(S+R), C_{25}/C_{26}(S+R) trycyclic terpane ratio; C_{24} Tet / (C_{26} (S+R) + C_{24} Tet), tetracyclic terpane ratio.

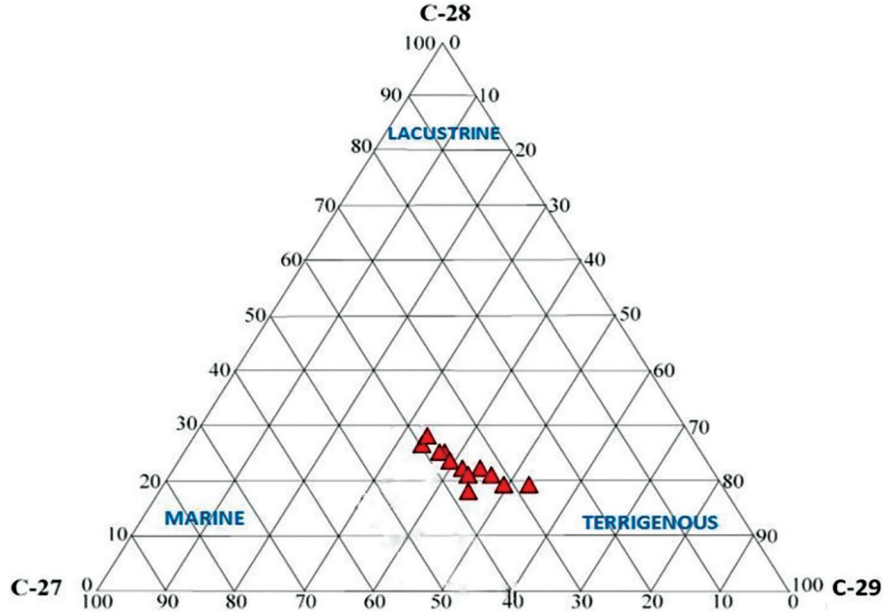

Figure 11: *Ternary plot showing distribution of C_{27}, C_{28}, and C_{29} steranes for EE-1 Well. (After Huang and Meinschein [49]).*

during and immediately after the deposition of the source sediments [31]. The studied samples have a low homohopane index (0.05 – 0.17) (Table 4), which suggests a suboxic depositional environment [43].

The 17α (H)-hopanes/regular steranes ratio reflects input of prokaryotic (bacteria) versus eukaryotic (mainly algae and higher plants) organisms to the source rock. The hopane/ sterane ratio values for the well sediments

ranged from 1.53 to 16.11, indicating both terrigenous and marine organic matter input. It has been suggested by Qiuhua et al. [44] that C_{21}/C_{23} trycyclic terpane ratios < 0.5 are indicative of marine-sourced organic matter. In this study, this ratio ranged from 0.33 to 0.82, further indicating a mixed marine and terrigenous input to the sediments. The values of the gammacerane index ranged from 0.03 to 0.10 (Table 4), indicating a normal salinity environment of deposition of the initial organic matter [45]. The tetracyclic terpane ratio – C_{24} Tet / (C_{26} (S+R) + C_{24} Tet) – ranged from 0.45 to 0.72 (average: 0.57), indicating a low salinity environment of deposition for the study well [31]. The abundance of 1, 2, 5-TMN (trimethyl naphthalene) observed in the samples has been reported to be indicative of significant land plant contribution to the organic matter [46, 47]. In addition, the occurrence of 1, 7-DMP (dimethyl phenanthrene) in the analyzed samples indicates a strong terrestrial organic matter input for the sediments [48].

Conclusions

Subsurface samples from EE-1 Well, offshore Eastern Dahomey Basin, have been analysed for their lithofacies distribution, hydrocarbon potentials, and paleodepositional environment based on Rock-Eval studies and biomarker evaluation. The sediments have adequate to excellent source rock potential. Organic matter type indicated the presence of mainly types II and III kerogen, implying a prospect to generate both oil and gas at appropriate thermal maturity. Evaluations of saturate and aromatic biomarker parameters indicate the thermal immaturity status, organic matter of mixed terrigenous and marine origin with higher terrigenous input, as well as deposition under oxic – suboxic conditions. It can be deduced that the sediments have adequate organic richness, deposited under mixed marine/terrigenous environment under oxic – suboxic conditions with significant terrestrial organic matter input and potential to generate both oil and gas at appropriate thermal maturity.

Acknowledgements

The authors thank the members and staff of Geomark Research Lab, Humble, Texas for their technical assistance in analyses. We are grateful to the management and staff of Exxon Mobil Geochemistry Lab, Qua Iboe Terminal, Eket for permission to use its laboratory facilities for some aspects of the work. Special thanks to Dr. Babatunde Alalade and Dr. Chidi Eneogwe, for all their assistance during different phases of this work.

References

[1] Obaje, N.G. (2009): *Geology and Mineral Resources of Nigeria*. Springer: Berlin, 221 pp.

[2] Nton, M.E. (2001): *Sedimentological and geochemical studies of rock units in the Eastern Dahomey Basin, Southwestern Nigeria*. Ph.D Thesis. University of Ibadan, Faculty of Science, Department of Geology: Ibadan, 315 pp.

[3] Adekeye, O.A., Akande S.O. (2010): The principal source rocks for petroleum generation in the Dahomey Basin, Southwestern Nigeria. *Continental Journal of Earth Sciences*, 5(1): ISSN: 2141–4076, pp. 42–55.

[4] Adegoke, O.S. (1969): Eocene stratigraphy of Southern Nigeria. *Bulletinin Bureau de Research Geologic ET Miners Memoir*, 69, pp. 23–48.

[5] Omatsola M.E., Adegoke O.S. (1981): Tectonic evolution and Cretaceous stratigraphy of the Dahomey Basin. *Journal of Mining and Geology*, 18, pp. 130–137.

[6] Jan Du Chene, R.E., Salami, M.B. (1978): Palynology and micropaleontology of the Upper Eocene of the well Nsukka-1 (Niger Delta). *CompteRendu des Séances de la Société de Physique etd'HistoireNaturelle de Genève*, 13, pp. 5–9.

[7] Ekweozor, C.M. (1990): Geochemistry of Oil Sands of Southwestern Nigeria. In: *Occurrences, Utilization and Economics of Nigeria Tar Sands*, Ako, B.D., Enu, E.I. (eds). *Nigeria Mining and Geosciences Society Publication on Tar Sands Workshop*, Ago-Iwoye, pp. 50–62.

[8] Billman, H.G. (1992): Offshore stratigraphy and paleontology of Dahomey (Benin) Embayment. *NAPE Bulletin*, 70(2): pp. 121–130.

[9] Okosun, E.A. (1998): Review of the Early Tertiary stratigraphy of Southwestern Nigeria. *Journal of Mining and Geology*, 34(1), pp. 27–35.

[10] Elueze, A.A., Nton, M.E. (2004): Organic geochemical appraisal of limestones and shales in part of Eastern Dahomey Basin, Southwestern Nigeria. *Journal of Mining and Geology*, 40, pp. 29–40.

[11] Brownfield, M.E., Charpentier, R.R. (2006): Geology and total petroleum systems of the West-Central Coastal Province (7203), West Africa. *U.S. Geological Survey Bulletin* 2207-C, 52 pp.

[12] Nton, M.E., Ikhane, P.R., Tijani, M.N. (2009): Aspect of rock-eval studies of the Maastrichtian-Eocene sediments from subsurface in the Eastern Dahomey Basin, Southwestern Nigeria. *European Journal of Scientific Research*, 25(3), pp. 417–427.

[13] Kaki C., d'Almeida G.A.F., Yalo, N., Amelina, S. (2013): Geology and petroleum systems of the offshore Benin Basin (Benin). *Oil & Gas Science and Technology - Rev. IFP Energies nouvelles*, 68 (2), pp. 363–381.

[14] d'Almeida, G.A.F., Kaki, C., Adeoye, J.A. (2016): Benin and Western Nigeria Offshore Basins: A Stratigraphic Nomenclature Comparison. *International Journal of Geosciences*, 7, pp. 177–188.

[15] Billman, H.G. (1976): Offshore stratigraphy of the Dahomey embayment, West Africa. *7th African Micropaleontology College*, pp. 16–17.

[16] Nwajide, C.S. (2013). *Geology of Nigeria's Sedimentary Basins. CSS Bookshop Ltd: Lagos, Nigeria*, 565 pp.

[17] Kingston, D.R., Dishroon, C.P., Williams, P.A. (1983): Global basin classification system. American Association of Petroleum Geologists Bulletin, 67, pp. 2175–2193.

[18] Burke, K.C., Dessauvagie, T.F.J., Whiteman, A. J. (1972): Geological history of the Benue Valley and adjacent areas. In: *African Geology*, Dessauvagie, T.F.J., Whiteman, A.J. (eds.). University of Ibadan Press: Ibadan, Nigeria, pp. 187–218.

[19] Jones, H.A., Hockey, R.D. (1964): The geology of part of Southwestern Nigeria. *Geological Survey Bulletin*, 31, pp. 1–101.

[20] Enu, E.I., Adegoke, O.S. (1988): Microfacies of shallow marine carbonates (Paleocene) in the Eastern Dahomey Basin, Southeastern Nigeria. *Journal of Mining and Geology*, 24, pp. 89–97.

[21] Fayose, E.A., Asseez, L.O. (1972): Micropalaeontological investigations of Ewekoro Area, Southwestern Nigeria. *Micropaleontology*, 18, pp. 369–385. http://dx.doi.org/10.2307/1485014

[22] Adebiyi, A.O. (2015): Upper Cretaceous to Paleogene palynosequence stratigraphy of H-1 well offshore Eastern Dahomey Basin, Southwestern Nigeria. *International Journal of Research and Innovations in Earth Science* (IJRIES), 2, pp. 82–88.

[23] Ogbe, F.G.A. (1972): Stratigraphy of strata exposed in the Ewekoro quarry, Western Nigeria. In: *African Geology*, Dessauvagie, T.F.J., Whiteman, A.J. (eds.). University of Ibadan Press: Ibadan, Nigeria, pp. 305–322.

[24] Coker, S.J.L. (2002): Field excursion guide to tar sand outcrops in Benin Basin. *Nigerian Association of Petroleum Explorationists Mini-Conference*, 32 p.

[25] Olabode, S.O. (2006): Siliciclastic slope deposits from the Cretaceous Abeokuta Group, Dahomey (Benin) Basin, Southwestern Nigeria. *Journal of African Earth Sciences*, 46, 187–200. http://dx.doi.org/10.1016/j.jafrearsci.2006.04.008.

[26] Emordi, E.E. (2021): *Hydrocarbon Potential, Biomarker Evaluation and Palynological Studies of EE-1 Well, Offshore Eastern Dahomey Basin, Southwestern Nigeria*. MSc Thesis, University of Ibadan, Faculty of Science, Department of Geology: Ibadan, Nigeria, 120 pp.

[27] Tissot, B.P., Welte, D.H. (1984): *Petroleum formation and occurrence*, 2nd ed. Spinger Verlag: Berlin, 699 pp.

[28] Peters, K.E. (1986): Guidelines for evaluating petroleum source rocks using programmed pyrolysis. *AAPG Bulletin*, 70, pp. 318–329.

[29] Van Krevelen, D.W. (*1961*): *Coal typology, chemistry, physics and constitution*. Elsevier: Amsterdam, 514 p.

[30] Jackson, J.M., Powell, T.G., Summons, R.E., Sweet, I.F. (1986): Hydrocarbon shows and petroleum source rocks in sediments as old as 1.7 x lO'years. *Nature*, 322, pp. 727–729.

[31] Peters, K.E., Moldowan, J.M. (1993): *The Biomarker Guide; Interpreting Molecular Fossils in Petroleum and Ancient Sediments*. Prentice Hall: Englewood Cliffs, New Jersey, 363 pp.

[32] Peters, K.E., Cassa, M.R. (1994): Applied source-rock geochemistry. In: *The Petroleum System, From Source to Trap*, Magoon, L.B., Dow, W.G., (eds.). AA PG Memoir, American Association of Petroleum Geologists: Tulsa, OK, USA. 60, pp. 93–120. DOI: https://doi.org/10.1306/M60585C5

[33] Jackson, K.S., Hawkins, P.J., Bennett, A.J.R. (1985): Regional facies and geochemical evaluation of Southern Denison Trough. *Australian Petroleum Exploration Association Journal*, 20, pp. 143–158.

[34] Peters, K.E., Walters, C.C., Moldowan, J.M. (2005): Biomarker guide: Biomarker and isotopes in

petroleum exploration and earth history. Cambridge: Cambridge University, 1155 pp.

[35] Ten Haven, H.L. (1996): Applications and limitations of mango's light hydrocarbon parameters in petroleum correlation studies. *Organic Geochemistry*, 24, pp. 957–976.

[36] Bray, E.E, Evans, E.D. (1961): Distribution of n-paraffins as a clue to recognition of source beds. *Geochimica et Cosmochimica Acta*, 22, pp. 2–5.

[37] Hunt, J.M. (1979): *Petroleum geochemistry and geology*. W.H. Freeman and Company: San Francisco, California, 617 p.

[38] Scalan E.S., Smith, J.E. (1970): An improved measure of the odd-even predominance in the normal alkanes of sediment extracts and petroleum, *Geochimica et Cosmochimica Acta*, 34(5), pp. 611–620.

[39] Cortes, J.E., Niñoa, J.E., Poloa, J.A., Toboa, A.G., Gonzaleza, C., Siachoquea, S.C. (2013): Molecular organic geochemistry of the Apiay field in the Llanos Basin, Colombia. *Journal of South American Earth Sciences*, 47, pp. 166–178.

[40] Ekweozor, C.M., Strausz, O.P., (1982): Tricyclic terpanes in Athabasca oil sands: their geochemistry, In: *Advances in Organic Geochemistry*, Bjoroy, M. (ed). J. Wiley and Sons: New York, pp. 746–766.

[41] Radke, M., Welte, D.H., Willsch, H. (1986): Maturity parameters based on aromatic hydrocarbons: influence of the organic matter type. *Organic Geochemistry*, 10, pp. 51–63.

[42] Ekweozor, C.M., Udo, O.T. (1987): The oleananes: origin, maturation and limits of occurrence in Southern Nigeria sedimentary basins. In: *Advances in Organic Geochemistry*, Mattavelli, L., Novelli L., (eds.). Pergamon Press: Oxford, pp. 131–140.

[43] Moldowan, J.M., Sundararaman, P., Schoell, M. (1986): Sensitivity of biomarker properties to depositional properties and/or source input in the Lower Toarcian of S.W. Germany. *Organic Geochemistry*, 10, pp. 915–992.

[44] Qiuhua, Y., Zhigang, W., Youjun, T. (2011): Geochemical characteristics of Ordovician crude oils in the northwest of the Tahe Oil Field, Tarim Basin. *Chinese Journal of Geochemistry*, 30, pp. 93–98.

[45] Xia, G., Ji, C., Chen, L., Yi, H. (2017): Biomarkers of the lower Jurassic black shale in the Shuanghu area of the Qiangtang Basin, northern Tibet, and their geological significance. *Oil Shale*, 34, (1), pp. 55–69.

[46] Strachan, M.G., Alexander, R., Kagi, R.I. (1988): Trimethylnaphthalenes in crude oils and sediments: Effects of source and maturity. *Geochimica Cosmochimica Acta*, 52, pp. 1255–1264.

[47] Sonibare, O.O., Adedosu, T., Ekundayo, A.O., Jarvie, D.M. (2008): Hydrocarbon potential and organic geochemistry of coals from Benue Trough, Nigeria. *Journal of Applied Sciences Research*, 4(11), pp. 1511–1520.

[48] Simoneit, B.R.T. (1986): Cyclic terpenoids of the geosphere. In: *Biological Markers in the Sedimentary Records*, Johns, R.B. (ed.). Elsevier Science Publishers: Amsterdam, pp. 43–99.

[49] Huang, W.Y., Meinschein, W.G. (1979): Sterols as ecological indicators. *Geochimica et Cosmochimica Acta*, 43, pp. 739–745.

Original Scientific Article • DOI: 10.2478/rmzmag-2021-0010

Received: October 16, 2021
Accepted: January 11, 2022

Improvement of Blast-induced Fragmentation Using Artificial Neural Network and BlastFrag© Optimizer Software

Izboljšanje učinka vpliva miniranja na fragmentacijo z uporabo umetne nevtronske mreže in napredne programske opreme

Blessing Olamide Taiwo*, Babatunde Adebayo
Department of Mining Engineering, Federal University of Technology, Akure, Nigeria
*Corresponding author: E-mail: taiwoblessing199@gmail.com

Abstract in English

The Golden Girl dolomite quarry was selected by the authors to develop predictive artificial neural network (ANN) models and software for optimization of blast fragment size distribution. Blast images from the quarry were analysed using WipFrag©. Seven controllable and two uncontrollable blast parameters, and WipFrag© image analysis results for fifty blasts were used to train ANN models. The reliability of the established models was tested, and the Bayesian regularization algorithm with the architecture of 9-8-3 was found to be superlative. The superlative model was compared with the modified Kuz-Ram model and found to be accurate. The optimum ANN models were translated into mathematical formulas and used to develop user-friendly software called BlastFrag optimizer. The software was validated with R^2 greater than 80% for all models and was found suitable for predicting blast fragment size distribution. The optimized result revealed that percentages for oversize and mean-size fragments were reduced from 68.4% and 418 mm to 27.83% and 101.6 mm, respectively, and undersize fragments increased from 50% to 72.17%.

Keywords: blasting, muck-pile, fragment size, ANN model, Bayesian regularization

Abstract in Povzetek

V članku je predstavljen razvoj napovednega modela z uporabo umetne nevronske mreže ANN (ang. Artificial Neural Network) in programske opreme za optimizacijo porazdelitve velikosti fragmentacije miniranja na primeru kamnoloma dolomita. Slike iz miniranja v kamnolomu so bile analizirane z uporabo programske opreme WipFrag©. Za usposabljanje modela ANN je bilo uporabljenih sedem nadzorovanih in dva nenadzorovana parametra miniranja ter slikovna analiza WipFrag© za 50 odstrelov. Preizkušena je bila zanesljivost modelov. Izkazalo se je, da je bajezijski algoritem z arhitekturo 9-8-3 superlativen. Superlativni model je bil primerjan z modificiranim modelom Kuz-Ram, ki je bil natančen. Optimalni modeli ANN so bili prevedeni v matematične formule in uporabljeni za razvoj uporabniku prijazne programske opreme, imenovane BlastFrag optimizer. Razvita programska oprema je bila potrjena z R^2 večjim od 80 % za vse modele. Ugotovljeno je bilo, da je primerna za napovedovanje porazdelitve velikosti fragmentacije miniranja. Optimizirani rezultat je pokazal, da se je odstotek s preveliko in povprečno velikostjo delcev zmanjšal iz 68,4 % oziroma 418 mm na 27,83 % oziroma 101,6 mm ter odstotek s premajhno velikostjo delcev zvišal s 50 % na 72,17 %.

Ključnebesede: miniranje, odstreljen material, velikost fragmentacije, ANN model, bajezijska regularizacija

Introduction

The profitability of a blasting operation depends on the ability of the mining engineer to produce a fragment size distribution as close as possible to the optimal range for downstream operations. In practical terms, *oversize* is defined as size ranges greater than the crusher's gape and that therefore require secondary breakage before further handling. In hard rock mining strategies, drilling and blasting are the most broadly utilized techniques for fragmenting the rock in preparation for transportation and stock-piling [1]. Sang and Katsuhiko [1] defined an optimal blast as that which yields the predetermined fracture size dispersion by means that are compatible with safety ecological, and financial guidelines. An ineffectively initiated rock blast would most likely end in useless fracture and may create dangerous impacts like fly rocks, ground vibration, air impact, and back break [2]. The presence of boulders in the blasted muck causes problems in production, and additionally increases the expense of hauling. Everything considered, the expense and effectiveness of mucking, stacking, and comminution (crushing and granulating) operations will be profoundly impacted by the outcome of the blasting operation. A few fragmentation-estimating techniques are available [3], some of which incorporate oversized rock count techniques, sieving, visual investigation, and scoop stacking rate as well as picture examination strategies [1, 4–6]. The research reported here uses WipFrag as an example of a picture examination strategy for the investigation of blasting operations. The drilling and blasting activities have huge significance in the productivity of mining operations. The high degree of automation and coordination that define the nature of the production framework embraced in the mining industry require precise planning so that all units work dependably to achieve the projected production targets [7].

Although some efforts have been made to further develop insightful, experimental, and soft computing approaches that would positively impact results [2, 8–9], less consideration has been given to small-scale and artisanal miners whose blast operations depend on the use of pneumatic, hand-held jackhammer drill holes. It is important that more consideration be given to limited, small-scale mine blast design because the generation of oversized fragments during blasting affects the economy and efficiency of the downstream tasks. This can be achieved by using available fragmentation prediction software and models to anticipate the fragment size distribution resulting from a particular set of blasting parameters. However, the cost of buying the available software packages is too high for local mining industries. Therefore, this research was initiated in order to develop a blasting optimization software application that could predict the percentage of oversized, undersized, and mean particle size resulting from a blast.

Materials and Methods

In order to develop the models, blasting data that include controllable and uncontrollable factors related to different blasts were used to cover a wide range of values for the following parameters: burden (B), spacing (S), hole depth (H), drill hole diameter (D), stemming length (T), powder factor (K), uniaxial compressive strength (U), rock density (M), and charge weight (W). A total of 50 blasting operations were monitored in Golden Girl Quarry (10 blasts from Gate axis, 5 blasts from Zack axis, 5 blasts from S.K axis, 21 blasts from Timothy axis, 5 blasts from akakagbe axis, 4 blasts from golden building axis). The quarry is located at the Akoko Edo local government area, Edo state, Nigeria as shown in Figure 1. Blast images were analysed with WipFrag© software. Intact rock samples were collected from blasts using the grab-sampling method. The samples were tested for uniaxial compressive strength and density according to The International Society for Rock Mechanics (ISRM) methods[10]. A database of WipFrag analyses and blast parameters obtained from the monitored blasts is presented in Tables 1 through 3, which will enable general application of the proposed model The data set was trained and validated using ANN and a modified Kuz-Ram model. The generated models were used to develop the BlastFrag optimizer software, which was adopted for the optimization of the Golden Girl Quarry blasting operation.

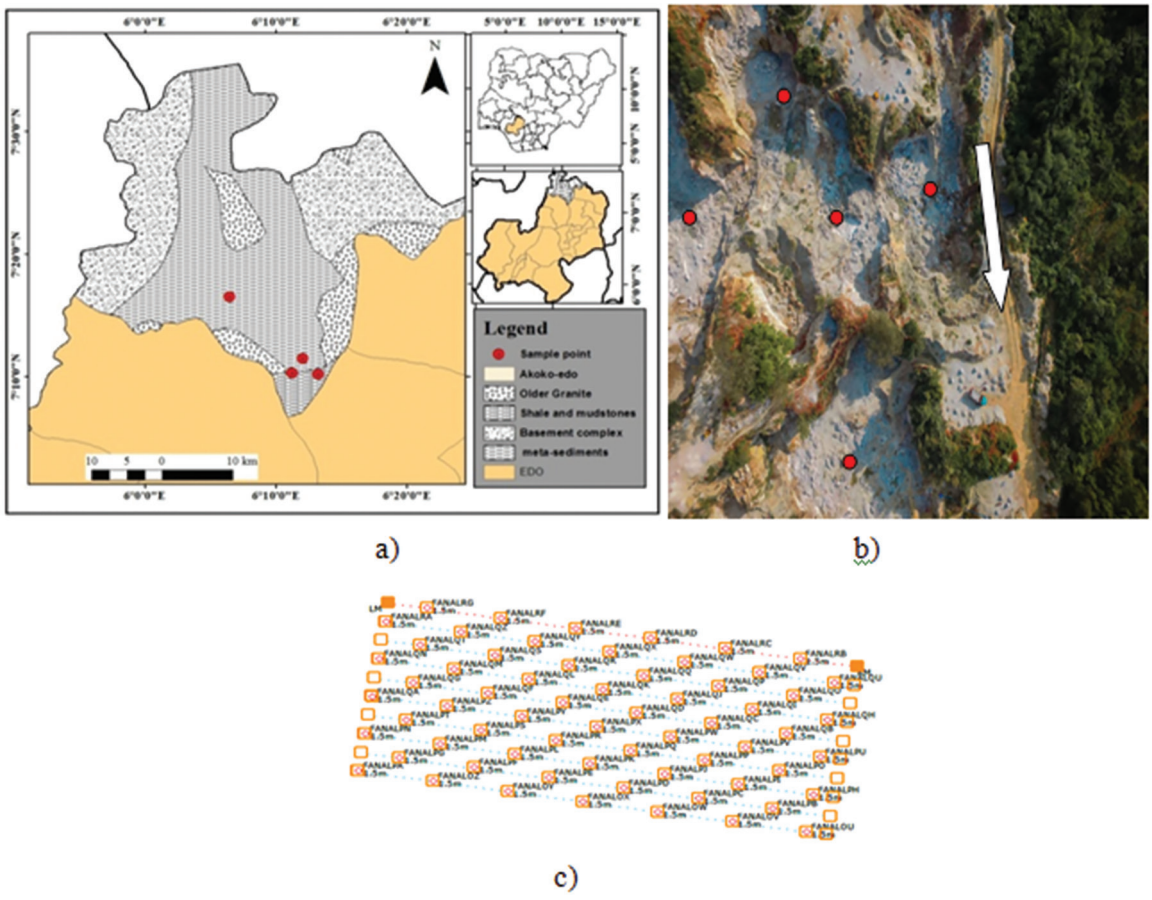

Figure 1: *a) Geological map of Akoko Edo, showing case study area. b) Quarry face showing the sampling points marked with red circles. c) Quarry scheme of the drilling patterns.*

Table 1: *Explosive data and information about the quarry*

Parameter	Pit 1	Pit 2	Pit 3	Pit 4	Pit 5	Pit 6
Charge length (m)	0.65-0.7	0.67-0.76	0.6-0.76	0.6-0.7	0.6-0.78	0.6-0.8
Type of explosive	Dynogel	Dynogel	Dynogel	Dynogel	Dynogel	Dynogel
Density of ANFO (kg/m^3)	820	820	820	820	820	820
Density of explosive (kg/m^3)	1190	1190	1190	1190	1190	1190
Powder factor (kg/m^3)	0.8-0.0.9	0.0.7-0.8	0.5-0.6	0.5-0.86	0.6-1.0	0.7-0.85
RWS	1.45	1.45	1.45	1.45	1.45	1.45
VOD (m/s)	5250	5250	5250	5250	5250	5250
Explosive strength	1.45	1.45	1.45	1.45	1.45	1.45

Rock properties

The rock properties were determined in the laboratory following the method suggested by ISRM [11] and conform to ISRM standards [10].

Fragmentation analysis

In the mining industry, accurate fragmentation measurement can be used to evaluate the behaviour and efficiency of explosive energy

Table 2: *Blast design parameters for the quarry*

Parameter	Pit 1	Pit 2	Pit 3	Pit 4	Pit 5	Pit 6
Burden (m)	0.7	0.82	0.85	0.85	0.7	0.85
Spacing (m)	0.85	0.96	1.10	1.1	1.0	1.1
Hole depth (m)	1.25	1.3	1.35	1.3	1.35	1.35
Drill pattern	staggered	Staggered	staggered	staggered	staggered	square
Hole diameter (m)	0.04	0.04	0.04	0.04	0.04	0.04
Drill hole depth (m)	1.25	1.3	1.35	1.3	1.35	1.3
Stemming (m)	0.65	0.7	0.66	0.66	0.7	0.6
Drilling accuracy	0.054	0.054	0.054	0.054	0.054	0.054
Charge length (m)	0.65-0.7	0.67-0.76	0.6-0.76	0.6-0.7	0.6-0.78	0.6-0.8
Charge weight (kg)	0.96-1.02	0.80-0.95	0.9-1.14	0.8-0.85	0.6-0.8	0.65-0.85
Crusher gap (m)	0.28	0.28	0.28	0.28	0.28	0.28

Table 3: *Summary of the rock characterization of Golden Girl Quarry*

Parameter	Pit 1	Pit 2	Pit 3	Pit 4	Pit 5	Pit 6
Uniaxial compressive strength (MPa)	173.75	178.75	171.25	167.75	168.75	186.25
Joint spacing (m)	0.76	0.26	0.64	0.20	0.32	0.28
Dip direction (^{0})	298	312	260	034	312	064
Dip angle (^{0})	58	30	74	42	48	78
Rock density (kg/m^3)	2804	2790	2886	2760	2860	2800
Young modulus (GPa)	60	75	75	68.5	60	75

released during charge detonation for rock blasting. Maerz and Germain [12] established that fragmentation analysis can be used along with in situ block size to evaluate the productivity of blasting and the accuracy of blasting simulations. It can be used to reduce downstream production costs and to improve the mine production rate [13].

WipFrag system

WipFrag is a picture examination framework for sizing materials, for example, blasted or crushed stone heaps; it has likewise been found to be appropriate for assessing the molecular transport of ammonium nitrate prills, glass dabs, and zinc concentrate for an accurate fixation measurements. WipFrag estimates 2-D net and reproduces 3-D dispersion utilizing the standard of geometric likelihood [14]. Maerz [15] established that WipFrag is a state-of-the-art, image-based granviometry system designed primarily for high-contrast graytone images, despite the fact that it can also evaluate hued prints. Pictures are uploaded to the software, which changes the picture into a parallel picture comprising a net of square diagrams as displayed in Figure 2b. Fifty blast images were collected using after-blast image capturing with a scaling object in place (0.5 m by 0.5 m, white helmet and 1 m by 1 m frame as shown in Figure 2a. Maerz et al. [16] established three analysis methods using WipFrag, including basic, calibrated, and zoom merge methods. The zoom merge method was recommended by Maertz et al. [16] as accurate and was used in this paper for blast image analysis.

The WipFrag analysis as shown in Figure 2c was performed for each blast using the case study primary jaw crusher gape size as the base limit to calculate the percentages of undersized and oversized fragments with "undersized" defined as fragments that pass through the gape and "oversized" being fragments that are retained without passing through the gape.

Artificial neural network model development

Artificial neural networks (ANNs) are systems modelled on the human brain that attempt to simulate the functioning of the human cerebrum and sensory system. Simpson [17] defined ANNs as computational models inspired by natural neural organization that are used to assess large amounts of information with complex interactions, that is, structured as networks rather than as linear interactions. Construction of an ANN has three major components: transfer function, network design, and learning law [17]. Kosko [18] explains that ANNs are created from calculations based on natural standards. Execution of the ANN network model relies upon the neuron connections and network's architecture [19], which can be designed with neurons connected in multiple ways. The adoption of the feed-forward approach was suggested by Shahin et al. [20] to solve extremely nonlinear dependent parameters that are not involved in the input variables. The multilayer perception (MLP) neural network is a well-recognized feed-forward ANN [8, 17, 21]. The neuron connection technique has several nodes in three layers (the input layer, the hidden layer, the output layer) all connected by weights and bias as shown in Figure 3.

Training of the network was trained using Levenberg-Marquardt back-propagation and

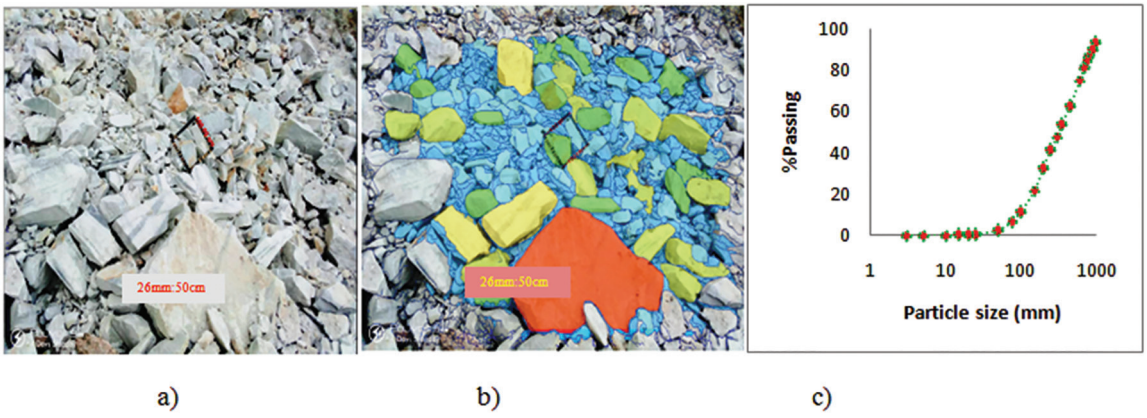

Figure 2: *a) Blast image with 1 m by 1 m scaling frame and image scale, b) Delineated image with scale, and c) WipFrag result particle size distribution curve.*

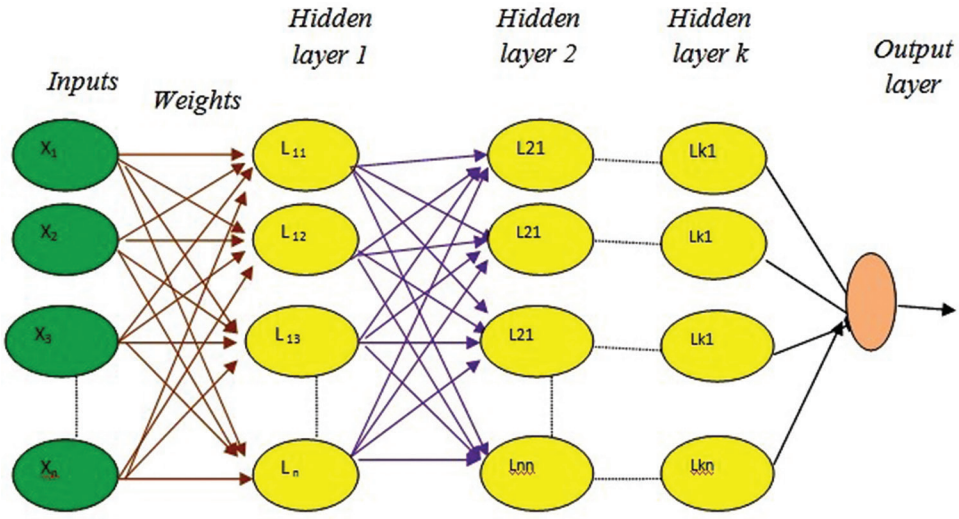

Figure 3: *ANN connection network structure.*

Table 4: *Input parameters and their symbols*

Parameter	Symbol	Range	Parameter	Symbol	Range
UCs	U	160–186.25Mpa	% oversize	Q	23.3%–70%
Density	M	2800–2886 kg/m^3	% undersize	Y	32%–72.1%
Spacing	S	0.8–1.1 m	Mean size (mm)	V	220%-–480 mm
Hole depth	D	1.25–1.35 m			
Stemming length	T	0.6–0.7 m			
Hole diameter	H	0.04 m			
Powder factor	K	0.6–1.0 kg/m^3			
Charge weight	W	0.6–0.96 kg			
Burden	B	0.7–0.85 m			

the Bayesian regularization algorithm. The Levenberg-Marquardt back-propagation algorithm ordinarily takes more memory yet less time. Training ends when speculation stops improving, as demonstrated by an increase in the mean square error of the approval tests. The Bayesian regularization algorithm ordinarily takes additional time but can result in good generalization for troublesome, small, or boisterous, datasets. Training ends as indicated by versatile weight minimization (regularization). Equation (1) shows the general form of the principle of operation of the ANN model as noted by Lawal et al. [22].

$$p_j = f_{sig/purlin}\left\{ b_0 + \sum_{k=1}^{n}\left[f_{sig}\left(b_{nk} + \sum_{i=1}^{m} w_{ik}\,\Gamma_i \right)^{wk\times\ldots} \right] \right\} \quad (1)$$

where, n is the number of neurons in the hidden layer; b_{nk} is the bias in the k^{th} neuron of the hidden layer; b_0 is the bias in the output layer; w_k is the weight of connection between the k^{th} of the hidden layer and the single output neuron; w_{ik} is the weight of connection between the i^{th} input parameter and the hidden layer; Γ_i is the input variable i; p_j is the output variable; and f_{purlin} and f_{sig} are the linear and nonlinear transfer functions, respectively.

The datasets required for the ANN training in this research were extracted from fifty blast operations traversing six distinctive selected pits at the Golden Girl Quarry situated at Akoko, Edo State, Nigeria. Nine input and three output parameters were utilized for the ANN training. The proposed ANN models were created on MATLAB© version R2017a utilizing Bayesian regularization and the Levenberg-Marquardt back-propagation training algorithm. Eight different ANN models were used for the prediction of percentage of oversize, undersize, and mean-size fragments. The input data considered for the research are presented in Table 4 and are made up of those parameters that are generally sensitive to the output. Nine input variables representing U, M, S, D, T, H, K, M, and B were utilized in each model. A three-layer Bayesian regularization algorithm—defined by nine input layers, eight neurons, and three output layers—was selected for building the proposed ANN models. A three-layer neural network was used to predict rock percentage oversize blast materials and percentage undersize blast materials because of its ability to accommodate large amounts of input data and its capabilities for solving vastly complex problems.

Results and Discussion

ANN models for the prediction of blast fragmentation size distribution

According to the training performance for different ANN network architectures and training algorithms, the Bayesian algorithm takes more time in data training as compared to the Levenberg-Marquardt algorithm. In order to determine the optimal ANN network architecture, mean square error (MSE), root mean square error (RMSE), maximum relative error

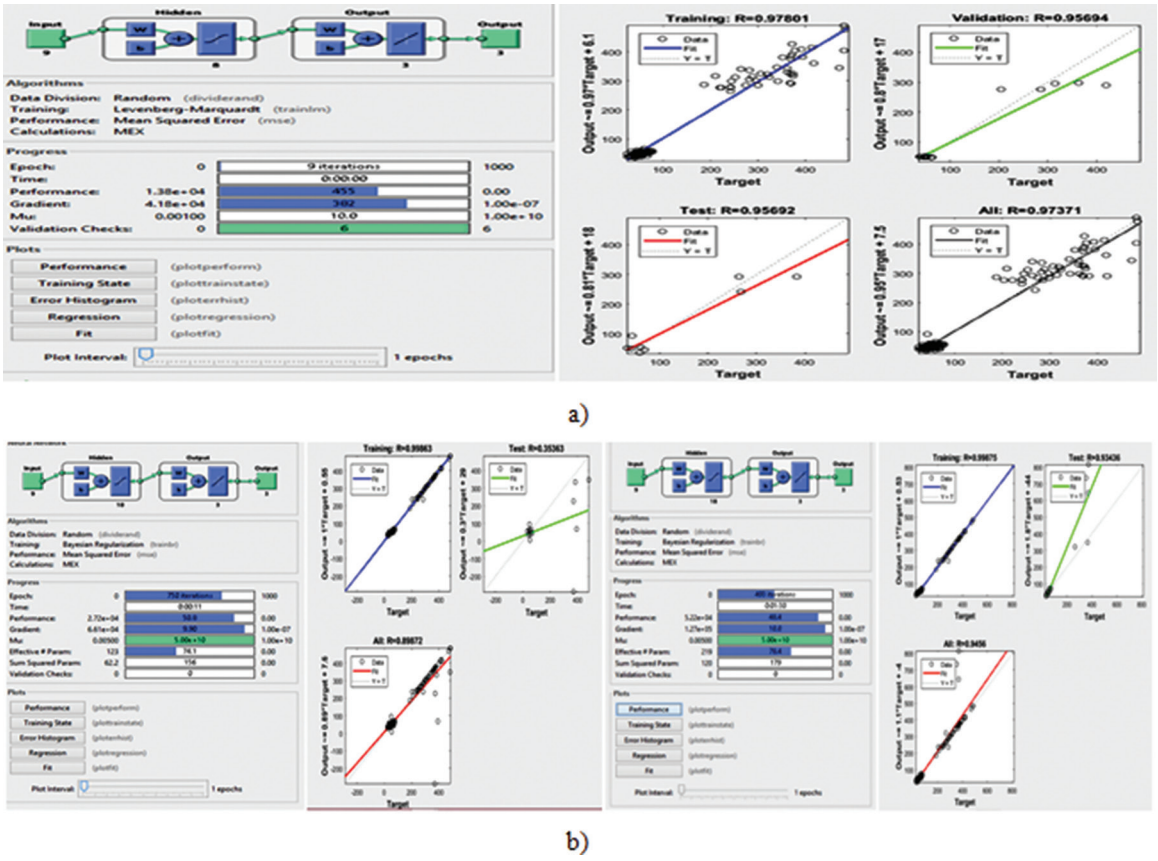

Figure 4: *a) Levenberg-Marquardt models architecture and network regression curves, b) Bayesian regularization algorithm models architecture and network regression curves.*

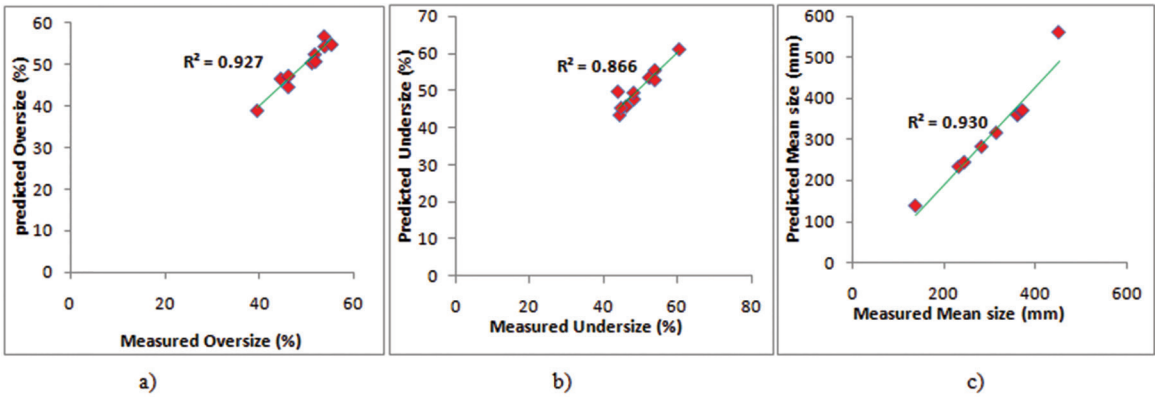

Figure 5: *Relationship between predicted and measured a) percent oversize; b) percent undersize; c) mean size using ANN.*

(MRE), and determination coefficient (R^2) were determined as described by the literature [23–25] for the various models.

The various algorithm performances were analysed using statistical tools, and the trained ANN regularization algorithm models made predictions with the highest accuracy. Figure 4 shows that the R-value for the model training, validation, and test is above 90%. Therefore, the proposed ANN model can successfully predict the blast fragmentation percentage for oversize, undersize, and mean-size fragments. The optimum models were validated with ten datasets. Figure 5 shows the model validation

results, the correlation between predicted and measured outputs for the three outputs (percentage oversize, percentage undersize, and the mean size) provided a high coefficient of determination (R^2) of between 87% and 93%, making the proposed models suitable for the prediction of blast fragmentation size percentages.

The proposed models were transformed into mathematical expressions through the weights and biases based on the ANN general equations presented in Equation (1) in order to enable the easy application of the proposed ANN models for the prediction of blast fragment particle size distribution. The mathematical models obtained for percentages of oversize, undersize, and mean size are presented in Equations (2-4). The proposed model equations were used to develop a software application called the BlastFrag optimizer.

The software requires that the user input the nine input parameters; it then predicts the possible output for the given data and optimizes the supply data using the basting rule of thumb using the Langford blasting formula. Figure 6 shows the software user display interface, the programming code of the software. The predictions obtained directly as outputs from the ANN models and those from the BlastFrag optimizer software were compared to validate the mathematically transformed ANN as shown in Figure 7. It was found that the coefficient of determination for the software is 100%, indicating that the proposed equations are replicates of their respective ANN models.

$$Q = 11.55\tanh\left(\sum_{i=1}^{8} Xi - 0.1603\right) + 45.415 \quad (2)$$

Where;

X_1 = -1.264[tanh(-0.9371+0.5511U+ 0.2418M-1.6908S+3.2295H+1.2932T- 0.92D-1.6066B+……+1.3196W+1.601K)]

X_2 = 1.1026[tanh(0.1053+0.9892U+ 0.5419M+1.3026S-0.5298H- 1.3373T+ 0.6678D-1.0059B+…… .2.5979W+0.4762K)

X_3 = 1.73[tanh(-2.214+0.4549U-0.3531M+ 1.0911S+1.9649H+2.7928T-0.8829D- 0.1656B+…….+0.4334W+0.8929K)]

X_4 = -1.9205[tanh(-0.511-1.1043U- 1.2781M-4.1108S-1.8184H- 1.6006T.0,5101D+2.2472B+...- 1.0147W+1.3332K)]

X_5 = -1.1692[tanh(0.8712-0.5419U+ 0.1954M+3.0582S-1.1224H- 0.0046T+0.1026D-0.8198B+.....- 1.3481W-1.368]

X_6 = -1.5332[tanh(-0.6763+0.204U-1.5771M+ 0.3394S+1.4095H-1.9506T-1.17056D- 1.9912B+...-0.8562W+0.4285K)]

X_7 = -1.2113[tanh(0.407+1.2402U+0.1091M+ 0.8108S-0.1397H+0.1418T+0.1424D- 0.6376B+...+1.3727W-0.2674K)]

X_8 = -1.1239[tanh (0.2348+3.5206U +0.338M+ 2.3944S+2.102H+1.0452T+0.0895D+3.43 36B....+1.5461W-1.6191K)]

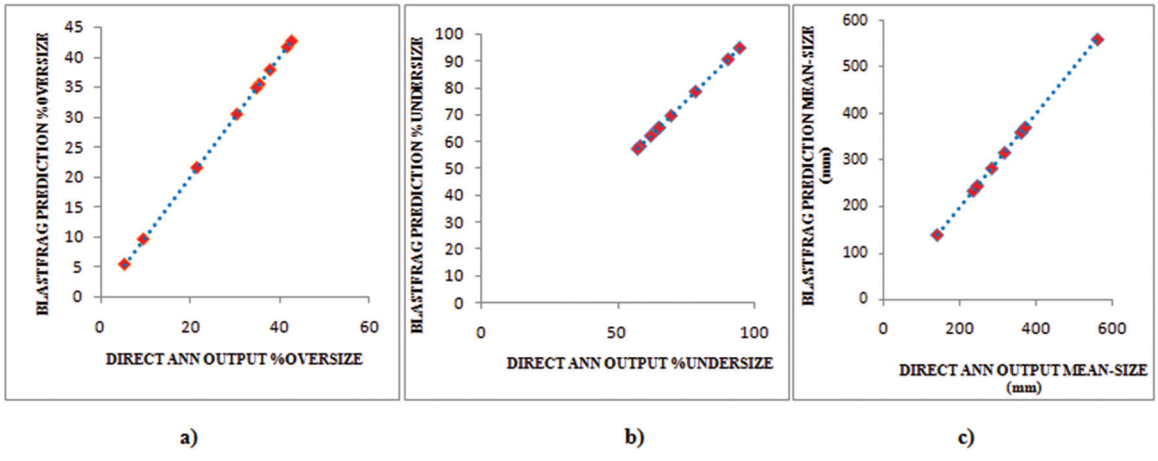

Figure 6: *Comparison of the ANN simulation input with the software (a) %oversize; (b) %undersize; (c) mean size.*

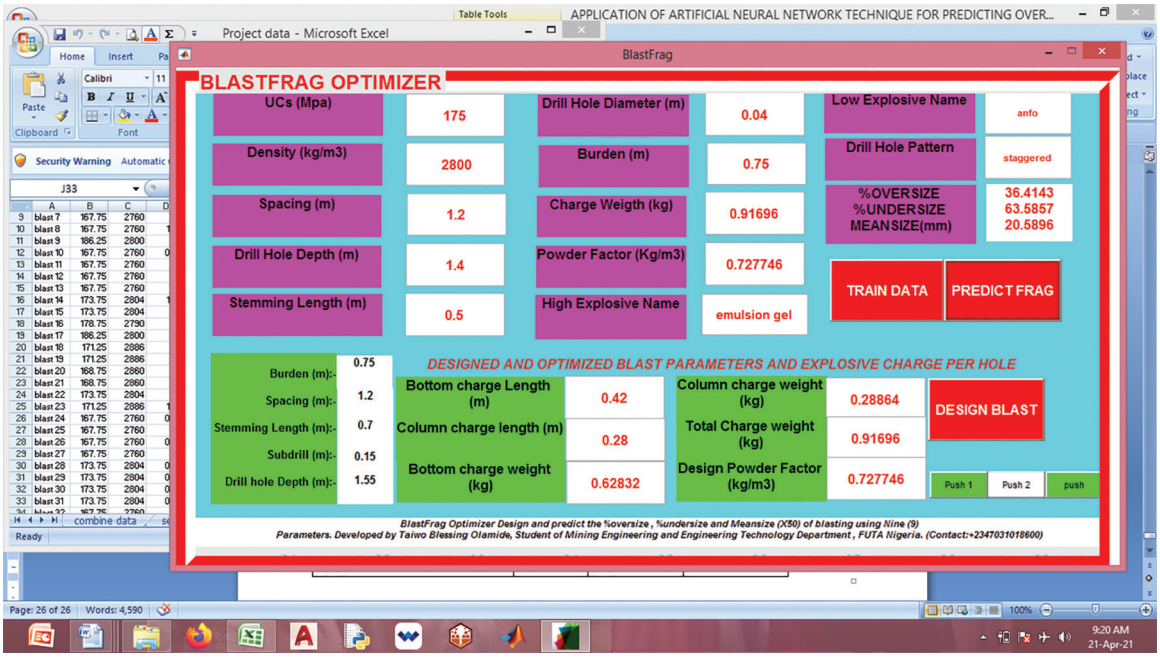

Figure 7: *BlastFrag optimizer user interface.*

$$Y = 23.105\tanh\left(\sum_{i=1}^{8} Xi + 0.1603\right) + 69.52 \quad (3)$$

Where;

X_1 = 1.264[tanh(-0.9371+0.5511U+0.2418M-1.6908S+3.2295H+1.2932T-0.92D-1.6066B+.....+1.3196W+1.601K)]

X_2 = -1.1026[tanh(0.1053+0.9892U+0.5419M+1.3026S-0.5298H-1.3373T+0.6678D-1.0059B+.....-2.5979W+0.4762K)]

X_3 = -1.73[tanh(-2.214+0.4549U-0.3531M+1.0911S+1.9649H+2.7928T-0.8829D-0.1656B+.....+0.4334W+0.8929K)]

X_4 = 1.9205[tanh(-0.511-1.1043U-1.2781M-4.1108S-1.8184H-1.6006T.0,5101D+2.2472B+.....-1.0147W+1.3332K)]

X_5 = 1.1692[tanh(0.8712-0.5419U+0.1954M+3.05825S-1.1224H-0.0046T+0.1026D-0.8198B+...-1.3481W-1.3658K)]

X_6 = 1.5332[tanh(-0.6763+0.204U-1.5771M+0.3394S+1.4095H-1.9506T-1.17056D-1.9912B+...-0.8562W+0.4285K)]

X_7 = 1.2113[tanh(0.407+1.2402U+0.1091M+0.8108S-0.1397H+0.1418T+0.1424D-0.6376B+.....+1.3727W-0.2674K)]

X_8 = 1.1239[tanh (0.2348+3.5206U 0.338M+2.3944S+2.102H+1.0452T+0.0895D+3.4336B+1.5461W-1.6191K)]

$$V = 148.205\tanh\left(\sum_{i=1}^{8} Xi - 0.1654\right) + 171.515 \quad (4)$$

Where;

X_1 = -2.7975[tanh(-0.9371+0.5511U+0.2418M-1.6908S+3.2295H+1.2932T-0.92D-1.6066B..+1.3196W+1.601K)

X_2 = -0.1986[tanh(0.1053+0.9892U+0.5419M+1.3026S-0.5298H-1.3373T+0.6678D-1.0059B+.....-2.5979W+0.4762]

X_3 = 2.6124[tanh(-2.214+0.4549U-0.3531M+1.0911S+1.9649H+2.7928T-0.8829D-0.1656B+....+0.4334W+ 0.8929K)]

X_4 = -2.3725[tanh(-0.511-1.1043U-1.2781M-4.1108S-1.8184H-1.6006T.0,5101D+2.2472B+.....-1.0147W+1.3332K)]

X_5 = -3.1791[tanh(0.8712-0.5419U+0.1954M+3.05825S-1.1224H-0.0046T+0.1026D-0.8198B+....-1.3481W-1.3658K)]

X_6 = -2.9608[tanh(-0.6763+0.204U-1.5771M+0.3394S+1.4095H-1.9506T-1.17056D-1.9912B+...-0.8562W+0.4285K)]

X_7 = 1.297[tanh(0.407+1.2402U+0.1091M+0.8108S-0.1397H+0.1418T+0.1424D-0.6376B+.....+1.3727W-0.2674K)]

X_8 = -2.6255[tanh (0.2348+3.5206U+0.338M+2.3944S+2.102H+1.0452T+0.0895D+3.4336B+.....+1.5461W-1.6191K)]

Where, U is the UCS in MPa; M is the rock density in kg/m^3; S is the spacing in m; H is the drill hole depth; T is the stemming length in m; D is the hole diameter in m; K is the powder factor in kg/m^3; W is the charge weight in kg; B is the burden in m; Q is the %oversize material; Y is the %undersize material; and V is the mean size of the blast muck pile.

Modified KUZ-RAM model

The Kuz-Ram model predicts fragmentation from blasting in terms of mass percentage of fragments passing; according to Choudhary and Gupta, [26] the following assumptions, drawn from explosive energy utilization, can be made: finer fragmentation is generated from higher explosive energy; weak rocks and smaller blast-hole diameters produce more regular fragmentation sizing as a result of uniform distribution of explosives in the rock mass; small burdens and a greater spacing-to-burden ratio produces a high percentage of oversize materials. The modified Kuz-Ram model is similar to the original Kuz-Ram model, but the Kuznetsov equation is modified by an additional factor of 0.073, which is included in the formula for the prediction of the mean fragment size [27]. The reason for adding the additional factor is that joint aperture is considered an effective parameter. The uniformity index of the Kuz-Ram model is also replaced by a modified uniformity index, which is based on the original uniformity index equation proposed by Cunningham and a blast ability index (BI). Table 5 compares the optimum ANN model as we have developed it with the modified Kuz-Ram model, the ANN model predicted outputs were compared with those of the modified Kuz-Ram and found to be more accurate than the modified Kuz-Ram model with the root mean square error (RMSE) relatively lower relatively compared to those of the modified Kuz-Ram model for the same parameters. Also, the coefficient of determination (R^2) for the parameters in the ANN model is closer to unity compared to those of the modified Kuz-Ram. Hence, the ANN model predicts output with suitable accuracy compared to the modified Kuz-Ram model. Percentage oversize prediction by the ANN model as seen in Table 6 is the best with an R^2 of 0.927. The modified Kua-Ram model also predicted mean size (X_{50}) better than it did for percentage oversize and undersize even though the Kuz-Ram model is not as accurate as that predicted by the ANN models that we have developed.

Table 6: *Computed RMSE and R^2 for comparing ANN and modified KUZ-RAM models*

Models	Blasting Parameters	R^2	RMSE
ANN model	Oversize (%)	0.927	1.09
	Undersize (%)	0.866	1.14
	Mean-size (mm)	0.930	3.46
Modified Kuz-Ram model	Oversize (%)	0.111	4.48
	Undersize (%)	0.073	4.58
	Mean-size (mm)	0.157	14.03

Blasting parameters and production optimization with BlastFrag

Table 7 shows the blast outputs and cost per hole blast statistics before and after optimization. An increase in the percentage of undersized fragments and a decrease in the percentage of oversized fragments is an indication of enormous improvement following simulation of the input blast parameters using BlastFrag software prior to blasting. The productivity and charge cost per drill hole were improved by 45.2% and 5%, respectively. There was also a 45.17% gain in productivity as illustrated in Table 7.

Conclusions

This paper reports on an attempt to improve blast preplanning design using the artificial neural network technique. The following conclusions have been drawn:

1. ANN prediction models were developed using seven controllable parameters obtained from fifty monitored blasts and two uncontrollable rock properties determined in the laboratory following the standard procedures suggested by Gheibie et al. [27]. The rock properties conform to ISRM standards [10] for six dolomite pits.

Table 7: *Blasting output statistics and cost per hole blast*

Blast parameters	Blast before ANN model design	Blast with BlastFrag model design
Diameter (mm)	0.04	0.04
Burden (m)	0.7	0.8
Spacing (m)	1.1	1.2
Drill hole length (m)	1.3	1.4
Rock average specific gravity	2.8	2.8
Production per hole blasted (Tonnes)	2.59	3.76
Percent oversize	68.4%	27.83%
Percent undersize	50%	72.17%
Mean size (mm)	418.0	101.6
Profit from blast per hole (Naira)	10,360	15,040
Cost per hole charge (Naira)	1000	950

2. Fifty data sets with seven input parameters and three outputs were trained with ANN using the Levenberg-Marquardt and Bayesian-Regularization Training Algorithms.
3. Error analyses were performed to further compare the performance of the ANN models generated from the Levenberg-Marquardt and the Bayesian-regularization training algorithms adopted for this study. Indices of RMSE, R^2, and MRE are calculated for predicted outputs and compared with the real outputs. It was found that the performance of the Bayesian regularization training algorithm model had maximum accuracy and minimum error compared to the Levenberg-Marquardt training algorithm model.
4. The prediction models that have been developed have strong prediction accuracy and can be used to determine fragmentation size distribution in a dolomite quarry. The models we have developed were deployed in BlastFrag optimizer software for user-friendly implementation.
5. The newly developed software was compared with the modified Kuz-Ram model for predicting the percentage of fragments passing, percentage of fragments that were undersize, and the mean fragment size of dolomite blast results. For all the blasting results investigated, the BlastFrag optimizer showed a higher coefficient determination than the modified Kuz-Ram model. The performance of the proposed models can be used for field blast design for the dolomite quarry.

Acknowledgements

This research blasting images were analysed on WipFrag software with the assistance of Barry McCreadie, Drilling and Blasting Operational Engineer of MBMinBlast Ltd. Company N0:09198751/ 2 Halliwell Court, Elworth, Sandbach, CW11 3AQ, England. Email: barry@minblast.co.uk mobile: +447596455438.

References

[1] Sang Ho, C., Katsuhiko, K. (2004): Rock fragmentation control in blasting. *The Mining and Materials Processing Institute of Japan*, (1), pp. 1722–1730.

[2] Tiile, R.N. (2016): *Artificial neural network approach to predict blast-induced ground vibration, airblast and rock fragmentation*. Masters Thesis. Missouri University of Science and Technology, Faculty of the Graduate School, Department of Mining Engineering: Missouri, 7571 p.

[3] Paley, Na. (2001): Adjusting Blasting to Increase SAG Mill Throughput at the Red Dog Mine. In: *Proceedings of the 27th ISEE Annual Conference*, USA: Orlando, Florida, pp. 65–80.

[4] Atasoy, Y., Valery, W., Skalski, A. (2001): Primary Versus Secondary Crushing at St Ives (WMC) SAG

Mill Circuit. *University of British Columbia*, (1), pp. 248–261.

[5] Grundstrom, C., Kanchibotla, S., Jankovich, A., Thornton, D., Pacific, D.D.N.A. (2001): Blast Fragmentation for Maximizing the Sag Mill Throughput at Porgera Gold Mine. In: *Proceedings of the Annual Conference on Explosives and Blasting Technique*, Papua New Guinea: Porgera, pp. 83–400.

[6] Valery W., Morrell, S., Kojovic, T., Kanchibotla, S.S., Thornton, D.M. (2001): Modeling and Simulation Techniques Applied for Optimisation of Mine to Mill Operations and Case Studies. *CETEM/MCT*, Brazil: Rio de Janeiro, pp. 107–116.

[7] Singh, S.P., Narendrula, R. (2009): Causes, Implications and Control of Oversize During Blasting. In: *Proceedings of the Ninth International Symposium, Fragblast 9: Rock Fragmentation by Blasting, Held in Granada, Spain,* Sanchidrian Blanco, J. (ed.). ISEE: Cleveland, Ohio.

[8] Monjezi, M., Mehrdanesh, A., Malek, A., Khandelwal, M. (2013): Evaluation of effect of blast design parameters on flyrock using artificial neural networks. *Neural Computing and Applications*, 23(2), pp. 349–356.

[9] Mostafa, T. (2009): Artificial neural network for prediction and control of blasting vibrations in Assiut (Egypt) limestone quarry. *International Journal of Rock Mechanics and Mining Sciences*, 46(2), pp. 426–431.

[10] International Society for Rock Mechanics (ISRM) (1989): ISRM Suggested methods for the quantitative description of uniaxial compressive strength test and discontinuities in rock masses. In: *Rock Characterization, Testing and Monitoring: ISRM Suggested Methods,* Brown, E.T. (ed.). Pergamon: New York, p. 256.

[11] International Society for Rock Mechanics (ISRM) (1981): *Rock Characterization Testing and Monitoring: ISRM Suggested Methods.* Published for the Commission on Testing Methods. Brown, E.T. (ed.). Pergamon Press: New York, pp. 75–105.

[12] Maerz, N.H., Germain, P. (1996): In: *Proceedings of the ISRM/Fragblast 5 Workshop and Short Course on Fragmentation Measurement* (meeting held in Montreal, Canada), Franklin J.A., Katsabanis T. (eds.). A.A. Balkema: Brookfield, VT, USA.

[13] Joel, E. (2018): *Optimization of Drilling and Blasting Practices at a Western US Open Pit Copper Mine.* Masters Thesis, Montana Technological University, Department of Geoscience, Option in Geological Engineering, Butte, Montana, USA, pp. 11–18.

[14] Maerz, N.H. (1996): Reconstructing 3-D block size distributions from 2-D measurements on sections. In: *Proceedings of the ISRM/Fragblast 5 Workshop and Short Course on Fragmentation Measurement*(held in Montreal, Canada), Franklin J.S., Katsabanis T. (eds.). A.A. Balkema: Brookfield, VT, USA.

[15] Maerz, N.H. (1996): Image sampling techniques and requirements for automated image analysis of rock fragments. In: *Proceedings of the ISRM/Fragblast 5 Workshop and Short Course on Fragmentation Measurement* (meeting held in Montreal, Canada), Franklin J.S., Katsabanis T. (eds.). A.A. Balkema: Brookfield, VT, USA.

[16] Maerz, N.H., Franklin, J.A., Rothenburg, L., Linncoursen, D. (1987): Measurement of rock fragmentation by digital photoanalysis**.** In: *ISRM, 6th International Congress on Rock Mechanics* (held in Montreal: Canada). ISRM: Lisboa, Portugal, pp. 687–692.

[17] Simpson P.K. (1990): *Artificial Neural Systems. Foundation, Paradigms, Applications, and Implementations.* Pergamon Press: New York, NY, 212 pp.

[18] Kosko, B. (1992): *Neural Networks and Fuzzy Systems.* Prentice-Hall, Hoboken, NJ, USA, 67 pp.

[19] Fausett, L. (1994): *Fundamentals of Neural Networks: Architectures, Algorithms and Applications.* Prentice-Hall: Hoboken, NJ, USA, pp. 102–120.

[20] Shahin, Mohamed A., Mark B.J., Holger R.M. (2002): Artificial neural network applications in geotechnical engineering. *Australian Geomechanics*, 36(1), pp. 49–62.

[21] Haykin, S. (1999): *Neural Networks: A Comprehensive Foundation*. 2nd Edition, Prentice Hall: Englewood Cliffs, NJ, USA, pp.134–187.

[22] Lawal, A.I., Aladejare, A.E., Onifade, M., Bada, S., Idris, M.A. (2021): Predictions of elemental composition of coal and biomass from their proximate analyses using ANFIS, ANN and MLR. *International Journal of Coal Science and Technology*, 8(1), pp. 124–140. https://doi.org/10.1007/s40789-020-00346-9

[23] Pearson, A.L. (1995): Class C scavenger receptor: a macrophage-specific pattern recognition receptor: Proceedings of the 36th Annual Drososphilia Research Conference*. Journal of Muscle Research and Cell Motility* 36: 15A.

[24] Neaupane, K.M., Adhikari, N.R. (2006): Prediction of tunneling-induced ground movement with the multi-layer perception. *Tunnelling and Underground Space Technology,* 21(2), pp. 151–159.

[25] Enayatollahi, I., Aghajani B.A., Asadi, A. (2014): Comparison between neural networks and multiple regression analysis to predict rock fragmentation in open-pit mines. *Rock Mechanics and Rock Engineering*, 47(2), pp. 799–807.

[26] Choudhary, B.S., Gupta, A. (2012): A comparative study on fragmentation measurement techniques. *Mining Engineers' Journal, Mining Engineers' Association of India*, 14, pp. 16–24.

[27] Gheibie, S. Aghababaei, H., Hosienie, S.H., Pourrahimian, Y. (2009): Modified Kuz-Ram fragmentation model and its use at the Sungun copper mine. *International Journal of Rock Mechanics and Mining Sciences,* 46, pp. 967–973.

Original Scientific Article • DOI: 10.2478/rmzmag-2021-0013

Received: October 02, 2021
Accepted: December 06, 2021

Returning Electrostatic Precipitators to the Fe-Ni Production Process

Vrnitev elektrostatičnih filtrov v proizvodni proces Fe-Ni

Zarife Bajraktari-Gashi[1], Izet Ibrahim[1,*], Donjeta Sylejmani[1]

[1]Faculty of Geoscience, Department of Materials and Metallurgy, University of Mitrovica "Isa Boletini", St. Ukshin Kovacica, 40000, Mitrovica, Republic of Kosovo

*Corresponding author: E-mail: izet.ibrahimi@umib.net

Abstract in English

The process of frying the Fe-Ni charge in rotary kilns inherently produces large amounts of process dust, which rotary kilns clean out through the use of electrostatic precipitators [1].

One kiln contains two sections of electrostatic precipitators as a safety mechanism [1]. Electrodes installed in the sections produce electric fields when electricity passes through them, and ionize the dust.

The timing of the process must be coordinated carefully, and these electrodes are struck with hammers and occasionally shaken, generating quantities of dust which are then collected in a snail dust conveyor, then returned to the production process and recycled. In addition, a smaller amount of dust is derived from the gas chamber, which returns to production without entering the cleaning process in the electro filters. The difference between the two types of dust is their granulation size [1].

We conducted the research during the years from 2017 through 2020, calculating the components of the rotary kiln process. Here, we present a linear equation as a result of the ratio of calcine and electrofilter dust.

Keywords: dust, calcine, electro filter, adhesion, rotary kiln

Abstract in Povzetek

Proces žganja Fe-Ni vložka v rotacijskih pečeh proizvede velike količine procesnega prahu, ki ga rotacijske peči očistijo z uporabo elektrostatičnih filtrov [1].

Ena peč vsebuje dve vrsti elektrostatičnih filtrov kot varnostni mehanizem [1]. V odseku kjer so nameščene elektrode se ob prehodu elektrike ustvarjajo električna polja in prah ionizira.

Pravi čas je skrbno usklajen. S pomočjo kladiv, ki te elektrode udarjajo in občasno stresajo, nastanejo znatne količine prahu. Te se nato zberejo v polžjem transporterju za prah, ki se nato reciklira in vrne v proizvodni proces. Poleg tega se iz plinske komore pridobi manjša količina prahu, ki se vrne v proces brez vstopa v proces čiščenja v elektrofiltrih, pri čemer je razlika med obema vrstama prahu v granulaciji [1].

Raziskavo smo izvedli v letih 2017–2020, pri čemer smo izračunali komponente procesa rotacijske peči in predstavili linearno enačbo kot rezultat razmerja žganega in elektrofiltrskega prahu.

Ključnebesede: prah, žganje, elektrofilter, adhezija, rotacijska peč

Introduction

The ferronickel plant in Drenas uses ores that contain a high percentage of moisture, in which the average humidity over the years reaches about 30% [2]. This amount of ore is not subject to drying before the frying process; therefore, the amount of fuel that makes up the charge is high, leading to a large amount of dust and process gasses.

Ores used in the ferronickel plant are the following:

- Ores from Kosovo (mines of Çikatove and Gllavice)
- Ores from Albania
- Ores from Guatemala

The rotary kiln compartment consists of two kilns, both 100 m in lengthand 4 m in; the angle of inclination with respect to the horizontal is 20 degrees [1]. The capacity of the wet charge per day is 2400 tons (t). Moreover, until the end of 2019, the refractory material was chamotte; beginning from the end of 2019, however, the refractory material has been anchored concrete.

The process occurs in the following three zones:

- Drying zone
- Heating zone
- Frying zone

Nickel oxide ores make up significant amounts of fine fractions. During the frying of ore with exhaust gases, a range of up to 8–12% of the Fe-Ni ore is subjected to metallurgical processing.

The return of dust, that is, the ore that passes to cleaning in the processing system is an additional requirement of the dust-cleaning system [1]. In order to clean the dust from the gases of the rotary kilns, the following structures are used: a chamber for charging the rotary kiln, the carrier structure of the dust chamber, and the electronic filter.

The ring for filling the rotary kiln is made in such a way that even large changes in the trajectory of movement of gases are taken into account. In this case, the large fractions fall into the chambers to fill the rotary kiln, where they accumulate together with the charge poured. The gas flowing through the conductor system encounters the the electrical field forming the filter. Two sections of electronic filters of type 2PAA-4040-90100-1 are placed in every kiln [1].

The electronic filters have four dust collectors, 14 control holes, and one filter section has 1485 and the other 10,500 cleaning electrodes, both sets of electrods being 2-mm in thickness. The gas is purified at a rate of 7300 m^3n/min at a temperature of 375°C, and the gas is dusted at a rate of 50 g/m^3n. This process results in a gas purification level of 99% [1].

FLS MT 315 S fans are used to suck the gases from the rotary kilns. The first kiln contains two fans, and the second kiln contains four fans. In the collectors of rotary kilns, the frying process provides a system for the return of dust from electric filters and chambers. In the dust chambers, conveyors 7 and 7a, 8 and 8a and coils 1 and 1a, 2 and 2a place the dust in an elevator. A portion of the spill from conveyors 7-7a and 8-8a is recovered and also placed in the elevator [1].

The transport capacity and conditions consist of the following: 10 t/h, 300-mm diameter, up to 250°C temperature, 6- to 25-mm length, and an electric motor power of 2.2–5.5 kW. The yield of dust on the side of the evaporator increased to +25.7 m from a previous yield of +1.32 and +2.29 m [1].

In the receiving collectors of the rotary kilns, two elevators are placed for the purpose of returning dust to the rotary kilns N-1 and N-2. By means of the ninth conveyor, it is possible for the dust, which is attached to the gas-cleaning system of the rotary kiln N-1, to be thrown into the elevator, which delivers the dust captured by the gas-cleaning system of the N-2 rotary kiln. From the elevators, the dust is poured into conveyors 10 and 10a, which are poured through conveyors 11-11a into the equipment for filling the rotary kiln. The filling device enables the transfer of the dust inside the oven along with the dust in the charge. This operation reduces the circulation of dust.

If the furnace breaks down, it creates and collapses the rings glued to its inner walls, which contributes to the increase in the size of the pieces of ore. As a result, the ore cannot pass through the sieve placed at the bottom of the furnace. The enlarged pieces of ore are transported to the special base and from there the loading equipment loads the ore into trucks, which return it to the processing department.

Methodology

Our methods for this study were based on the industrial working processes of rotary kilns during the four years analysed (2017–2020).

Figure 1 shows the industrial data for the charge composition for rotary kilns, which comprises the product of the rotary kiln (calcine), moisture composition, adhesion composition, and dust composition calculated as percentages of total content [2].

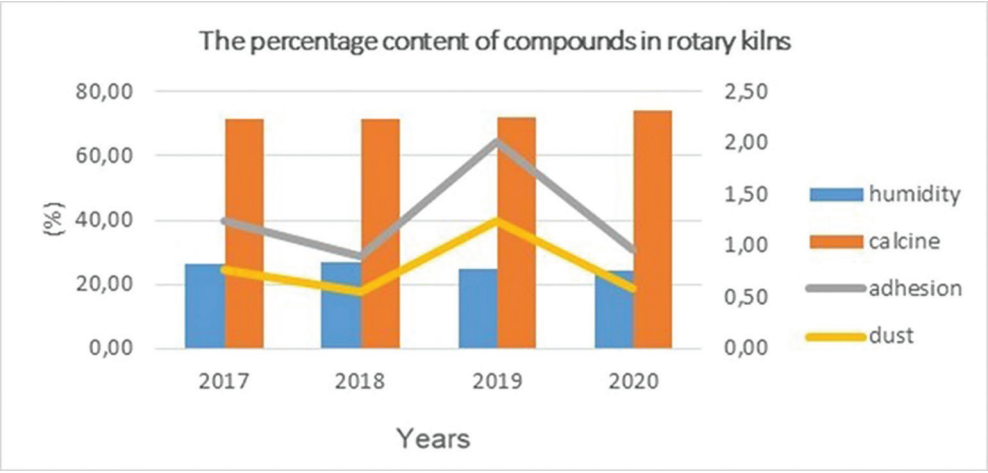

Figure 1: *Graphical representation of the amount of ores, moisture, calcine, adhesion, and dust in the product of rotary kilns.*

The return of the electrofilter dust into the production process benefits the environment.

Discussion of results

The dust has the same composition as the calcine produced in rotary kilns. Therefore, its return to the process has economic and environmental benefits, the main purpose being the reduction of nickel losses to a minimum.

The graphic representation (Figure 1) shows that the amount of calcine and the composition of the ore moisture as products of charge reached adhesions of 1% in 2018, 2% in 2019, and 1% in 2020 of the calcine produced [3].

Moreover, calculations of the moisture content of the ore the amount of calcine produced, and the adhesives (Figure 1), allowed us to calculate the amount of dust created during the years analysed. In 2017, the amount of dust was 0.77% of the amount of calcine produced. In 2018, the amount of dust came to 0.55% of the amount of calcine produced, and the amount of adhesives reached 1.25% of the amount of calcine produced. In 2020, however, the amount of dust scored 0.59% that of calcine produced [3].

Figure 1 shows that during the year 2019 the amount of dust produced as a result of processing Guatemalan ore was high. Guatemalan ore contains large amounts of moisture, which in turn leads to the creation of more dust [1]. Figure 2, however, shows the amount of Fe-Ni ore spent during the years 2017–2020, where it is worth noticing the significant drop in production in 2018 due to a halt in use of the rotary kilns.

From analysing industrial practice, we have reached the conclusion that 1800 kg of dust is formed in one hour from 80 t/h of pure charge.

Dust comes as a consequence of:

- Equipment overload
- Amortization of snails
- The low capacity (12 t/h) of snails
- The large amounts of dust generated from processing ores from Guatemala and Albania

We obtained the linear equation presented in Figure 3 from the ratio of calcine to dust generated from using the electrofilter process of rotary kilns.

As a result of all the factors in our analysis, we can conclude that the amount of dust increases as the moisture content contained by Fe-Ni ore increases [4].

Because the composition of the dust is the same as the composition of the calcine produced in rotary kilns, returning to the use of electrostatic precipitators should be a well-accepted process. because they result in improved recovery of valuable components of the process. Moreover, the use of electrostatic precipitators is favourable from an environmental point of view.

If the electrofilter dust were to be released into the atmosphere, it would have a

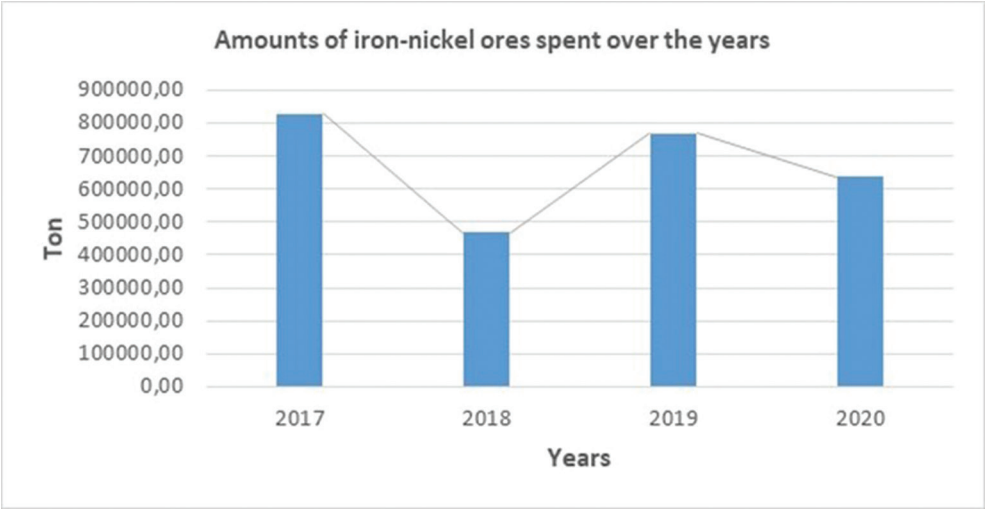

Figure 2: *Graphical representation of the amount of Fe-Ni ore used during the years 2017–2020.*

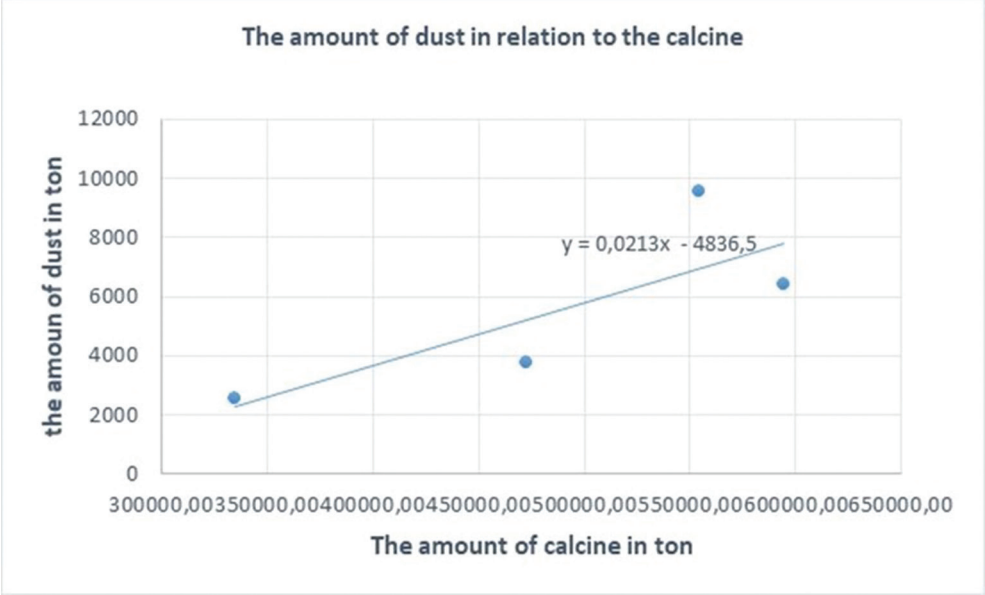

Figure 3: *The representation of the amount of dust in relation to calcine.*

negative impact on the environment, particularly people and plants, as well as animals that graze around the Ferronikeli plant, thereby making a harmful impact on all chains of life.

Recommendations:

- Installation of two dryers at the Ferronikeli plant for drying of Fe-Ni ore
- Granulation of Fe-Ni ore
- Use of a greater amount of Kosovo's dry lignite

References

[1] Bajraktari Gashi, Z. (2012): *Theoretical and experimental research in order to reach optimum technical, technological and productive parameters during qualitative reduction of Ni ore in Fe-Ni Plant in Drenas*. Ph.D. Thesis. University of Prishtina "Hasan Prishtina", Faculty of Geoscience of Technology in Mitrovica, Department of Materials and Metallurgy: Kosovo, 108 pp.

[2] Bajraktari-Gashi, Z., Halilaj, B. (2018): Material balance of the technological process in the New

Foundry of New Ferronikel in Drenas during 2017. *Journal of Technology and Exploitation in Mechanical Engineering*, 4(1), pp. 29–35, DOI:10.35784/jteme.90.

[3] New Ferronickel Complex L.L.C. (2017–2020). Official Documentation of Melting.

[4] Bajraktari Gashi, Z., Zabeli, M., Halilaj, B. (2018): The impact of pet-kok in the technological process of production of Fe-Ni in the new foundry of the new Ferronickel in Drenas. *Journal of International Environmental Application and Science*, 13(1), pp. 72–77.